ULTRASOUND ALIGNMENT OF A HIGH WEIGHT FRACTION OF CARBON NANOTUBES IN A POLYMER MATRIX

by

Leora Homel

A thesis submitted to the faculty of
The University of Utah
in partial fulfillment of the requirements for the degree of

Master of Science

Department of Mechanical Engineering

The University of Utah

August 2017

THE UNIVERSITY OF UTAH GRADUATE SCHOOL

STATEMENT OF THESIS APPROVAL

The thesis of Leora Homel

has been approved by the following supervisory committee members:

Bart Raeymaekers, Chair	Date Approved
Bruce Gale, Member	06/08/2017 Date Approved
Brittany Coats, Member	06/08/2017 Date Approved

and by Timothy Ameel, Chair of the

Department of Mechanical Engineering,

and by David B. Kieda, Dean of The Graduate School.

ABSTRACT

This research introduces a new process to fabricate polymer nanocomposite materials reinforced with an ultra-high weight fraction of aligned carbon nanotubes (CNTs). This process is based on ultrasound directed self-assembly, which employs the force associated with a standing ultrasound wave to concentrate and align the carbon nanotubes in a user-specified pattern. In contrast with existing processes, which typically limit fabricating nanocomposite materials with a CNT weight fraction on the order of 1 weight percent (wt.%), polymer nanocomposite materials were fabricated to contain a weight fraction of aligned CNTs in excess of 10 wt. %. The fabrication process, dispersion of CNTs in the polymer matrix, appropriate acoustic wave propagation velocity in the matrix material, and degradation of polymer mechanical properties from exposure to ultrasound stimulation are described.

The mechanical properties of these polymer nanocomposite specimens were experimentally measured and it was found that the ultrasound alignment process resulted in specimens that displayed a significant increase in ultimate tensile strength, Young's modulus, and moduli of resilience and toughness, compared to specimens including polymer nanocomposite materials with randomly oriented CNTs, and "processed polymer".

The research demonstrates that by combining ultrasound alignment with microwave

radiation exposure, the Young's modulus and ultimate tensile strength of the polymer nanocomposite material is further enhanced. Specimens were affected differently by microwave radiation exposure, depending on the type of alignment and dispersion used to create the specimen. These observations may guide further optimization of the process.

TABLE OF CONTENTS

ACKNOWLEDGEMENTS

I gratefully acknowledge the contributions of Prof. Bart Raeymaekers, whose guidance and patience made this work possible. I'm also grateful for the work of Michael Haslam and John Greenhall, which laid the foundation for this effort.

I'm thankful for the love and support of my parents and my husband, who provided encouragement and support during graduate school and the process of writing this thesis.

The author also acknowledges support from Army Research Office contract W911NF-14-1-0565. We thank Prof. Daniel O. Adams for access to the mechanical testing infrastructure in the Structural Integrity Laboratory at the University of Utah – Department of Mechanical Engineering.

CHAPTER 1

INTRODUCTION

Carbon nanotubes (CNTs) were discovered in the early 1990s [1] and researchers have attempted to use them as a reinforcement fiber in polymer composite materials because of their ultra-high strength-to-weight and stiffness-to-weight ratio [2]. Thus, successfully embedding CNTs in a polymer matrix could yield low-density materials with mechanical properties that vastly outperform those of state-of-the-art composite materials and other high strength-to-weight ratio materials, enabling a myriad of engineering applications. Such applications include structural materials that are for instance used in lightweight structures, military equipment, and aerospace components. Military applications include strong lightweight body armor and helmets for ballistic protection of soldiers and military assets, whereas aerospace components include low-density aircraft panels and parts, which save weight and reduce fuel consumption. Other critical applications include multifunctional materials. Successfully embedding CNTs in a polymer matrix would enable electromagnetic shielding combined with low-density materials, which is of primary importance to the aerospace industry and satellite manufacturers. Also, electrically-conductive bonded joints find use in spacecraft to eliminate the buildup of static charge on the structure. Thus, successfully manufacturing polymer nanocomposite materials reinforced with CNTs would address an important need in several industries and

enable several engineering applications. As a result, many researchers attempt to manufacture polymer nanocomposite materials reinforced with CNTs, to obtain low-density materials with mechanical properties that significantly outperform those of state-of-the-art materials.

However, while an active research topic, polymer nanocomposite materials reinforced with CNTs have not yet achieved the mechanical properties that are theoretically expected based on the strength of the CNTs. Three primary reasons are often cited for this reduced performance [3], [4]. First, dispersion of the CNTs in the polymer matrix is needed to ensure intimate contact between each CNT and the matrix material. Second, alignment of the CNTs in the direction of the anticipated mechanical loading of the material is required to take advantage of the strength of the CNTs. Third, adhesion between the CNTs and the polymer matrix is critical to ensure load transfer from the weak matrix material to the strong CNTs. To meet these requirements, the concentration of CNTs in the polymer matrix is typically limited to less than 1-2 weight percent (wt. %) because larger concentrations of CNTs make it increasingly difficult to obtain dispersion, alignment, and intimate contact between all CNTs and the polymer matrix material [5]. Consequently, based on these limited CNT weight fractions, researchers have only demonstrated modest improvement of the mechanical properties of polymer nanocomposite materials reinforced with CNTs compared to polymer composite materials without CNTs. However, the ability to significantly increase the CNT weight fraction could enable further increasing the strength and stiffness of polymer nanocomposite materials reinforced with CNTs.

This research specifically focused on aligning CNTs in the direction of the anticipated mechanical loading, and relied on existing, well-known methods to obtain dispersion and

adhesion of the CNTs in the polymer matrix. The goal of this research was to develop a novel method, based on ultrasound waves, to manufacture polymer nanocomposite materials reinforced with an ultra-high weight fraction (> 10 wt. %) of aligned CNTs, and to significantly improve the mechanical properties of polymer nanocomposite materials reinforced with aligned CNTs compared to state-of-the-art polymer nanocomposite materials. In addition, the research employed microwave radiation to further improve the mechanical properties of polymer nanocomposite materials with aligned CNTs following the work of Sweeney *et al*. [6].

Thus, the objectives of this research were (1) to devise a novel manufacturing process, based on ultrasound waves, that enabled synthesizing polymer nanocomposite materials with an ultra-high weight fraction of aligned CNTs, and (2) to experimentally evaluate the mechanical properties of such materials compared to materials without CNTs, and materials reinforced with randomly oriented CNTs.

The research employed the following tasks to achieve this objective:

(1) Use ultrasound standing waves to align CNT weight fractions ranging between 9 and 13 wt. % in a liquid polymer matrix material.

(2) Manufacture a polymer nanocomposite material with aligned CNTs by cross-linking the polymer matrix in a standard dogbone-shaped mold.

(3) Measure the mechanical properties of the polymer nanocomposite material with aligned CNTs, including ultimate tensile strength, Young's modulus, and moduli of resilience and toughness.

This thesis is organized as follows. Chapter 2 presents the background and literature survey related to composite materials with focus on polymer nanocomposite materials

reinforced with CNTs, and processes to align CNTs in a polymer matrix. Chapter 3 discusses the materials and processes used to manufacture polymer nanocomposite materials with aligned CNTs in excess of 10 wt. %. The methods also include those for testing the mechanical properties of the manufactured polymer nanocomposite material specimens and statistical analysis of the data. Chapter 4 presents the mechanical properties of the polymer nanocomposite materials with aligned CNTs, and compares these results to materials without CNTs and materials reinforced with randomly oriented CNTs. Chapter 5 summarizes the key findings of the work presented in this thesis and outlines a plan for future work.

CHAPTER 2

BACKGROUND

2.1 Introduction

Composite materials are defined as materials that contain at least two constituents or phases that are physically or visibly distinguishable [7]. In this thesis, the term "composite material" is used to refer specifically to a solid, structural material that consists of a reinforcement phase suspended in a matrix phase [8]. The reinforcement phase is the primary source of structural integrity in the composite material. The matrix phase maintains the position of the reinforcement phase, protecting it against external damage, and transferring external mechanical loads to the reinforcement phase [9]. By adjusting the type, weight fraction, and microstructure of the constituent phases, it is possible to vary the mechanical properties (*e.g.*, the strength, Young's modulus, resilience, toughness, and fatigue life) across a broad spectrum. This manipulability affords a degree of control and customization not possible with single-phase engineering materials [10]. The choice of matrix material and reinforcement phase, their properties, and the interplay between these constituents significantly affects the mechanical properties of the resulting composite material.

The engineering value of composite materials has been recognized throughout history. For thousands of years, humans have constructed structures with composite materials based

on natural, indigenous materials. Several cultures have mixed straw into mud/clay bricks (adobe) to improve binding of the material while curing [11]. The Chinese added bamboo to structurally reinforce the Great Wall [12], the Egyptians added gypsum to the mortar for the Great Pyramids [13], and the Romans made concrete with sand, lime, and volcanic ash [14], [15]. Synthetic composite materials were first engineered in the 1930s [16]. This thesis focuses on synthetic composite materials reinforced with CNTs. As such, Section 2.2 presents an overview of the diverse spectrum of synthetic composite materials. The subsequent sections then describe the family of carbon composite materials, with specific attention to polymer nanocomposite materials reinforced with aligned CNTs, which are the focus of this thesis.

2.2 Synthetic composite materials

Synthetic composite materials are commonly described in three major groups, as illustrated in Figure 2.1, which shows: (a) particle-reinforced composite materials, (b,c) fiber-reinforced composite materials, and (d-f) laminated structures [17], [18]. Figure 2.2 diagrams the taxonomy of these major composite material types, along with common sub-classifications. Particle reinforcement in composite materials is sub-classified into two groups: large-particle reinforcement and dispersion-strengthened reinforcement. Laminar composite materials are also sub-classified into two groups: layered structures and sandwich panels. Fiber reinforcement in composite materials is sub-classified into two groups: continuous fiber reinforcement and discontinuous fiber reinforcement. Each of these sub-classifications is described in the paragraphs that follow.

Particle-reinforced composite materials are classified by particle size, which governs the mechanism of reinforcement. For *dispersion-strengthened* reinforcement, the matrix

material provides primary structural support, and the reinforcement particles enhance mechanical properties by mitigating inelastic deformation within the matrix phase [18], [19]. There is significant disagreement in the literature as to the range of particle sizes to which this classification applies, (*c.f.* Akovali [19], which gives 0.01-0.1 mm or Askeland and Wright [18], which gives 10-250 nm) but it is generally applied for particles smaller than 0.1 mm. When the particle size is larger than this limit, the term *large-particle* reinforcement is used. For such materials, the particles are stiffer than the matrix and occur at a sufficient volume fraction that the majority of the load is supported by the reinforcement phase [19].

Laminated structures comprise two or more bonded layers. Each laminated layer, or *lamina*, may be a different material, or several laminae of the same anisotropic material may be combined at differing orientations [20]. In some cases, the individual lamina may themselves be composite structures such as fiber-reinforced composite materials or epoxy-impregnated woven fabrics [21], [22]. When the laminae have similar thicknesses, the structure is termed a *laminate* [18]. Another common configuration is a *sandwich panel* comprising two higher-stiffness face laminae (approximately 10% of the total panel thickness) bonded to a lower-density (*e.g.*, foam or honeycomb structure) inner core. This configuration is used to maximize the strength and stiffness in bending while minimizing weight [8], [23].

Fiber-reinforced composite materials are classified based on the aspect ratio (l/d) of the reinforcement fibers, which affects the failure mechanisms of the composite material. *Continuous fibers* are manufactured in lengths of several meters to several thousand meters, and have a length-to-diameter ratio of approximately 10,000 [24]. Since the fibers can span

the dimensions of an entire part, the potential for failure due to matrix or polymer cracking is mitigated or reduced [25]. *Discontinuous fibers* are classified as either *short* (l < 3 mm [24], with a length-to-diameter ratio of approximately 100 [26]) or *long* (3-25 mm, with a length to diameter ratio of 300-2000 [24]). For short-fiber composite materials, the fibers can be *randomly-oriented* or can be *aligned* to some preferential orientation.

Fiber-reinforced composite materials can be reinforced with either natural or synthetic fibers. This discussion will focus on synthetic fibers, which are engineered to have superior mechanical properties compared to their natural counterparts. Figure 2.3 depicts an overview of the types of synthetic fibers that are commonly used to reinforce composite materials[1].

Synthetic organic fibers have high strength (1.9-3.6 GPa) [28], high stiffness (59-186 GPa) [28], [29], and low density (1,300-1,500 kg/m³) [28]; these fibers are used when it is desirable to maximize specific strength or specific stiffness. Aramid is one of the most commonly used synthetic organic fibers for reinforcement, and has a reported specific strength as high as 2,514 kN·m/kg [28], [30]. Synthetic inorganic fibers have comparatively higher strength (3.4-4.8 GPa) [28] and higher stiffness (81-370 GPa) [28], but they also have a higher density (1,800-2,500 kg/m^3) [31], resulting in a lower specific strength but similar specific stiffness to synthetic organic fibers [32]. CNTs are an

[1] These fibers can be broadly classified as either *organic* or *inorganic*. In the study of organic chemistry, the term organic is commonly taken to mean, "containing carbon". But, for historical reasons, certain simple carbonaceous compounds (*e.g.*, carbonates, carbides, etc.) are considered inorganic [27]. Following this convention, which is adopted in much of the composite materials literature, this thesis uses the term organic to refer to molecules and compounds that contain both carbon and hydrogen, so the allotropes of carbon (*e.g.*, diamond, graphite, CNTs) are classified as inorganic.

exception and have a reported specific strength up to 46,238 kN·m/kg [33].

Synthetic inorganic fibers are brittle materials, for which strength depends on the orientation and distribution of microcracks and defects within the material [34]. The probability of a defect existing within a volume decreases as the size of the volume is reduced, producing a significant scale effect in the apparent strength of a brittle material [35]. As a result, brittle materials are stronger and stiffer in fiber form than in their bulk form, increasing the effectiveness of fiber reinforcement [26], [36]. Because of this scale effect, synthetic inorganic fibers are most advantageous when used as short-fiber reinforcement [37].

The strength and stiffness of fiber reinforcement depends on the type, length, weight fraction, and orientation of fibers in the matrix material, but the bulk mechanical properties of the composite material are also strongly dependent on the properties of the matrix material [7]. Metals, polymers, and ceramics are used as the matrix material in synthetic composite materials. Figure 2.4 gives examples of each class of matrix material commonly found in synthetic composite materials.

Ceramic matrix materials have high strength (300-1000 MPa) [38] due to ionic bonding and high-temperature resistance but are very brittle with low fracture toughness (3-8.5 $MNm^{-3/2}$) [39], [40]. Silicon nitride and silicon carbide can withstand temperatures of up to 1,700°C, making them ideal matrix materials for composite materials used in high-temperature applications [41].

Metal matrix materials are typically nonferrous alloys that require high processing temperatures [10]. Aluminum and titanium are the alloys most commonly used as metal matrix materials, because of their low densities (1,700-2,700 kg/m^3) [17], high strength

(60-370 MPa) [39], and high stiffness (69-120 GPa) [38]. They are used to make lightweight, thermal-resistant (400-750°C) [29], [42], high strength composite materials, but they have limited application potential due to their high cost (2.65-160 $US/kg) [39] and potential to corrode in certain environments [42]. In some cases, the matrix material has a desirable physical property such as high density (*e.g.*, lead) or high electrical conductivity (*e.g.*, copper), and the reinforcement phase is added to provide structural support.

Polymer matrix materials are the most common of all matrix materials used in manufacturing of composite materials due to low cost (1.05-105 $US/kg) [39], high specific strength (8.97-33.95 kN·m/kg) and toughness (185.9-304.9 kN·m/kg) [39], ease of manufacture, and chemical compatibility [36]. Of the three basic polymer types, elastomers, thermoplastics, and thermosets, thermoset polymer matrix materials are the most common [8]. Thermoset matrix materials begin as a low-viscosity resin that reacts and cures during processing to form a solid material [42]. The reinforcement phase can be added to the resin at room temperature, which simplifies the manufacturing process [26], [39]. Adding reinforcement can reduce the cost, enhance the mechanical properties, and alter the surface characteristics of the polymer [39].

Maximizing strength and stiffness while minimizing density is desirable for many structural applications [43]. Figure 2.5 shows a material selection chart comparing the stiffness versus density for several families of engineering materials by plotting, for each material, the Young's modulus (E) on the ordinate and the density (ρ) on the abscissa [44]. Composite materials are shown to be the highest-stiffness option for densities in the range of 100-1000 kg/m^3 [45]. Many of the stiffest materials in this range are polymer composite

materials.

Carbon is a widely used reinforcement phase for polymer matrix composite materials. It has many different forms including carbon fiber, diamond, graphite, fullerene, carbon nanofiber, and CNT [46]. These allotropes can all be used as reinforcement for polymer matrix composite materials to enhance one or more properties. The addition of carbon to a polymer typically increases the strength, stiffness, thermal conductivity, and electrical conductivity of the composite material. Carbon fiber is the most widely used form of carbon for enhancing the mechanical properties of composite materials.

To increase the performance of a fiber-reinforced composite material beyond that achievable with carbon fiber reinforcement, it is necessary to increase the strength or stiffness of either the fiber, the matrix, or the adhesion at the interface. The following section describes CNTs, which have outstanding mechanical properties relative to other synthetic fibers. However, many technical challenges must be overcome to economically produce polymer nanocomposite materials reinforced with aligned CNTs that exhibit the properties theoretically achievable with a CNT reinforcement phase.

2.3 Carbon nanotube polymer nanocomposite materials

CNTs can be conceptualized as a graphene sheet rolled into a cylindrical structure. CNTs are classified by the number concentric cylinders in a CNT. Figure 2.6a shows a single-walled CNT (SWCNT), whereas Figure 2.6b shows an example of a multi-walled CNT (MWCNT), which can comprise two or more concentric graphene cylinders.

The unique properties of CNTs have garnered much excitement for their potential applications, but thus far, their widespread use has been limited by current manufacturing technology. Common methods to manufacture CNTs include arc discharge, laser ablation,

and chemical vapor deposition (CVD). Arc discharge was the first successful method and is the easiest approach, but it produces a low-purity product that may contain as much as 30 percent impurities [1]. Laser ablation produces higher-purity CNTs, but can only produce SWCNTs and has limited yield [47]. Most recent attention has been paid to CVD, which can produce larger quantities by using a continuous process [48].

The CVD method requires the decomposition of a hydrocarbon with the assistance of a catalyst. The hydrocarbon is decomposed at high temperature (550-750°C) [49] in the presence of an inert gas and a catalyst such as iron, nickel, or cobalt [48] (Figure 2.7). The solubility of carbon in these catalysts is sufficiently low at these temperatures that carbon precipitates on the catalyst surface; the energy of formation for CNTs is lower than for other allotropes of carbon, so CNTs form preferentially [50].

CNTs created using CVD, laser ablation, and arc discharge have defects and contaminants present [51], and subsequent purifications steps may be required [48]. For each of these production methods, the process parameters, catalyst selection, and doping agents will affect the structure of the product.

Table 2.1 compares the mechanical properties of CNTs to those of other engineering materials used as reinforcement in polymer composite materials, illustrating the extraordinary strength and stiffness of CNTs. Since CNTs have a low density for a solid, their specific strength is amongst the highest of any known engineering material.

The need for materials with improved specific strength and stiffness arises in many applications and has driven the development of polymer composite materials reinforced with aligned CNTs. The idea of adding reinforcements to a matrix made of polymer has been around for many decades. The addition of CNT reinforcement to a polymer matrix

material increases the strength and stiffness of the polymer.

When the reinforcement phase is much stiffer than the matrix phase and the weight fraction of the reinforcement phase is high (> 10 wt. %), the elastic stiffness will be limited by the adhesion between the matrix and reinforcement [52]. A good adhesion allows effective load transfer to the reinforcement phase, enhancing the mechanical properties of the composite material. With sufficient adhesion, a polymer composite material with aligned CNTs is much stronger, stiffer, and lighter than polymer matrix composite materials that are reinforced with carbon or glass fibers [53].

There are several methods to estimate mechanical properties of a composite material from its composition and constituent properties. The classical "rule of mixtures" and "inverse rule of mixtures" are based on assumptions of uniform strain or uniform stress in the material, respectively. Various modified rules of mixtures [17], as well as the generalization to 3D by Hashin and Strikham [54], expand upon these principles.

Using a rule of mixtures [26], the theoretical value of the Young's modulus was estimated for a polymer nanocomposite material with aligned CNTs as

$$E_c = E_f v_f + E_m v_m , \tag{2.1}$$

where E_c, E_f, and E_m are the Young's modulus of the composite, fiber[2], and matrix, respectively, and v_f and v_m are the volume fractions of the fiber and the matrix [26]. The implied assumption of constant strain is valid for a large volume of CNTs that is well-

[2] To be consistent with the standard nomenclature in the mechanics literature for composite materials, this thesis uses the subscript *f* to denote "fiber" as a synonym for reinforcement phase.

adhered to the matrix phase. Similarly, a rule-of-mixtures estimate for the density is

$$\rho_c = \rho_f v_f + \rho_m v_m , \tag{2.2}$$

where ρ_c, ρ_f and ρ_m are the densities of the composite, fiber, and matrix, respectively.

This research used the rule of mixtures for estimating the performance of polymer composite materials with a high weight fraction of aligned CNTs. For the polymer matrix material used in this research (thermoset resin) with a density of 1050 kg/m^3 and Young's modulus of 0.962 GPa, and with 10% volume fraction of perfectly dispersed, aligned CNTs added as reinforcement, the theoretical values for the composite material density and Young's modulus are 1121.9 kg/m^3 and 151 GPa, respectively. For comparison with other engineering materials, these values are plotted in Figure 2.8h, which illustrates the remarkable specific stiffness of a polymer composite material reinforced with aligned CNTs.

The actual performance of a polymer composite material with aligned CNTs may be substantially lower than the theoretical value, and is affected by (1) dispersion of the CNTs in the matrix, (2) adhesion at the matrix-reinforcement interface, and (3) alignment of the reinforcement phase relative to the applied load. These factors are discussed in the following sections.

2.3.1 Dispersion of carbon nanotubes

CNTs have a tendency to entangle and aggregate due to van der Waals forces [55]. *Dispersion* refers to the process to reduce these attractive forces, mitigating the formation of aggregate CNT bundles. Dispersion of the CNTs is one of the most important procedures when manufacturing polymer nanocomposite materials with aligned CNTs, and the extent

of CNT dispersion in a nanocomposite material correlates strongly with its mechanical properties [56]. When CNTs aggregate into bundles, the interfacial area between the CNT and the polymer matrix material decreases, which degrades the capability for stress transfer between the matrix material and the reinforcement phase. Additionally, the strength and stiffness of a CNT bundle is much lower than that of a single CNT [57]. Thus, dispersion is expected to increase the strength of a polymer nanocomposite material reinforced with aligned CNTs, unless the dispersion method itself degrades the strength of the matrix material, the reinforcement phase, or the interfacial strength [57].

A small number of chemical and physical dispersion methods exist that have been used to disperse CNTs in a liquid polymer material. Polymers, surfactants, acids, or a combination of these materials are used as chemical dispersing agents [58]–[60]. There are two methods that are used to chemically disperse CNTs into a polymer matrix. The first method is to simply combine the dispersing chemical, the CNTs, and the polymer matrix solution. The second method is to combine the dispersing chemical and the CNTs, but to then remove the dispersing chemical before adding the CNTs to the polymer matrix solution. This is done to avoid degrading or diluting the matrix material with the dispersing agent, but it has been widely reported that the first approach is more effective in creating a thoroughly dispersed composite material [61]. An additional consideration is that these dispersing agents are hazardous to human health, and their use involves complex and time consuming procedures (*e.g.*, removal of the dispersing agent), which may not be amenable to mass production. A less hazardous alternative is mechanical dispersion using sonication, stirring, and/or shear mixing. Sonication is the excitation of a solution by a vibrating surface or probe, typically at ultrasound frequencies [62]. While mechanical methods can

effectively disperse a CNT solution, prolonged exposure to sonication can damage the CNTs [63]. By combining sonication with the use of a dispersing agent, the required sonication time can be reduced, producing a synergistic result [64].

Many researchers have attempted to identify the most ideal dispersing agent [3], [4], [62], [65], [66]. Most of these approaches use either surfactants or polymers. Adding a surfactant or a polymer to CNTs chemically alters the surface of the CNT, and is a form of *functionalization* (*i.e.*, the creation of functional groups on a surface). Functionalization of CNT surfaces can affect the dispersive properties of the CNT or can affect the adhesion at the interface between the CNTs and the polymer matrix material. CNT functionalization typically takes advantage of defects on the CNT walls and endcaps [56] and is termed *chemical* if the bonds are covalent and *physical* if the bonds are noncovalent [57]. Physical functionalization preserves the mechanical properties of the CNT [63]. Both chemical functionalization and physical functionalization of CNTs have been shown to improve the adhesion at the interface [56].

Gong *et al.* [58] were the first to demonstrate the importance of a nonionic surfactant to assist with dispersion in an epoxy-matrix nanocomposite material with aligned CNTs. This type of dispersant molecule wraps around the CNT and causes a strong noncovalent bond with the matrix. Using this surfactant, they were able to increase the Young's modulus of the epoxy by 30%, with the addition of a weight fraction of approximately 1 wt. % CNTs. In contrast, the addition of the CNTs alone (with sonication but no chemical dispersion) resulted in an increased stiffness of just 6% relative to that of the epoxy matrix.

More recently, Matarredona *et al.* [64], Islam *et al.* [67], and others have found that the addition of the surfactant, sodium dodecylbenzene sulfonate (NaDDBS), to the matrix

solution causes an exfoliation (separation of a layer of CNT from a bundle) and dispersion of the CNTs [64], [67]. In their method, the chemical dispersion is followed by a short period of sonication, which could also be a cause of the observed exfoliation of the CNTs. This exfoliation is followed by the adsorption of the surfactant molecules on the CNT surfaces. Dispersion has been found to only be temporary [2], [4], [68], but steric repulsion of the adsorbed NaDDBS molecules helps to mechanically stabilize the suspension of CNTs.

Once the polymer solution has hardened, the degree to which the CNTs are dispersed in the polymer matrix material is quantified using a host of different methods, including the ones described by Haslam and Raeymaekers [69]. In addition to being well dispersed, a strong interfacial bond is necessary to maximize the mechanical properties of the polymer nanocomposite material with aligned CNTs.

2.3.2 Adhesion between carbon nanotubes and the polymer matrix

The adhesion at the interface between the polymer matrix and the CNTs can critically limit the mechanical properties of the composite material, because it determines the degree of stress transfer between the matrix material and the CNT reinforcement phase.

CNT reinforced nanocomposite materials can fracture in four ways, CNT pull-out (Figure 2.9a), CNT fracture (Figure 2.9b), CNT/matrix debonding (Figure 2.9c), and matrix cracking (Figure 2.9d). The type of failure that occurs is dependent on the strength of the polymer matrix relative to that of the CNT, the CNT-polymer interface area, and the adhesion between the CNT and polymer [25].

The CNT/polymer interfacial shear strength is the maximum shear stress that occurs before the interface reaches failure. This interfacial shear strength determines the

maximum shear stress that is transferred from the polymer matrix material to the CNT. If the strength of the interface between the polymer matrix material and the CNTs is not the limiting factor in the nanocomposite material strength, the interface will not fail during mechanical loading.

A nonlinear relationship exists between the strength of the nanocomposite material and the interfacial strength between the matrix material and the reinforcement phase. The type of bonding (covalent, noncovalent) [66], and the fraction of the CNT surface that is bonded to the polymer matrix material (a result of dispersion) [70] are the most important factors to consider when creating a structural polymer composite material. The CNT/matrix strength for a noncovalent bonded composite material is around 50 MPa. The strength varies for a covalently bonded composite material, but is typically a few hundred MPa [71]. The Liao *et al.* molecular dynamic simulations of fiber pull-out predict an interfacial shear strength range of 100-160 MPa [72]. The strength can be further enhanced by functionalization of the CNTs during the dispersion process [56].

The manufacturing method of the CNTs, contaminants, and defects affect the CNTs mechanical properties and can also therefore affect the strength of the nanocomposite material. In addition to dispersion and a strong adhesion at the interface, alignment of the CNTs is necessary to incorporate the effect of the CNTs' high uniaxial modulus as a reinforcement fiber. Techniques for alignment of CNTs are discussed in the following section.

2.3.3 Alignment of carbon nanotubes

CNTs have strongly anisotropic mechanical properties, *e.g.,* the longitudinal modulus is 1-2 TPa, whereas the transverse modulus is approximately 15 GPa [49], [73]. CNTs, like carbon fiber, are most effective as reinforcement if the fibers are aligned in the direction of maximum tensile stress. Thostenson and Chou compared a polymer nanocomposite material with randomly oriented SWCNTs to one with aligned SWCNTs and found that the former only displayed a 10% increase in the Young's modulus, whereas the latter showed a 49% increase when compared to the bulk polymer [74].

There are two main approaches to introduce aligned CNTs as reinforcement for polymer nanocomposite materials. In the first approach, *bulk alignment,* CNTs are directly added into the liquid polymer matrix material, as described previously in the discussion of dispersion and adhesion, so that dispersed CNTs form the reinforcement phase. The CNTs are dispersed and aligned in the liquid polymer matrix material, which is then hardened by cross-linking the liquid polymer. The second approach, *fiber alignment*, creates long fibers consisting of pure CNTs or of polymer composite fiber reinforced with CNTs that are aligned during the manufacturing process.

Polymer composite fibers reinforced with CNTs could be used as a substitute for traditional carbon fibers. Research has been devoted to making long fibers with CNTs aligned in the longitudinal direction of the fiber, to best exploit the uniaxial mechanical properties of the CNTs. Fiber spinning and mechanical stretching are the most common methods to align CNTs into a fiber that is used as reinforcement for nanocomposite materials. Fiber spinning includes methods such as melt spinning, electrospinning, and coagulation spinning. Melt spinning uses the shear force and drawing force in a mechanical

stretching process to align the CNTs in the polymer composite fiber [75]–[77]. Electrospinning uses electrostatic drawing forces on small jets of polymer solution; this causes the CNTs to rotate around their center of gravity and align along the drawing direction in order to reduce the torque being applied to them [78], [79]. Andrews *et al.* obtained polymer composite fibers reinforced with CNTs by spinning dispersed SWCNTs in isotropic petroleum pitch [80]. The fibers obtained with this process display a Young's modulus of approximately 15 GPa, much lower than that of pitch-carbon fibers (400-960 GPa) [80]. Dalton *et al.* created polymer composite fibers with an ultra-high weight fraction of CNTs (they reported approximately 60 wt. %) [81]. These fibers showed a Young's modulus of 80 GPa and a tensile strength of 1,800 MPa [81], and have a higher energy-to-fracture (570 J/g) than Kevlar fibers (33 J/g) and graphite fibers (12 J/g), which makes them a good candidate for impact applications [81]. The Dalton *et al.* fibers also exhibit a high strain-to-failure (30%), enabling weaving and sewing [81].

Fiber stretching can further enhance the strength and stiffness of a polymer composite fiber with CNTs, which was demonstrated in conjunction with coagulation spinning, developed by Vigolo *et al.* [82]. Their work produced flexible fibers with a Young's modulus of 15 GPa that could be tied into knots [4], and the strength and stiffness of the fibers were improved by stretching the fiber when wet [82]. The stretching process produced fibers with a Young's modulus and ultimate tensile strength of approximately 40 GPa and 230 MPa, respectively [82].

Bulk alignment of CNTs in a polymer matrix material is less common than fiber alignment methods. Bulk alignment methods allow the CNTs to align during the fabrication process of the polymer nanocomposite material. Tailoring the degree of CNT alignment is

of fundamental concern during the synthesis of the nanocomposite material. Bulk alignment methods can be categorized as either *substrate* or *substrate-free*.

Dai and Mau were the first to create a controlled method to vertically align CNT arrays on a substrate [83]. This thesis defines *vertical* to be perpendicular to the substrate plane, and *horizontal* to denote a preferred alignment in any direction parallel to the substrate plane. Horizontal alignment is easier to achieve than vertical alignment, since the CNTs are susceptible to collapse when incorporated into a polymer matrix [84], [85]. Despite this, vertical alignments are being widely performed by adding a liquid polymer matrix material to a pre-aligned CNT-array. The liquid polymer fills in the gaps between the CNTs, but can disrupt the vertical alignment as it flows through the array [84].

Shear pressing is a horizontal alignment method that is applied to arrays of CNTs that are grown in vertical alignment on a substrate. The CNTs are compressed using a shear pressing plate under horizontal motion, into an aligned CNT array. The deformed array is infiltrated with a liquid polymer. Once hardened, the film material is removed, forming a paper-like layer that can be used in a nanocomposite material [84].

Several researchers have studied different methods to maintain the mechanical properties of vertical alignment of substrate-grown CNT arrays during the polymer infiltration process. One approach is to enhance the vertical stability of the CNT themselves through process control of the diameter, length, and number of walls. Even with such process control, for this approach to be successful, the CNT surface must be fully wetted by the polymer. As such, the polymer matrix material must be of low viscosity to enable the infiltration within a reasonable timescale, to limit degradation of the polymer [85]. Hinds *et al.* manufactured a membrane structure by incorporating an array of aligned

MWCNTs across a polymer film [86]. They used polysulfone to fill in the gaps between the vertically aligned CNTs through a spin-coating technique [86]. This approach allows for the CNTs to maintain their vertical alignment in the polymer matrix after processing and it allows the weight fraction of CNTs to be varied for different applications. This process for incorporating a liquid polymer matrix material into a CNT array has been adopted by other research groups. Pei *et al.* fabricated a CNT polyimide membrane by combining this spin-casting infiltration approach with a shear-pressed CNT array under a silicon substrate [87]. Jung *et al.* used polydimethylsiloxane to infiltrate the gaps between CNTs in the vertically aligned array [88]. By removing an adjusted amount of the polydimethylsiloxane matrix prior to the curing process, the thickness of the nanocomposite material is controlled [88]. The resulting nanocomposite material displayed extreme flexibility and unique conductive properties.

Lim *et al.* used acoustic waves to align CNTs in a polymer matrix solution. In their process, the CNTs must be attached to a substrate, so that the pressure created from the acoustic jetting bends the CNT in a preferred alignment direction [89] (Figure 2.11). While their result demonstrates the effectiveness of acoustic CNT alignment, the need for a substrate limits the applicability of their process to producing only thin films.

These vertical alignment methods, while good for manufacturing thin films and membranes, are not suitable for synthesizing nanocomposite materials for structural applications. Substrate-free methods provide an alternative, in which the alignment direction of the CNTs depends on the orientation of an external field. The external field can be electric, magnetic, or acoustic.

In the case of an external electrostatic field, the dipole moments induced in the CNTs

cause them to rotate into alignment with the direction of the electrostatic field. Depending on the nature of the electrostatic field, the CNT may then move towards the nearest electrode due to the Coulomb force that acts on each CNT [3], [46].

Ma *et al.* demonstrated MWCNT alignment in a polymethyl methacrylate matrix material driven by an electrostatic field [56]. Xie *et al.* showed that using an electrostatic field increased both dispersion and alignment of the CNTs in polymer matrix materials, thus increasing strength, stiffness, and electrical conductivity of the resulting nanocomposite material [3].

Magnetic field alignment of CNTs was first demonstrated by Kimura *et al.* [90]. Using dispersed MWCNTs in a polyester material, a constant magnetic field of 10 T was applied to align the MWCNTs. The anisotropic properties of the resulting nanocomposite material demonstrated that a unidirectional alignment of the MWCNTs had been produced. This process has been used and modified by several research groups to align CNTs [91]–[95]. Smith *et al.* [95] used a 25 T magnetic field to produce a polymer nanocomposite film with a thickness of approximately 7 micrometer reinforced with 2 wt. % aligned CNTs [95]. However, this method is limited as it does not allow higher weight fractions of CNTs to be aligned, and it also requires specialized equipment to produce the required magnetic field strength.

Novel methods to align CNTs include using lyotropic liquid crystals [96], ultrasound manipulation [89], [97], cutting/slicing [98], and shear pressing [84]. Lyotropic liquid crystals (LLC) assist with alignment of CNTs in the presence of an electric or magnetic field. The unique molecular structure of the LLC allows the CNTs to remain aligned even after the force field has been removed [3]. Haslam and Raeymaekers used ultrasound waves

to align CNTs in a liquid urethane resin and obtained a 6% increase in the ultimate tensile strength of the composite material with a MWCNT weight fraction of 0.15 wt. % [97]. The research presented in this thesis builds on these results using the same method for alignment, but at much higher nominal weight fractions. Compared to magnetic or electric field alignment methods, this method does not require expensive specialized equipment, and can produce nanocomposite materials at higher weight percentages (> 10 wt. %).

Cutting or slicing a cured CNT polymer nanocomposite will produce alignment of the CNT at the cutting surface, due to shear forces acting on the CNTs [98]. The applications of this method are limited, since the alignment occurs only at the cutting surface, and because the integrity of the matrix, and the interface between the polymer matrix material and the CNT, may be compromised by the cutting process. However, this method is remarkable in its ability to achieve alignment with very high (> 10 wt. %) weight fractions of CNTs [98]. Wood *et al.* used flow orientation and shear forces to align SWCNTs in an liquid polymer matrix material [99]. In this method, SWCNTs are dispersed in an ultraviolet (UV) curable polymer matrix material. This mixture is spread onto a glass slide and is screed twice with a thin blade to induce shear flow in the polymer that orients the SWCNTs. The resulting thin film must be cured immediately by exposure to UV radiation, to avoid relaxation of the SWCNT alignment [99]. The disadvantage of this flow-orientation technique is that it can only be used in UV curable polymer matrix materials and in geometries where the shear flow can be controlled.

While numerous methods have been developed to manufacture polymer nanocomposite materials with aligned CNTs, none of the available methods allow for high weight fractions of CNTs throughout a bulk material.

2.4 Problem statement and objective

Polymer nanocomposite materials reinforced with aligned CNTs have not yet achieved the theoretical mechanical properties that are expected from the specific strength and specific stiffness of CNTs. Achieving the theoretical mechanical properties requires dispersion, alignment, adhesion between the CNTs and the polymer matrix material, and a high weight fraction of the CNTs in the polymer matrix material. Dispersion using a surfactant combats alignment, because surfactant causes the CNTs to repel each other. High weight fractions of CNTs inhibit dispersion, because the bundling of the CNTs makes surfactant adsorption difficult. Additionally, increasing the CNT weight fraction increases the viscosity of the CNT/polymer mixture, which also promotes entanglement and clustering of the CNTs and inhibits dispersion and alignment of CNTs.

It is therefore necessary to develop a process that balances dispersion, alignment, and weight fraction to maximize the mechanical strength and stiffness of the polymer nanocomposite material with aligned CNTs. For widespread application and scalability, this must be a bulk, substrate-free process to avoid the limitations of thin-film or substrate methods. Hence, the objective of this thesis was to experimentally demonstrate a manufacturing process for fabricating polymer nanocomposite materials reinforced with a weight fraction in excess of 10 wt. % aligned CNTs. Using established methods, dispersion of the CNTs in the polymer matrix solution was controlled with a combination of chemical surfactant and tip sonication following the work of Matarredona *et al*. [64] and Islam *et al*. [67].

The mechanical properties of polymer nanocomposite materials reinforced with CNTs have been shown to improve when the nanocomposite material is exposed to microwave radiation [6], [100]. It is hypothesized that this is a result of localized melting at the

interface between the polymer matrix material and the CNTs, which either heals defects or welds the interface. Previous investigations of this process were limited to nanocomposite materials with small weight fractions of CNTs (< 1 wt. %), for which the CNT reinforcement produces only a modest enhancement to mechanical properties [100]. Thus, a secondary objective of this thesis was to characterize the effect of exposure to microwave radiation on high weight fraction MWCNT polymer nanocomposite materials.

The dogbone polymer nanocomposite material specimens were reinforced with aligned MWCNTs and the ultimate tensile strength, Young's modulus, and moduli of resilience and toughness of these specimens were quantified as a function of the MWCNT weight fraction, and were then compared to the mechanical properties of specimens without MWCNTs and specimens with randomly oriented MWCNTs.

The following chapter details the methods, procedures, and materials that were the focus of this research.

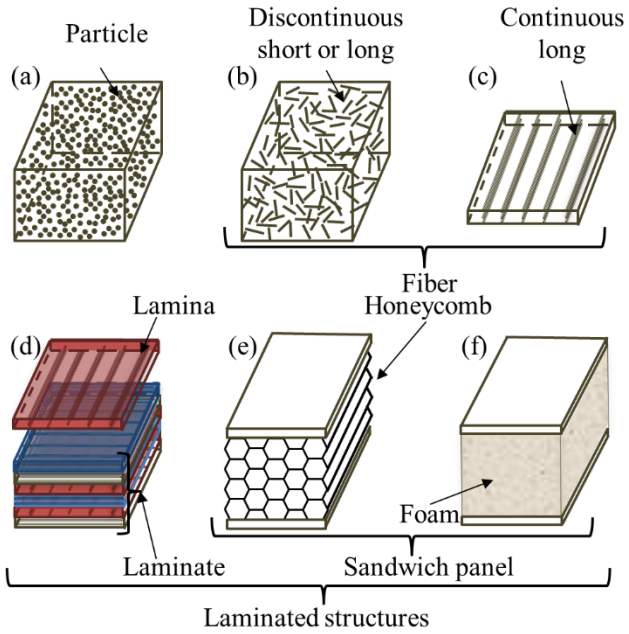

Figure 2.1 Illustration of composite material classes: (a) particle-reinforced, (b,c) fiber-reinforced, (d-f) laminated structures (adapted from Askeland [18] and Gibson [26]).

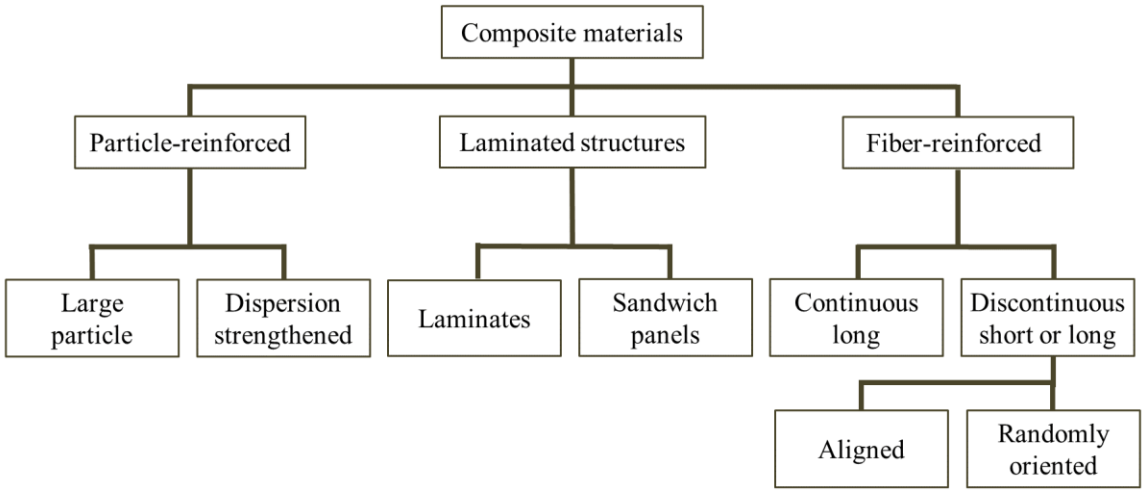

Figure 2.2 Taxonomy of common composite materials (adapted from Mitchell [17]).

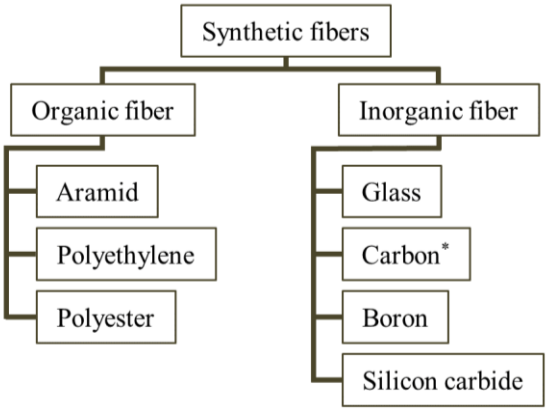

Figure 2.3 Common types of synthetic fibers used as reinforcement for composite materials (adapted from Kelly [37] and Rosato and Rosato [101]).

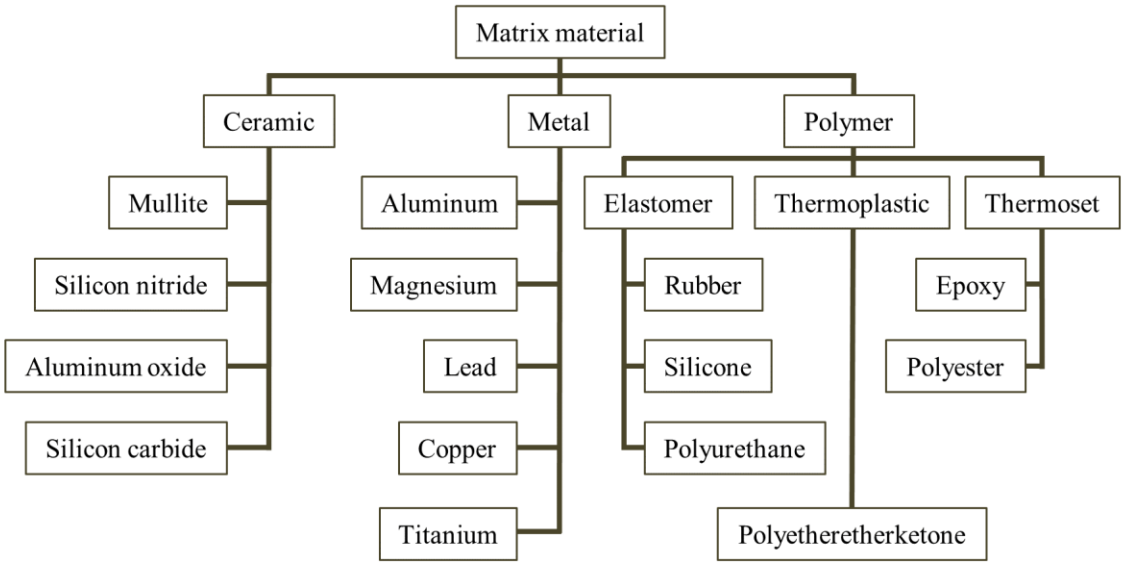

Figure 2.4 Categories of matrix materials for synthetic composite materials (adapted from Rosato and Rosato [101]).

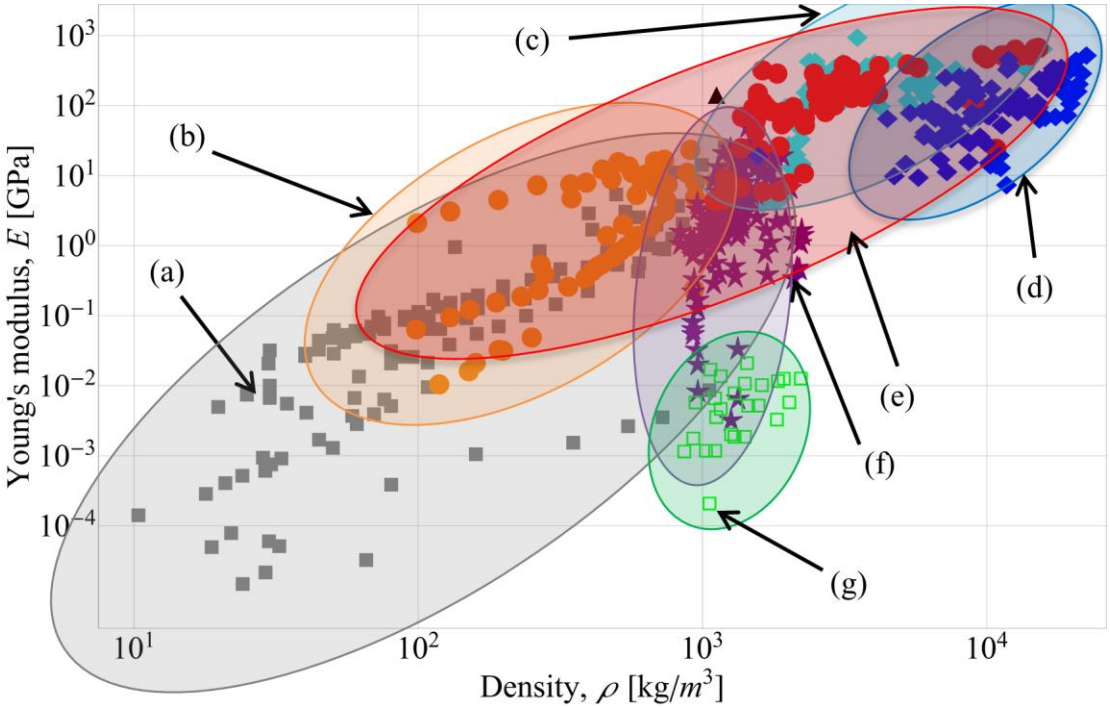

Figure 2.5 Comparison of the stiffness-density properties of engineering materials: (a) foam materials, (b) natural materials, (c) ceramic materials, (d) metals and alloys, (e) composite materials, (f) plastic materials, (g) elastomer materials (adapted from Cambridge Engineering Selector [45]).

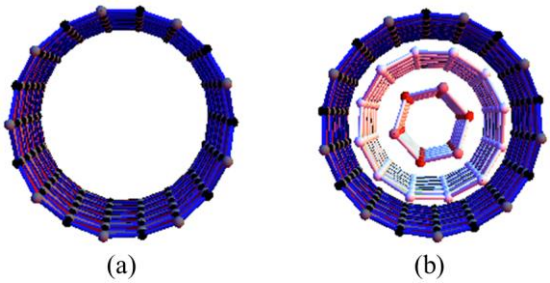

Figure 2.6 Schematic showing the different types of CNTs: (a) SWCNT, (b) MWCNT.

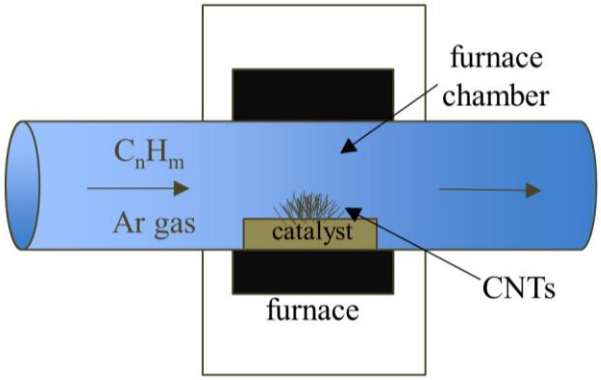

Figure 2.7 Schematic of CNT synthesis using CVD: argon gas and hydrocarbons enter the furnace chamber and react on a catalyst specimen creating CNTs (adapted from Poplov, 2004 [49]).

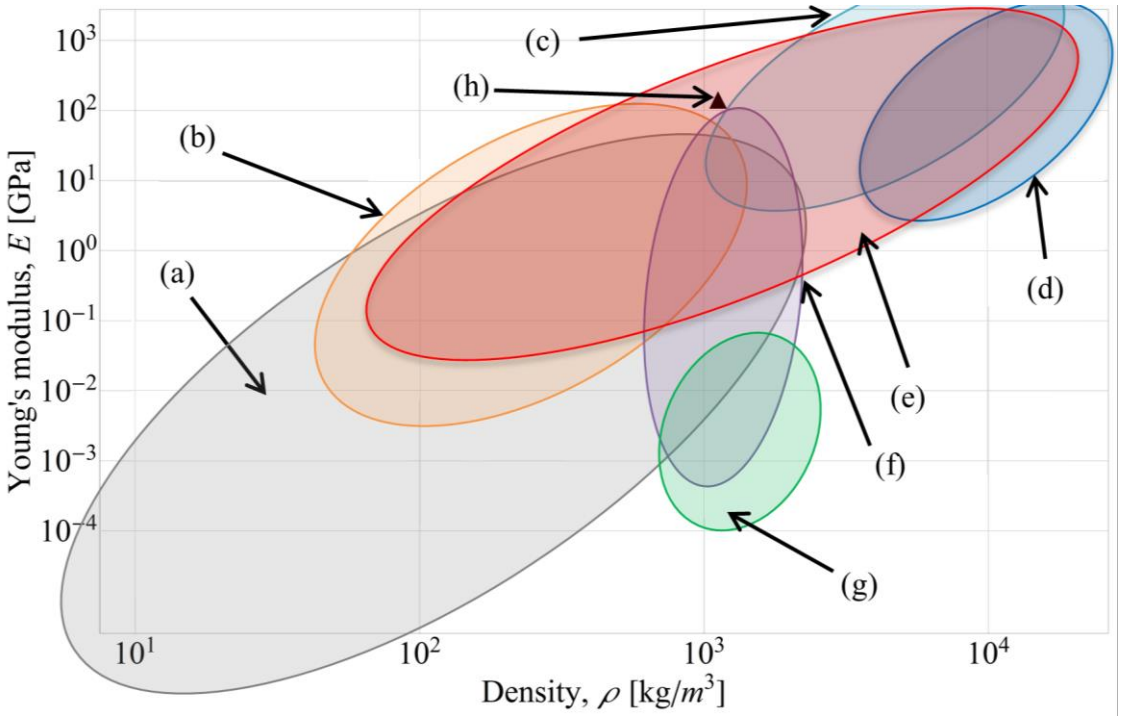

Figure 2.8 Comparison of the stiffness-density properties of engineering materials: (a) foam materials, (b) natural materials, (c) ceramic materials, (d) metals and alloys, (e) composite materials, (f) plastic materials, (g) elastomer materials (adapted from Cambridge Engineering Selector [45]), and (h) theoretical polymer nanocomposite material with 10 wt. % aligned CNT volume fraction.

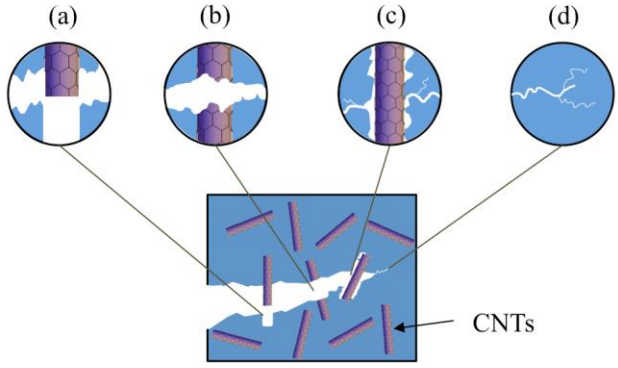

Figure 2.9 Possible failure mechanisms for polymer nanocomposite materials with CNTs: (a) CNT pull out, (b) CNT fracture, (c) CNT/matrix debonding, and (d) matrix cracking (adapted from Vajtai, 2013 [25]).

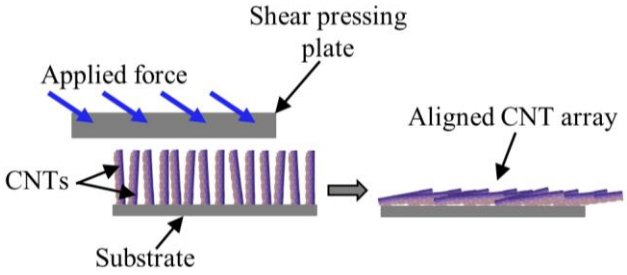

Figure 2.10 Horizontal alignment of a substrate-grown CNT array through the use of a shear pressing plate (adapted from Bradford *et al.*, 2010 [84]).

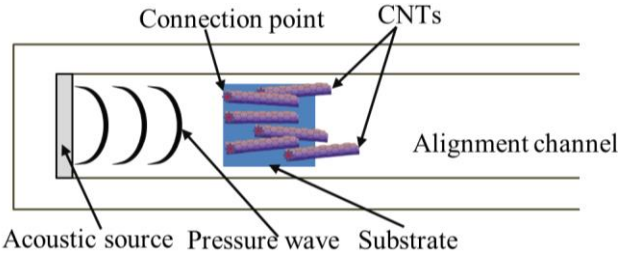

Figure 2.11 Schematic (top-view) of the method of Lim *et al.* for alignment of substrate-connected CNTs in a liquid polymer matrix material, driven by pressure waves in a channel (adapted from Lim *et al.*, 2007 [89]).

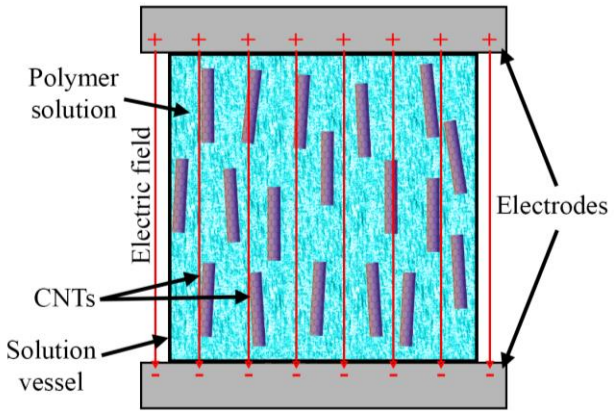

Figure 2.12 Alignment of CNTs in an electrostatic field. The direction of the alignment corresponds to the direction of the applied field (adapted from Xie *et al.*, 2005 [3]).

Table 2.1: Mechanical properties of engineering materials [102]–[105].

	Young's modulus [GPa]	Mass density [kg/m^3]	Tensile strength [MPa]	Strain at failure [%]	Specific strength [kN·m/kg]
CNTs	1,000-2,000	1,300-2,000	10,000-60,000	10-16	7,690-46,200
Stainless steel	200	7,500-8,00	400-1,600	<10	50-213
Polyarylonitrile-carbon fiber	200-600	1,700-2,00	1,700-5,000	0.3-2.4	850-2,940
Pitch-carbon fiber	400-1,000	2,000-2,200	2,200-3,300	0.3-0.6	1,000-1,650
S-glass	100	2,500	2,400	4.8	960
E-glass	100	2,500	4,500	4.8	1,800
Aramid fiber	100-200	1,400	3,600-4,100	2.-2.8	2,570-2,930

CHAPTER 3

MATERIALS AND METHODS

To obtain polymer nanocomposite materials with ultra-high strength and stiffness, dogbone specimens were made with aligned high weight fractions of MWCNTs within a liquid urethane resin, which was subsequently cured to form a polymer matrix containing MWCNTs aligned parallel to the direction of the anticipated external mechanical loading. To align a MWCNT weight fraction in excess of 10 wt. %, a small weight fraction (≤ 1 wt. %) of MWCNTs was dispersed in a reservoir of liquid urethane resin, and then ultrasound alignment was employed to concentrate and align the MWCNTs along a single line in the urethane resin, obtaining a locally high wt. % of MWCNTs.

3.1 Experimental apparatus for the fabrication of polymer nanocomposite specimens

Figure 3.1 shows a schematic of the experimental set-up used to fabricate macroscale dogbone specimens of polymer nanocomposite materials with aligned MWCNTs. Two polypropylene dogbone reservoir/mold were machined using a three-axis CNC mill (HAAS) from a geometry defined using CAD software (Solidworks), converted to NC code for the CNC mill using conversion software (FeatureCam). The reservoirs contained a liquid urethane resin with dispersed MWCNTs. Two parallel piezoelectric ultrasound transducers (PZT-4, 190 kHz center frequency and 1,500 kHz center frequency) are

positioned in recessed slots in the gage section to create a standing ultrasound wave that aligns the MWCNTs in the dogbone reservoir (see Section 3.3.3). The bottom of the reservoir consists of a glass plate coated with an anti-adhesion layer to facilitate evacuation of the specimen after the liquid urethane resin polymerizes.

The dimensions of the reservoirs and the resulting dogbone test specimens were based on the ASTM D638 standard for Type V plastic specimens [106]. The gage section of the first dogbone reservoir/mold had length L = 16 mm and width W = 3.65 mm, which was designed based on a center frequency (190 kHz) of the ultrasound transducers and the acoustic wave propagation velocity in the uncured urethane resin/MWCNT mixture (Section 3.3.3).

A second dogbone reservoir/mold was made with L = 20.1 mm and W = 7.5 mm, corresponding to a center frequency (1,500 kHz) of the ultrasound. This mold was used to make specimens for a baseline comparison following the work of Haslam and Raeymaekers [97].

The ultrasound transducers were connected to the output of a radio frequency (RF) power amplifier (E&I 440LA), which was driven by an arbitrary/function generator (Tektronix AFG3102). The function generator created a sinusoidal wave that causes the ultrasound transducers to act as a “piston source”, and establish a standing pressure wave in the gage section of the dogbone-shaped reservoir. The amplitude of the pressure wave was controlled through the amplitude of the sine wave produced by the function generator, and by the gain of the RF amplifier.

3.2 Materials

3.2.1 Polymer matrix material

A two-part thermoset resin (Smooth-Cast 300, Smooth-On, Inc.) was used, where Part A is methylene diphenyl diisocyanate (MDI) and Part B is a polymeric resin proprietary to the supplier. This liquid urethane resin uses a one-to-one mix ratio by volume; it has a density of 1,050 kg/m^3, a pot life of 3 minutes, and a demold time of 10 minutes [107]. Table 3.1 shows pertinent properties for this polymer matrix material.

The acoustic radiation force that drives the alignment of MWCNTs in the liquid urethane resin is described in Section 3.3.3, where alignment at a given frequency requires a constant acoustic wave propagation velocity. As the urethane resin starts to cure, the acoustic wave propagation velocity increases, which may diminish the effectiveness of ultrasound alignment. However, the viscosity of the urethane resin also increases during curing, slowing the movement of the MWCNTs from their aligned position. Thus, a fast curing time is essential to fixate the aligned MWCNTs in place, before they can migrate from their aligned position. The resin mixture has a low viscosity (80 cP at 25 °C) in its liquid state, and also has a fast cure (approximately 1-2 minutes), making it well suited for the ultrasound alignment process [67].

3.2.2 Carbon nanotubes

The MWCNTs used for reinforcement were fabricated using chemical vapor deposition (95 % pure) [108]. This material is commercially available in large (>1 kg) quantities and is therefore suitable for mass production of a polymer nanocomposite material with aligned MWCNTs. Table 3.2 shows the dimensions and density of the MWCNTs. Here, the “bulk density” is the tapped density of the poured material in air, and the “true density” is based

on the estimated outer dimensions of the individual MWCNTs, independent of the packing density.

The average length-to-diameter ratio of the MWCNTs is 230.8, which is at the upper end of the range of aspect ratios commonly defined as a “short-fiber” filler in a polymer matrix material [24]. The MWCNTs were weighed using a digital microgram scale (Mettler Toledo), before they were dispersed in the liquid urethane resin.

3.2.3 Surfactant

An anionic surfactant sodium dodecylbenzene sulfonate (NaDDBS) (Tokyo Chemical Industry Co., LTD) was used based on methods described by Islam *et al*. [109] and Matarredona *et al*. [64]. The NaDDBS molecule is a long hydrophobic chain with a benzylsulphonate group [110], which forms a monolayer of hemimicelles on the MWCNT surface, as illustrated in Figure 3.2.

The π-π interactions between the benzene rings of the NaDDBS molecules cause the surfactant hemimicelles to repel each other, dispersing the MWCNTs to which they are bonded [111]. Thus, addition of NaDDBS mitigated the formation of MWCNT aggregate bundles that would have otherwise degraded mechanical properties of the resulting polymer nanocomposite material.

An experimental analysis was performed to determine the optimum amount of NaDDBS surfactant that should be added as a function of MWCNT weight percent. MWCNTs were dispersed in the liquid urethane resin using a combination of chemical and physical dispersion. To remove moisture that would otherwise produce defects in the urethane resin, the MWCNTs were dried on a hotplate at approximately 65 °C for 1 minute and were immediately added to Part A of the liquid urethane resin. Then, the NaDDBS

surfactant was added to the mixture to reduce the van der Waals attraction between adjacent MWCNTs [67], [112]. After adding the surfactant, 10 minutes of tip sonication at 20 kHz and 300 W was applied following the work of Matarredona *et al.* [64] who found that this power level was sufficiently low to avoid damage to the MWCNTs. The tip sonicator was operated in a pulsed mode to avoid thermal degradation of the urethane resin that was observed for continuous-mode tip sonication. Figure 3.3 shows that the addition of surfactant and subsequent tip sonication removed visible aggregate bundles in the mixture. After tip sonication, Part B of the liquid urethane resin was added to initiate polymerization, and the mixture was cast in the dogbone reservoir/mold.

The optimum surfactant-to-MWCNT ratio was found experimentally by uniaxial tensile testing sixty-three nanocomposite material specimens with 0.1, 0.2, and 0.3 wt. % of randomly oriented MWCNT, and varying the surfactant-to-MWCNT ratio from 0.1 to 1.0. Figure 3.4 shows the ultimate tensile strength σ_{UT} normalized with the ultimate tensile strength of the polymer matrix material $\sigma_{UT,poly}$ as a function of the surfactant-to-MWCNT ratio.

The effect of the surfactant-to-MWCNT ratio was found to be similar for all MWCNT weight fractions in this range, and an optimal ratio was selected by finding the maximum of a quadratic curve fit to each data set, resulting in a value of approximately 0.6. In this work, the ratio of 0.6 was used for all subsequent fabrication of polymer nanocomposite material specimens with aligned and randomly oriented MWCNTs.

3.2.4 Ultrasound transducers

The ultrasound transducers were lead zirconate titanate (PZT-4, STEMiNC) piezoelectric ceramic plates with center frequencies of 190 kHz for the novel specimens and 1,500 kHz for the specimens manufactured as a baseline comparison. The ultrasound transducers were operated near their center frequencies to maximize their amplitude when operating as a piston source to establish a standing pressure wave in the liquid urethane resin contained in the dogbone reservoir/mold. The operating frequency, the spacing between the opposing ultrasound transducers, and the acoustic wave propagation velocity in the liquid urethane resin are related to each other (Section 3.3.3), and to establish a standing pressure wave in the gage section of the dogbone reservoir/mold the spacing between the two opposing ultrasound transducers must be equal to an integer N multiple of the half wavelength.

3.3 Methods

3.3.1 Fabrication process for polymer nanocomposite material specimens

A process was developed to fabricate macroscale dogbone specimens of polymer nanocomposite material with an ultra-high weight fraction of aligned MWCNTs. Figure 3.5 schematically illustrates the process steps: mixing of MWCNTs in Part A of a two-part thermoset liquid urethane resin (Figure 3.5a), dispersing and tip sonicating of the MWCNTs and NaDDBS surfactant in Part A of the liquid urethane resin (Figure 3.5b), adding of Part B of the liquid urethane resin to initiate polymerization (Figure 3.5c), casting of the mixture in a dogbone reservoir/mold (Figure 3.5d), energizing the opposing ultrasound transducers (Figure 3.5e) to establish a standing ultrasound wave that concentrates and aligns the MWCNTs along a central plane in the gage section of the

dogbone reservoir as the resin cures, evacuating the dogbone specimen from the reservoir (Figure 3.5f), and trimming of the polymer matrix from the dogbone gage section to retain only the region that contains an ultra-high weight fraction of aligned MWCNTs (Figure 3.5g).

3.3.2 Different types of polymer nanocomposite material specimens

Figure 3.6 shows the polymer nanocomposite material specimen types fabricated for this work. The ultra-high weigh fraction specimens (Figure 3.6a) were fabricated starting from a MWCNT weight fraction of approximately 1 wt. % dispersed in the liquid urethane resin. After aligning and concentrating the MWCNTs along a single plane (which manifests as a single line on the exposed surface), a local MWCNT weight fraction in excess of 10 wt. % was obtained by trimming the excess polymer surrounding the concentrated region, then sanding the part with 900 grit followed by 1200 grit sand paper. This fabrication process is different from existing work where MWCNTs are aligned along multiple lines in the gage section of the dogbone specimen and the entire gage section is left intact [97].

To interpret the mechanical performance (see Section 3.3.7) of these ultra-high MWCNT weight percent polymer nanocomposite material specimens, they were statistically compared to the performance of polymer nanocomposite materials with multiple lines of MWCNTs (Figure 3.6b) and also to specimens containing randomly oriented MWCNTs (Figure 3.6c) using a weight fraction of 0.1-10.0 wt. % (described in Section 4.2). The specimens with multiple lines were fabricated following the methods of Haslam and Raeymaekers [97] and have MWCNTs aligned along 16 planes with an alignment frequency of 1465.11 kHz. Finally, as a baseline reference, specimens of processed polymer without MWCNTs (see Section 4.1) were fabricated. In the sections

that follow, the specimen types in Figure 3.6a-d are referred to as “single-line”, “multi-line”, “randomly oriented”, and “processed polymer” specimens, respectively.

All dogbone specimens that contain MWCNTs (Figure 3.6a-c) were fabricated using a constant surfactant-to-MWCNT weight ratio of 0.6 (see Section 3.2.3); for the “processed polymer” specimens, an amount of surfactant was added equal to that of the “single-line” specimens. All dogbone specimens (Figure 3.6a-d) were exposed to the same amount of ultrasound energy, but for the “randomly oriented” specimens, the frequency was not tuned to yield alignment and was intended only to produce any ancillary effects of ultrasound exposure such as displacing bubbles or breaking up aggregate bundles of MWCNTs in the mixture. Additionally, a set of specimens were fabricated and exposed to microwave radiation (see Section 3.3.6) after evacuation from the mold to investigate the effect of this exposure on their mechanical properties. Photographs of the fabricated parts are shown in Figure 3.7.

3.3.3 Ultrasound alignment of MWCNTs in the liquid urethane resin

The ultrasound transducers were energized to create a standing ultrasound wave in the liquid urethane resin in the gage section of the dogbone reservoir. The acoustic radiation force associated with this standing ultrasound wave enables manipulating single particles [113], assembling patterns of multiple particles [114], [115], and aligning particles [97] dispersed in a fluid medium. The acoustic radiation force theory was first described for spherical particles in an inviscid medium [116], [117]. The acoustic radiation force acting on a spherical particle with radius R in an inviscid fluid medium and subject to a plane ultrasound standing wave with wavelength $\lambda \gg R$ and acoustic pressure $p = p_0 \sin(k_0 x)$ is given as [117]

$$F = \frac{\pi R^3}{3} p_0^2 k_0 \beta_m \Phi \sin\left(2k_0 x\right), \tag{3.1}$$

where p_0 is the pressure amplitude of the standing ultrasound wave, x is the distance from the ultrasound source, and k_0 is the wave number ($k_0 = 2\pi / \lambda = 2\pi f / c_m$ where f is the operating frequency of the ultrasound transducer and λ is the corresponding wavelength). The acoustic contrast factor is

$$\Phi = \frac{5\rho_p - 2\rho_m}{2\rho_p + \rho_m} - \frac{\beta_p}{\beta_m}, \tag{3.2}$$

where the subscripts m and p refer to the fluid medium and the particle, respectively, with density ρ, acoustic wave propagation velocity c, and compressibility $\beta = 1 / \rho c^2$. From Equation (3.1), it is observed that the sign of the acoustic contrast factor determines whether the acoustic radiation force drives the particle towards the nodes ($\Phi > 0$) or towards the antinodes ($\Phi < 0$) of the standing ultrasound wave [118].

Fenley *et al.* reported longitudinal and transverse acoustic wave propagation velocities for MWCNTs of 12 km/s and 7 km/s, respectively [119]. Hone *et al.* report c_p values for MWCNTs of 8, 10, and 20 km/s [120]. Lukes and Zhong estimate the acoustic wave propagation velocity of MWCNTs to be 11.26 km/s [121]. With ρ_p = 2,100 kg/m^3, ρ_m = 1,050 kg/m^3, E_p = 1 TPa, using the low estimate of c_p = 7 km/s, to evaluate Equation (3.2), Φ = 1.58. Using the high estimate of c_p = 20 km/s, to evaluate Equation (3.2), Φ = 1.60. Even though a wide range of values exist in the literature for the acoustic wave propagation velocities of MWCNTs, in all cases, $\Phi > 0$, indicating that the MWCNTs will align at the nodes of the standing ultrasound wave pattern.

Following Raeymaekers *et al.* [115], for a plane standing ultrasound wave [117], Figure 3.8 shows the acoustic pressure and the corresponding acoustic radiation force along the propagation direction of a standing ultrasound wave, where $x/\lambda = 0$ at the surface of the ultrasound transducer [115], [117], [122]. The magnitude of the pressure and acoustic radiation force are normalized with the amplitude of the respective waves. The horizontal arrows indicate the direction of movement of particles in the reservoir, driven by the acoustic radiation force. Particles accumulate where the acoustic radiation force is zero (*i.e.*, at the pressure nodes and pressure anti-nodes). However, the particles will only be in stable equilibrium where the gradient of the force is negative, which occurs only at the pressure nodes. Thus, particles will accumulate at the nodes of the standing pressure wave in the case of a positive acoustic contrast factor [123].

The acoustic radiation force theory has also been extended to include non-spherical particles (*e.g.*, MWCNTs) and to include viscous drag terms [124]. These extensions have shown that spherical and non-spherical particles align identically in viscous and inviscid media [125] and, thus, the acoustic radiation force theory for inviscid media is sufficient to describe the locations where MWCNTs align in a liquid urethane resin.

The standing pressure wave has two nodes per wavelength, so the width W of the gage section of the reservoir, measured between the surfaces of the opposing ultrasound transducers, must be an integer multiple N of half of the wavelength λ of the standing pressure wave, *i.e.*,

$$W = N\frac{\lambda}{2} = N\frac{c_m}{f_0}. \tag{3.3}$$

N is the number of nodes between the two ultrasound transducers, f_0 is the center frequency

of the ultrasound transducers, and c_m is the acoustic wave propagation velocity in the liquid urethane resin. For the "single-line" specimens, there was exactly one node and, thus, one line of aligned MWCNTs in the gage section of the reservoir ($N = 1$).

3.3.4 Determining the acoustic wave propagation velocity c_m in the liquid urethane resin

Figure 3.9 shows the experimental apparatus used to measure the acoustic wave propagation velocity c_m in the liquid urethane resin with a pulse-echo experiment.

In the pulse-echo experiment, the time Δt required for an ultrasound pulse to traverse a known distance W_{TR} was measured from a transmitting to a receiving ultrasound transducer. The unknown acoustic wave propagation velocity c_m of the medium was then determined as

$$c_m = \frac{W_{TR}}{\Delta t} . \tag{3.4}$$

The wave propagation velocity was found using this methodology with c_m =1.353 km/s for the liquid urethane resin.

Using cm and the width of the gage section W of the dogbone reservoir (Figure 3.1), the operating frequency of the ultrasound transducers required to establish an ultrasound standing wave was calculated with f = Ncm / W. The center frequency and the operating frequency of the ultrasound transducers may be slightly different due to imperfections during the fabrication of the dogbone reservoir, and minute misalignment of the ultrasound transducers. Starting from this calculated operating frequency, micro-adjustments of f were made until a single line of MWCNTs was formed. Because only two ultrasound transducers

were used in the experimental apparatuses, the MWCNTs were aligned within a plane. To get uniaxial alignment only in the direction of loading, two mutually perpendicular pairs of ultrasound transducers would need to be employed. This would complicate the manufacturing process. Figure 3.10 shows a dogbone "single-line" specimen, after curing and evacuation from the mold, which was fabricated using an operating frequency of 183.732 kHz, slightly less than the 190 kHz center frequency of the ultrasound transducers, for which the width of the gage section of the dogbone reservoir was designed. The cross-sectional image of the dogbone "single-line" specimen showed that the width of the line with ultra-high weight fraction of aligned MWCNTs was uniform through the thickness of the specimen.

3.3.5 Characterizing MWCNT weight fraction in the "single-line" specimen

The density of the material in the aligned region of the "single-line" specimens was used to estimate the weight fraction of MWCNTs in that region. After evacuating the cured "single-line" specimen from the dogbone reservoir (Figure 3.10), the material surrounding the concentrated region of aligned MWCNTs was removed. This was accomplished by uniformly sanding each side of the specimen with 900 grit sand paper to reduce the width of the gage section to a final "single-line" gage width, W_{SL} = 1.3 mm. The surface was finished by lightly sanding with 1200 grit sand paper to remove any remaining surface defects. This method does not guarantee that the surface is defect free, and the removal process could have affected the failure mechanism in the final specimens. Figure 3.11 shows a "single-line" specimen, which is typical of those used for mechanical testing.

The density of the polymer nanocomposite material specimen ρ_c was determined using

Archimedes' method, by measuring its weight in air and in water [126],

$$\rho_c = \frac{\rho_w m_c}{m_c - m_c^w}, \tag{3.5}$$

where ρ_w is the density of water, m_c is the measured weight of the polymer nanocomposite material in air, and m_w^c is the measured weight of the polymer nanocomposite material submerged in water [126]. The rule of mixtures (Equation (2.2)) was used with the density of the polymer matrix ρ_m = 1,050 kg/m^3 [107] and the bulk density of the MWCNTs ρ_f = 180 kg/m^3 [108] to determine the weight fraction of MWCNTs from the polymer nanocomposite material density. First, the volume fraction of the MWCNTs was computed as [26]

$$v_f = \frac{\rho_c - \rho_m}{\rho_f - \rho_m}, \tag{3.6}$$

which was converted into the weight fraction, as

$$w = v_f \rho_f / m_c. \tag{3.7}$$

For example, a "single-line" specimen was measured with m_c = 21.9 mg and m_w^c = 0.812 mg, for which Equation (3.5) yields ρ_c = 1,040 kg/m^3. Equation (3.6) and the material properties of the urethane resin and the MWCNTs (Table 3.1 and Table 3.2), respectively, were used to calculate v_f = 0.0132 and w = 10.9 wt. %.

To validate that a rule of mixture can be used to estimate the weight fraction of MWCNTs, seventy-one "randomly oriented" specimens were manufactured with w = 0.15-10.3 wt. %. These specimens had an exact known weight fraction at the time of

manufacture. The density of these known weight fraction specimens was computed from the weight of the specimens in air and the weight of the specimens in water using Equation (3.5). Figure 3.12 shows the measured density of "randomly oriented" specimens, and a plot of ρ versus w from the rule of mixtures Equations (3.6) and (3.7), using the bulk density of the MWCNTs (Table 3.2).

From Figure 3.12, the deviation between the individual density measurements and the rule of mixtures predictions ranges was calculated to be between -1.14% to 3.47%. The percent error is computed as follows,

$$Error = \frac{|\rho_m - \rho_t|}{|\rho_t|} \times 100\%, \tag{3.8}$$

where ρ_t is the theoretical density calculated with Equation (2.2) using the exact known weight fraction of the specimen, and ρ_m is the measured density of the corresponding specimen. These results were used to estimate the uncertainty in computing the weight fraction in the composite material from measured density. The general agreement between the data and the rule of mixtures suggests that the MWCNTs are acting in the composite material as though they have a density that is equal to their bulk density (180 kg/m^3) rather than their true density (2,100 kg/m^3), as would be expected for well dispersed individual particles. This counter intuitive result implies that either (1) the MWCNTs have air pockets within MWCNT agglomerate bundles that persist through the fabrication process, or (2) the NaDDBs surfactant hemimicelles are significantly affecting the density of the polymer nanocomposite material.

Figure 3.13 shows a schematic of the concentrated region of MWCNTs in the "single-line" specimens that was excised for density measurements after the samples had been

sanded. The excised regions for fifteen samples are weighed in both air and water to determine the density of the concentrated region.

Figure 3.14 shows the measured density of fifteen excised "single-line" specimens normalized by the density of the processed polymer with the weight fraction at each point computed using the rule of mixtures, Equation (2.2). In this analysis, the (currently unvalidated) assumption was made that the alignment process does not affect the dependence of ρ on w.

Figure 3.14 shows the variation in measured density and the associated computed weight fraction of MWCNTs for the concentrated excised region of fifteen "single-line" specimens. The computed MWCNT weight fraction was in the range of 9.88-12.69%, with a mean value of 11.35 wt. %. Assuming that the uncertainty in this measurement is equal to maximum deviation (3.47%) that was found from the results shown in Figure 3.12, the actual estimated weight fraction of the concentrated excised region of the "single-line" specimens was in the range of 9.53 wt. % to 13.13 wt.%.

For comparison, if the entire mass of MWCNTs added to the specimen were located in the volume of the concentrated region of the "single-line" specimen, the density of this concentrated region would be 258.3 kg/m^3, which equates to w = 91.8 wt. %. However, for aligned MWCNTs, Shaffer *et al*. report a theoretical maximum volumetric packing density of 0.55 [127]. The theoretical density of the composite material at this maximum packing density is 570 kg/m^3, which equates to w = 55.4 wt. %. Thus, the theoretical maximum weight fraction of MWCNTs in the concentrated region of the "single-line" specimen is limited by the packing density (as opposed to the availability of MWCNTs in the part), and the measured weight fraction was approximately 1/4th of theoretical limit. This weight

fraction of MWCNTs was higher than that of any bulk-alignment method for polymer nanocomposite materials that has been previously reported in the literature.

The width of the excised concentrated region of the "single-line" specimens used for the density measurements was smaller than the gage width of the "single-line" specimens used for uniaxial tensile testing, for which an area of unaligned material was retained so the specimens are robust enough to endure handling.

3.3.6 Microwave exposure

Sweeney *et al*. exposed polyactide-CNT 3D-printed composite materials to microwave radiation, and showed that this method improves the mechanical properties of the composite material; they concluded that exposure to microwave radiation welds the interface of the CNTs and polyactide matrix [6]. To investigate whether exposure to microwave radiation results in a similar enhancement of the mechanical properties of polymer nanocomposite materials with aligned MWCNTs, "single-line" specimens were exposed to varying amounts of microwave radiation in a commercial microwave oven (Panasonic 1200W).

Before exposing the specimens to microwave radiation, a calorimetry calibration sequence was performed to verify that the energy output of the microwave emitter is consistent with its power settings. A sample of water of mass m was heated in an insulated vessel at different power settings, while the exposure time was controlled so that the total energy was constant for each power level. The temperature difference ΔT of the water sample was measured using a digital thermometer. Using the heat capacity of water, C = 4.186 J/gK, the amount of heat, Q, added to the water was defined as

$$Q = C(\Delta T)m\,. \tag{3.9}$$

Table 3.3 shows the calibration results.

The energy absorption in water was found to be proportional to the power setting over the range of 600-1200W. “Single-line” specimens were exposed to microwave radiation at the 600W power setting for an exposure time ranging between 80 and 120 s, to experimentally determine the microwave exposure time that yields the greatest increase in Young’s modulus and ultimate tensile strength of the “single-line” and benchmark specimens, respectively.

3.3.7 Mechanical testing methods

The ultimate tensile strength, Young’s modulus, and moduli of resilience and toughness of the specimens were quantified using uniaxial tensile testing following the ASTM D638 standard test method for tensile properties of plastics [106]. Tests were performed on a universal testing machine (Instron 4303) using a 1 kN load cell, extensometer (MTS model 632.26), and data acquisition software (Bluehill 2). The extensometer was calibrated using an extensometer calibrator (MTS model 3590) prior to every set of uniaxial tensile tests. The specimens were loaded as per ASTM standard D638 for plastic specimens at a rate of 2 mm/min until the peak load dropped by 50% [106]. Seven to fourteen specimens were tested for each specimen type and each MWCNT weight fraction to assess specimen-to-specimen variability of the mechanical properties. The cross sectional area of each specimen was measured prior to testing. Figure 3.15 shows the experimental set-up.

Figure 3.16 shows a generic uniaxial tensile engineering stress versus strain curve. The

Young's modulus was determined as the slope of a linear function found using a least squares fit of the initial portion of the stress-strain curve. The ultimate tensile strength was defined as the maximum value of tensile stress before fracture. The yield stress σ_{yield} was found from E and a 0.2% offset strain, which was then used to specify a yield strain ε_{yield}.

The modulus of resilience U_R, which represents the energy absorbed per unit volume without plastic deformation [43], was computed as

$$U_R = \int_0^{\varepsilon_{yield}} \sigma d\varepsilon \,. \tag{3.10}$$

Similarly, the modulus of toughness U_T, which represents the energy absorbed per unit volume without fracture [43], was computed as

$$U_T = \int_0^{\varepsilon_{fracture}} \sigma d\varepsilon \,. \tag{3.11}$$

3.3.8 Statistical analysis

A one-way analysis of variance was performed using Mathematica [128] to determine whether the mechanical properties of each specimen type were statistically different from each other. When the data followed a normal distribution, a Student's T-test with a p value of 0.05 was used to determine the statistical significance. The results were examined for assumptions of normality and heteroscedasticity; if the test for normality failed, ($p > 0.025$) the results reported come from a Bonferroni and Tukey posttest in the Anova analysis with $\alpha = 0.05$. The Bonferroni correction allows for a comparison of specimens that are unequal in sample size while assuring that an overall confidence coefficient is maintained, whereas the Tukey posttest compares the differences in the means of the different specimen sample

sets and renders them statistically significant if the difference in the mean is greater than the standard error. In most cases, these posttests revealed similar results. When they did not agree, the Bonferroni result was used because it is more conservative.

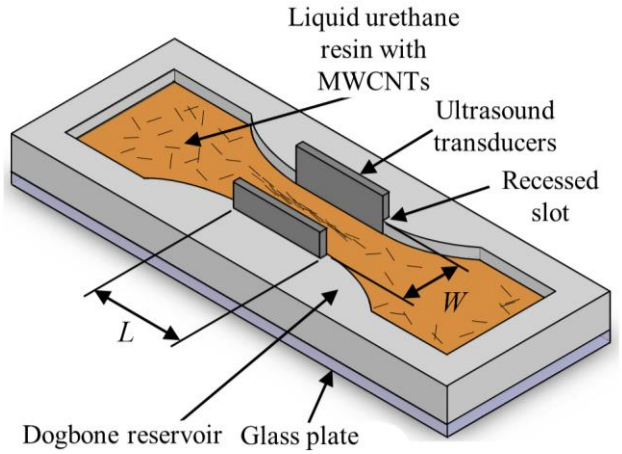

Figure 3.1 Schematic of the experimental set-up to fabricate macroscale dogbone shaped specimens of polymer nanocomposite material with aligned MWCNTs (not drawn to scale).

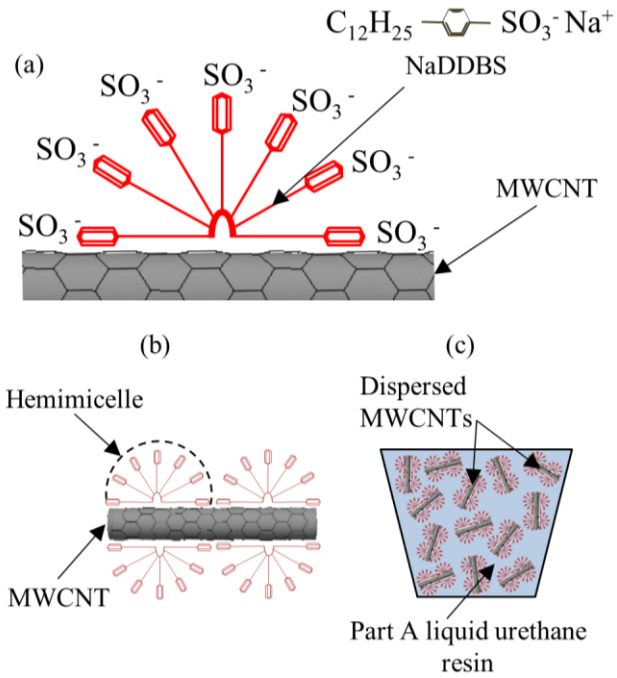

Figure 3.2 Dispersion of MWCNT with NaDDBS, (a) hemimicellar adsorption of NaDDBS onto the surface of a MWCNT (not to scale) (adapted from Vaisman *et al*. [59], and Xin *et al*. [110]), (b) multiple hemimicelles on a MWCNT, (c) dispersed MWCNT in Part A of the liquid urethane resin.

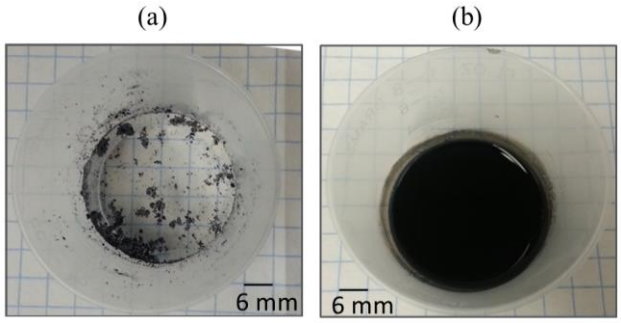

Figure 3.3 Dispersion of 0.2 wt. % MWCNTs in the liquid urethane resin (a) MWCNTs in Part A of the urethane resin without dispersion; (b) MWCNTs in Part A of the urethane resin with dispersion and tip sonication.

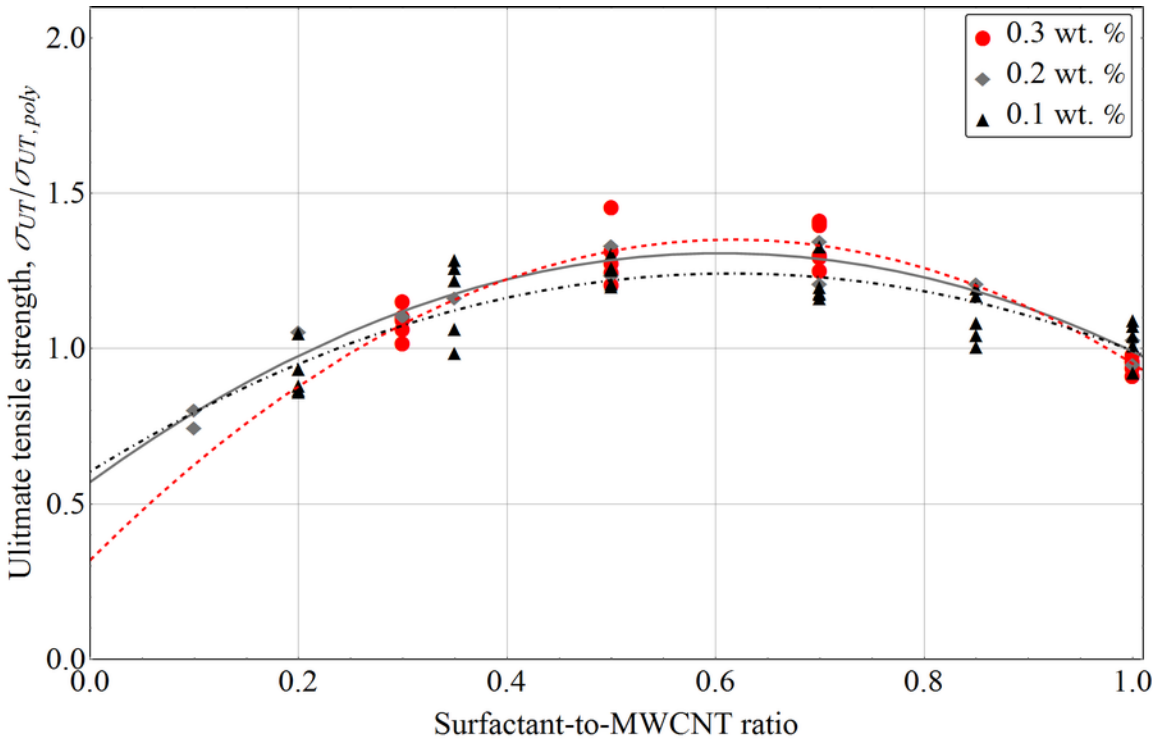

Figure 3.4 Ultimate tensile strength as a function of surfactant-to-MWCNT ratio at MWCNT weight fractions of 0.1, 0.2, and 0.3 wt. % for polymer nanocomposite specimens with randomly oriented MWCNTs.

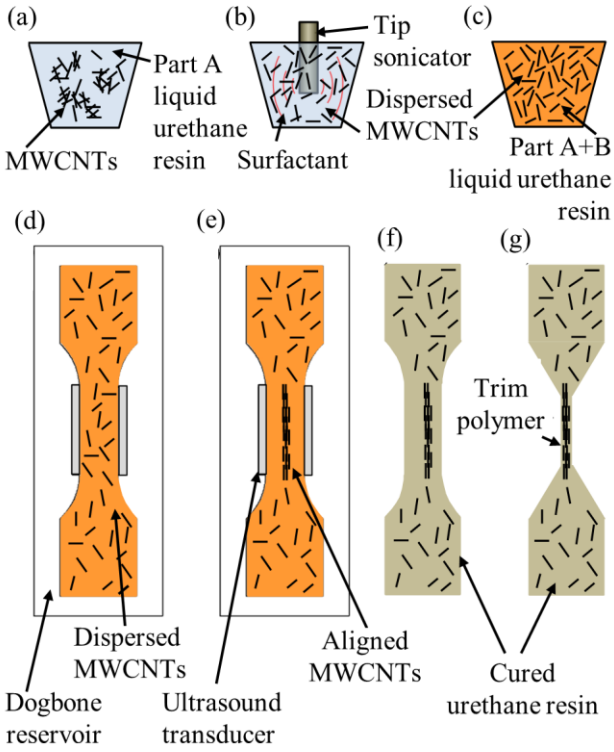

Figure 3.5 Schematic of the process to fabricate macroscale dogbone specimens of polymer nanocomposite material with aligned multi-walled carbon nanotubes (not to scale).

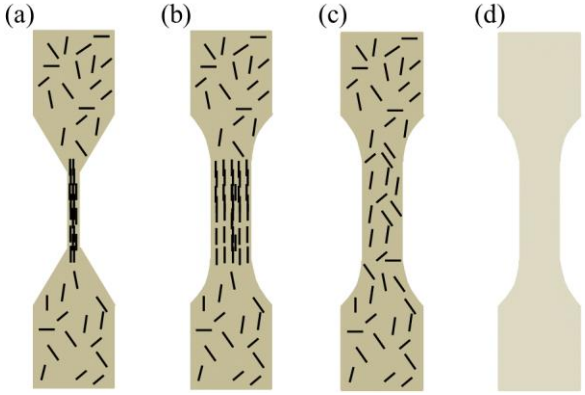

Figure 3.6 Dogbone specimens consisting of (a) the polymer nanocomposite material reinforced with a single line of aligned multi-walled carbon nanotubes (MWCNTs), (b) polymer matrix with multiple (N = 16) lines of aligned MWCNTs, (c) polymer matrix with randomly oriented MWCNTs, and (d) processed polymer matrix.

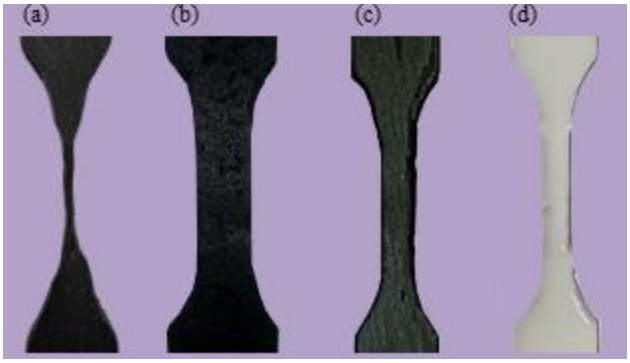

Figure 3.7 Photos of the dogbone specimens: (a) the polymer nanocomposite material reinforced with a single line of aligned multi-walled carbon nanotubes (MWCNTs), (b) polymer matrix with multiple (N = 16) lines of aligned MWCNTs, (c) polymer matrix with randomly oriented MWCNTs, and (d) processed polymer matrix.

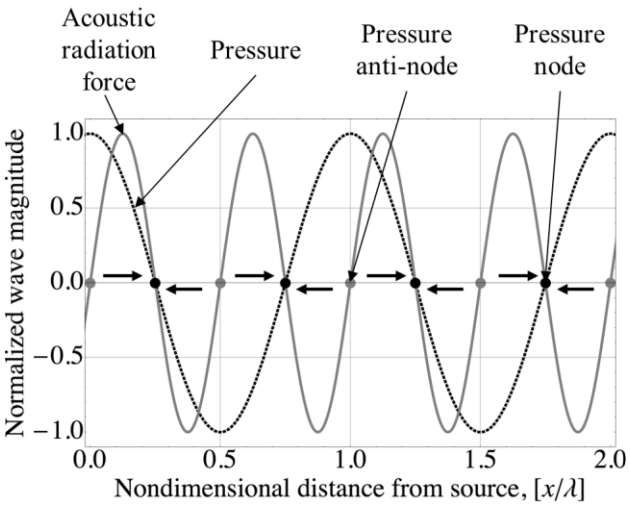

Figure 3.8 Normalized acoustic radiation force and pressure for ultrasound pressure resonance that creates nodes and anti-nodes (adapted from Raeymaekers *et al*., 2011 [115]).

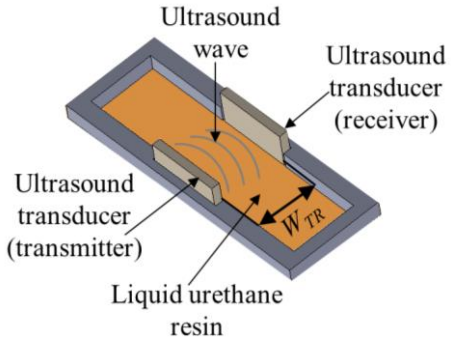

Figure 3.9 Apparatus to experimentally determine the acoustic wave propagation velocity in the liquid urethane resin based on the transit time of a propagating ultrasound wave between transmitting and receiving ultrasound transducers.

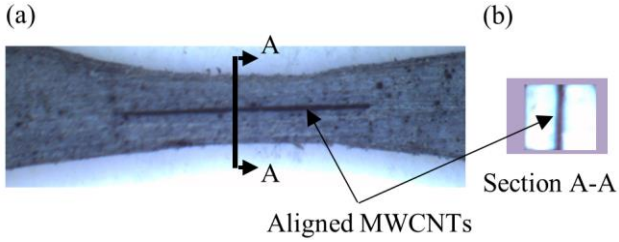

Figure 3.10 Photograph of the gage section of a "single-line" specimen (before trimming the polymer matrix material surrounding the MWCNTs) with an optical micrograph of a cross-section showing that the region of aligned MWCNTs runs uniformly through the thickness of the specimen.

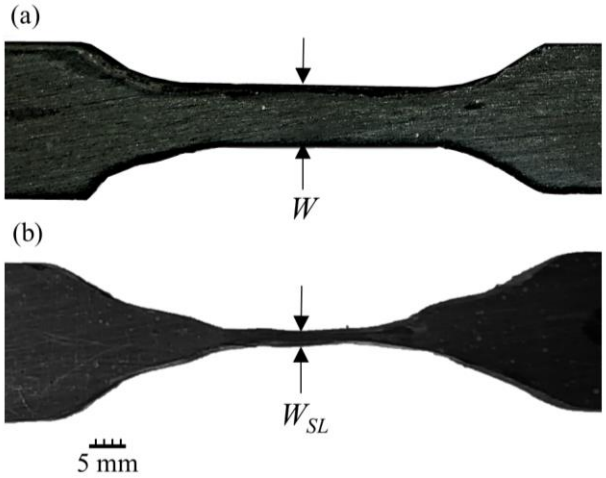

Figure 3.11 "Single-line" specimen showing the width of the gage section (a) before sanding, W, and (b) after removal of excess resin, W_{SL}.

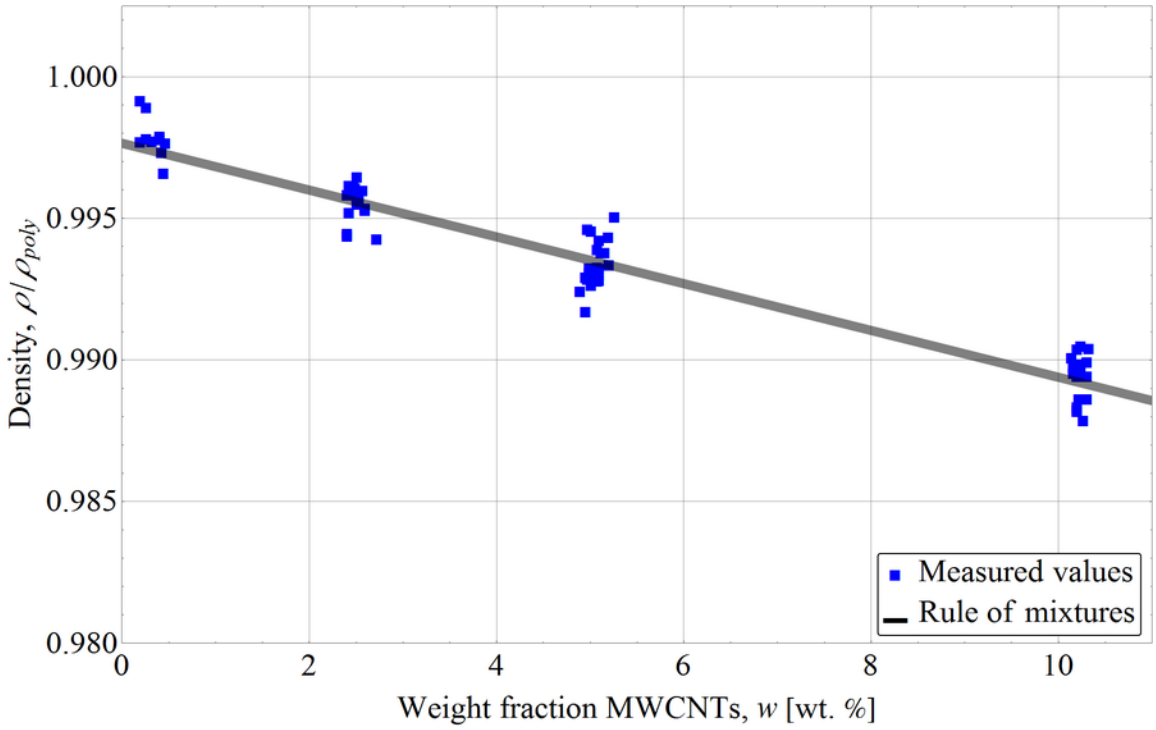

Figure 3.12 Normalized density measurements for polymer nanocomposite material specimens manufactured with known MWCNT weight fractions compared to the rule of mixtures.

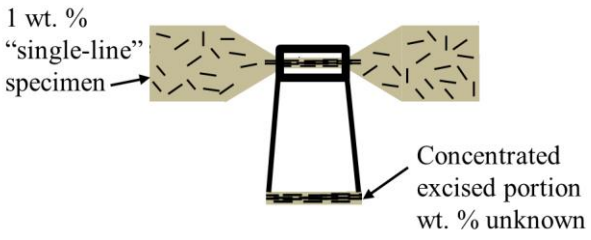

Figure 3.13 The concentrated region of the "single-line" specimen was excised after sanding to measure the density of the MWCNT concentrated region.

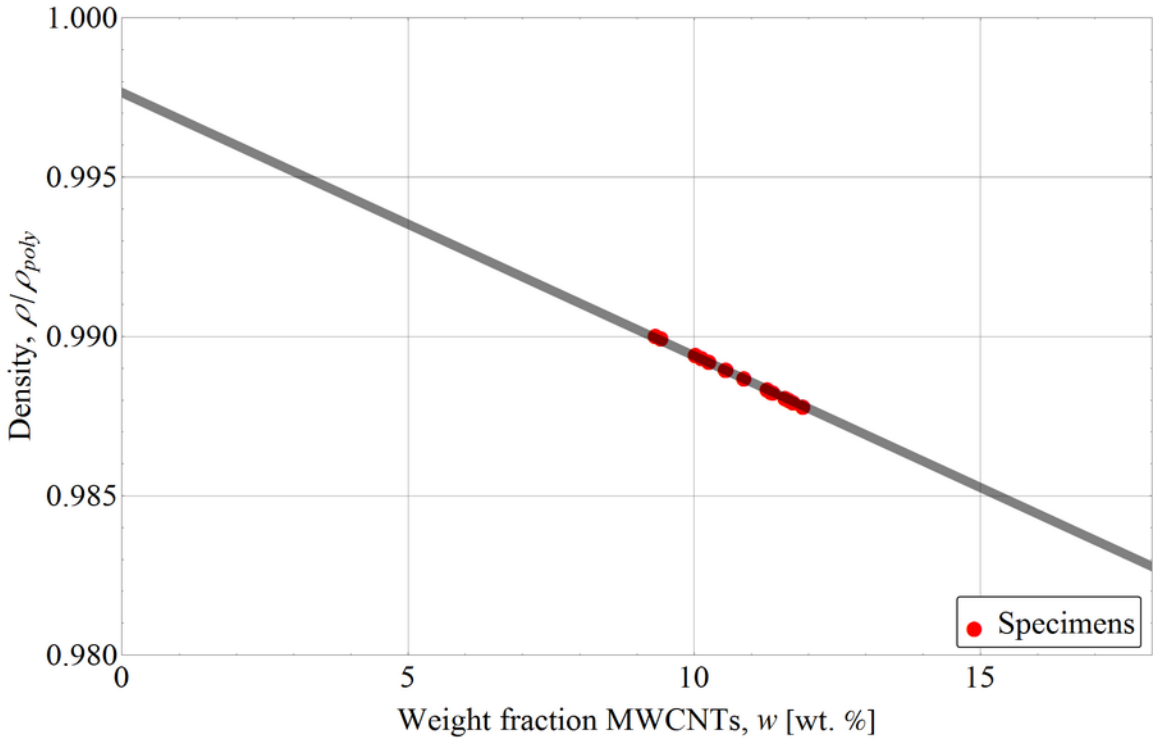

Figure 3.14 Normalized density measurement for the excised region of concentrated MWCNTs in a "single-line" specimen plotted at a weight fraction computed using a rule of mixtures.

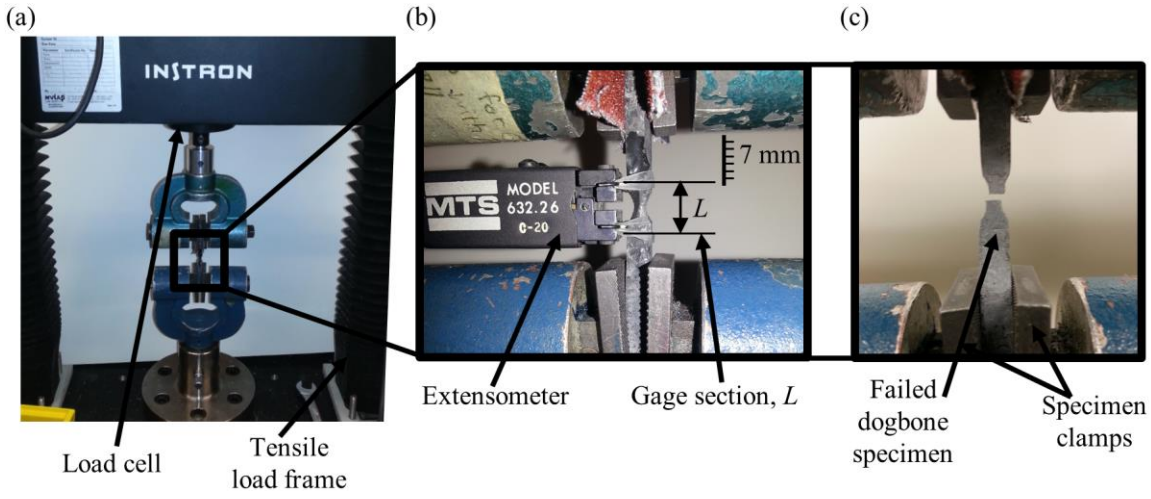

Figure 3.15 Uniaxial tensile test experimental set-up: (a) dogbone specimen clamped into the testing machine (Instron 4303); (b) Strain extensometer (MTS 632.26) attached to dogbone specimen; (c) dogbone specimen after testing is complete and extensometer has been removed.

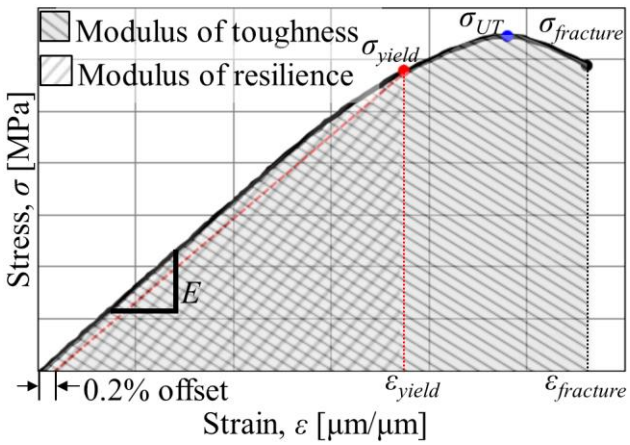

Figure 3.16 Generic stress-strain curve showing the Young's modulus E, the ultimate tensile strength σ_{UT}, the 0.2% offset strain (used to define the yield stress σ_{yield} and yield strain ε_{yield}), the modulus of resilience, the modulus of toughness, and the fracture stress $\sigma_{fracture}$.

Table 3.1 Smooth-Cast 300 two-part thermoset liquid urethane resin matrix properties [107].

	Value	Unit
Pot life	3	min
Cure time	10	min
Ultimate tensile strength, σ_{UT}	21	MPa
Young's modulus, E	0.962	GPa
Elongation at break	5	%
Mixed viscosity	80	cP
Density, ρ	1,050	kg/m^3

Table 3.2 MWCNTs properties [108].

	Value	Unit
Outside diameter	50-80	nm
Inside diameter	5-10	nm
Length	10-20	μm
Bulk density	180	kg/m^3
True density	2,100	kg/m^3

Table 3.3 Microwave calibration results showing heat added to water by varying exposure time and power setting with total energy remaining constant.

Power setting [W]	1200.	840.	600.	480.	360.	120.
Exposure time [s]	30.0	43.0	60.0	75.0	100.0	300.0
Temperature difference [K]	37.1	38.0	39.0	23.8	24.5	16.3
Water mass [g]	100.	100.	100.	100.	100.	100.
Total energy [kJ]	36.0	36.1	36.0	36.0	36.0	36.0
Heat added [kJ]	15.5	16.0	16.3	10.0	10.3	6.8

CHAPTER 4

RESULTS AND DISCUSSION

In this chapter, the mechanical testing results are reported and discussed for the different types of polymer nanocomposite specimens that were manufactured. First, the effect of different fabrication process steps on the mechanical properties of the cured urethane resin are detailed to fully characterize the "processed polymer" specimen (Section 4.1). Next, the mechanical properties of polymer nanocomposite material specimens were examined with aligned MWCNTs relative to specimens without MWCNT and "randomly oriented" specimens (Section 4.2). Finally, the effect of microwave radiation exposure on the mechanical properties of "single-line" specimens is examined (Section 4.3).

4.1 "Processed polymer" specimens

Table 4.1 shows the average Young's modulus and average ultimate tensile strength of ten to twelve "processed polymer" specimens (see Section 3.3), at different stages of the fabrication process. The results shown in Table 4.1 quantify the mechanical degradation of the urethane resin associated with each process step.

Table 4.1 shows that the experimentally determined average ultimate tensile strength and the average Young's modulus of the cured urethane resin (referred to here as the "measured polymer") was 3.3% higher and 26.8% lower, respectively, than that listed by

the manufacturer. Adding surfactant increased the average ultimate tensile strength and the average Young's modulus by 6.9% and 9.6%, respectively. Adding surfactant and exposing the specimens to ultrasound energy from both tip sonication (10 minutes at 20 kHz and 300 W) and standing ultrasound waves (2 minutes at 190.000 kHz) decreased the average ultimate tensile strength and average Young's modulus by 31.8% and 47.6%, respectively, relative to the values that were determined for the cured urethane resin. Figure 4.1 shows a stress-strain diagram for one specimen of each polymer type, the cured urethane resin in its virgin form, and the processed cured urethane resin.

Data for the "processed polymer" and "measured polymer" are included in Figure 4.2 through Figure 4.17. The "processed polymer" specimen was found to have significantly lower mechanical properties than the "measured polymer" using a Student's T-test ($p<<0.001$), including lower ultimate tensile strength, Young's modulus, modulus of toughness, and modulus of resilience.

Thus, the results show that the process that was used to disperse and align MWCNTs in the urethane resin degraded the mechanical properties of the cured urethane resin when MWCNTs were not present, and it is expected to have had a similar deleterious effect on the matrix material in the polymer nanocomposite material specimens. Throughout this chapter, to more clearly describe the effect of reinforcement with randomly oriented and aligned MWCNTs (independent of these matrix degradation effects), the mechanical properties of the polymer nanocomposite material specimens are plotted relative those of the "processed polymer" rather than the nominal values for the cured urethane resin listed in the manufacture's specifications. For completeness, the un-normalized values are also charted.

4.2 Aligned specimens

Mechanical properties are plotted in Figure 4.2 through Figure 4.18 and show the average Young's modulus, ultimate tensile strength, modulus of toughness, and modulus of resilience for "single-line" specimens, "multi-line" specimens, "randomly oriented" specimens, and "processed-polymer" specimens.

Figure 4.2 shows the ultimate tensile strength of the specimen types at various weight fractions. Here, and in the similar charts in this section, error bars indicate the standard error in the data with the mean value of the data shown above each error bar. The *n* value in each bar indicates the number of specimens that were tested for each weight fraction.

The "single-line" specimen had a significantly higher ultimate tensile strength compared to all of the other specimen types ($p<<0.001$). The "processed polymer" showed a statistically significant difference in the ultimate tensile strength from every specimen type with the exception of the "randomly oriented" specimen at 2.5 wt. %. In this data set, at least one of the *p*-values resulting from a test for normality is below 0.025. From an Anova one-way variance analysis, the "measured polymer" showed a significant difference ($p<<0.001$) in the ultimate tensile strength from the "randomly oriented" specimens at weight fractions of 1.0, 2.5, 5, and 10 wt. % and from the "multi-line" specimen at weight fraction of 5 wt. %.

Figure 4.3 shows σ_{UT} for all specimen types normalized with $\sigma_{UT,poly}$ as a function of the MWCNT weight fraction for the "single-line", "randomly oriented", and "multi-line" specimens. Here, and in all similar plots in this section, the error bars indicate the spread in the normalized experimental data.

From Figure 4.3, a 60% increase in σ_{UT} was observed for the "multi-line" specimens (triangle marker) relative to $\sigma_{UT,poly}$, which is approximately 20% greater than the maximum

increase observed for the "randomly oriented" specimens (square marker). This was attributed to alignment of the MWCNTs in the direction of the external mechanical loading, which enables transferring a greater fraction of that loading from the polymer matrix to the MWCNTs [97], and also inhibits formation of MWCNT aggregate bundles [129], [130]. Manufacturing nanocomposite materials at initial weight fractions greater than 2 wt. % of MWCNTs impedes dispersion [129] and increases the viscosity of the MWCNT/resin mixture [131], thus obstructing alignment of the MWCNTs using ultrasound. As a result, σ_{UT} decreased for both "multi-line" and "randomly oriented" specimens for a weight fraction above 2.5 wt. %. Finally, it was observed that the "single-line" specimens (circle marker) displayed σ_{UT} values significantly higher (10% to 185%) than those of the benchmark materials, which is in agreement with trends reported in the literature [4], [130], [132]. Here, poor dispersion at high weight fractions (> 2.5 wt. %) was avoided because during the fabrication process, dispersion was performed on liquid urethane resin containing a low weight fraction (< 1.0 wt. %) of MWCNTs.

Figure 4.4 shows the Young's modulus of the specimen types at various weight fractions.

The "single-line" specimen showed a statistically significant increase in the Young's modulus from all of the other specimen types ($p<<0.001$). The "processed polymer" showed a significant difference ($p<<0.001$) in the Young's modulus from every specimen type with the exception of the "randomly oriented" specimen at 10 wt. %. In this data set, at least one of the *p*-values resulting from a test for normality is below 0.025. From an Anova one-way variance analysis, the "measured polymer" showed a statistically significant difference in the Young's modulus from the "randomly oriented" specimens at

weight fractions of 10 wt. % and from the “multi-line” specimen at weight fraction of 0.2, and 5 wt. %.

Figure 4.5 shows E normalized by E_{poly} as a function of MWCNT weight fraction for “single-line” specimens and the benchmark materials.

Figure 4.5 shows that increasing w decreased E in the “randomly oriented” specimens (square marker) but increased E in the “multi-line” specimen (triangle marker). The average value of E for the “single-line” specimens (circle marker) is larger than that for all benchmark materials. This can be explained by the ultra-high axial stiffness (E = 1-2 TPa) of the MWCNTs [133], and the rule of mixtures, which shows that as w increases, the stiffness of the polymer nanocomposite material approaches that of the MWCNTs [4]. However, the polymer nanocomposite material can only take advantage of the exotic stiffness properties of the MWCNTs if they are aligned in the direction of the external mechanical loading. Adding MWCNTs to the polymer matrix resulted in a more significant increase in E (up to 200 %) as compared to the increase that was observed in σ_{UT} (up to 50 %), which is in agreement with other results documented in the literature [97], [132], [134].

Figure 4.6 shows the modulus of toughness for the specimen types at various weight fractions.

The “single-line” specimen showed a significant increase in the modulus of toughness from all of the other specimen types ($p<<0.001$), with the exception of “multi-line” specimens at weight fractions of 0.1 and 0.2 wt. %. The “processed polymer” showed a statistically significant difference in the modulus of toughness from most specimen types with the exception of the “multi-line” specimen at 2.5 wt. %, and the “randomly oriented” specimens at 0.2 and 1.0 wt. %. From an Anova one-way variance analysis, the “measured

polymer" showed a statistically significant difference in the modulus of toughness from the "randomly oriented" specimens at weight fractions of 1, 2.5, 5, and 10 wt. % and from the "multi-line" specimen at weight fraction of 5 wt. %.

Figure 4.7 shows U_T, and Figure 4.9 shows U_R, normalized with the corresponding moduli of the "processed-polymer" specimen, $U_{T,poly}$ and $U_{R,poly}$, as a function of MWCNT weight fraction, for the "single-line" specimens and the benchmark materials.

Figure 4.7 shows that for w of less than 1.0 wt. %, the "randomly oriented" (square marker) and "multi-line" (triangle marker) specimens displayed U_T values that are 60% and 40%, respectively, larger than that of the "processed polymer". However, increasing w beyond 1.0 wt. % decreased U_T in the benchmark specimens because the formation of MWCNT aggregate bundles lowered σ_{UT} without significantly lowering E. As a result, the low-σ_{UT} and high-E benchmark specimens were susceptible to plastic deformation even under small loads, as indicated by the small U_T values.

Figure 4.8 shows the modulus of toughness for the specimen types at various weight fractions.

The "single-line" specimen showed a significant increase in the modulus of resilience from all of the other specimen types ($p<<0.001$). The "processed polymer" showed a statistically significant difference in the modulus of resilience from "randomly oriented" specimens at 1.0 wt. %, and the "multi-line" specimens at 2.5 wt. %. From an Anova one-way variance analysis, the "measured polymer" showed a statistically significant difference in the modulus of resilience from the "randomly oriented" specimens at weight fractions of 1.0, 2.5, 5.0, and 10 wt. % and from the "multi-line" specimen at weight fraction of 2.5 and 5 wt. %.

Similarly, from Figure 4.9, it is observed that w in excess of 2.5 wt. % drastically reduced U_R of the benchmark "randomly oriented" (square marker) and "multi-line" (triangle marker) specimens.

Obtaining well-dispersed MWCNTs in the liquid urethane resin is challenging for high weight fractions (> 2.5 wt. %), and the resulting polymer nanocomposite materials became brittle and susceptible to fracture under small external mechanical loading. Physically, this is attributed to stress concentrations that typically occur in the vicinity of aggregate bundles of undispersed MWCNTs, and which initiate crack growth under small external mechanical loading [97]. In contrast, Figure 4.7 and Figure 4.9 show that the "single-line" specimens (circle marker) achieved U_T and U_R values that were approximately 200% and 450%, respectively, larger than those of the "processed polymer". These increases resulted from transferring the external mechanical loading from the polymer matrix material to the well-dispersed, aligned MWCNTs, which enabled the polymer nanocomposite material to withstand higher external mechanical loading before yielding or fracturing.

Figure 4.10 shows a stress-strain diagram for a representative specimen of each type: "single-line", "processed polymer", "measured polymer", and "randomly oriented".

These results indicate that the new manufacturing process demonstrated in this paper enabled obtaining an ultra-high weight fraction (>10 wt. %) of well-dispersed MWCNTs aligned favorably to the external mechanical loading, which resulted in a significant increase in the moduli of resilience and toughness.

4.3 Microwave-exposed "single-line" specimens

The effect of microwave exposure on the mechanical properties of "single-line" specimens was investigated. For comparison, the microwave-exposed "processed-

polymer" specimens were characterized along with "randomly oriented" specimens (1 wt. %), and "single-line" specimens without dispersion. Nanocomposite material specimens were exposed to microwave radiation at 600 W with exposure times, t_μ, of 80 s, 100 s, and 120 s. Figure 4.11 shows the ultimate tensile strength for the specimen types at microwave exposure times from 0 – 120s.

The "single-line" specimens without dispersion at a microwave exposure time of 100 s showed a statistically significant difference in the ultimate tensile strength from all of the other specimen types at all microwave exposure times. The "single-line" specimen with dispersion at t_μ = 100 s was not statistically significantly distinguishable from the "single-line" specimen without dispersion with t_μ = 120 s, but these two groups were significantly different from all other groups (p<<0.001). At each microwave exposure time, each specimen's ultimate tensile strength was significantly different than the others at the same t_μ, with the exception of the "single-line" specimen without dispersion at t_μ = 0 s, which was not discernable from the "measured polymer" specimen.

Figure 4.12 shows σ_{UT} normalized with $\sigma_{UT,poly}$ as a function of t_μ "single-line" specimens (with and without dispersion) and the benchmark materials.

From Figure 4.12, it is observed that exposure to microwave radiation increases σ_{UT} for both "randomly oriented" (square marker) and "single-line" (circle and diamond markers) specimens. The most prominent increase was for the "single-line" specimens (102.2 %), for which an exposure time of 100 s at 600 W maximized the σ_{UT} enhancement. Interestingly, while the "single-line" specimens with dispersion (circle marker) were stronger (26.5%) than the "single-line" specimens without dispersion (diamond marker) in the baseline case (no microwave radiation exposure), this trend reversed when both

specimen types were exposed to microwave radiation. The microwave-exposed "single-line" specimens without dispersion showed a 14% increase in σ_{UT} relative to the microwave-exposed "single-line" specimens with dispersion.

Microwave exposure is used in the curing of thermoset resin as a way to apply uniform heating in thick geometries [135]. There is some evidence that microwaves cause additional affects in curing beyond that of heating, but this remains an unresolved topic [136]. For polymer nanocomposite materials, microwave radiation may be selectively absorbed by one material, producing intense localized heating of that material or at the interface between matrix and filler in a composite material [6]. Thus, it is possible that intense local heating occurred around MWCNTs, healing defects in aggregate bundles of MWCNTs. In the absence of such defects, the MWCNT nanocomposite without dispersion would be expected to perform better, since the undispersed MWCNTs could align more easily to the direction of the applied external load. While this defect-healing mechanism is consistent with the observed response, further investigation is warranted to understand the complex interplay between microwave exposure and micromechanical response in aligned MWCNT composite materials.

Figure 4.13 shows the Young's modulus for the specimen types at microwave exposure times from 0 – 120s.

The "single-line" specimen without dispersion t_μ = 80 s, 100 s and 120 s and the "single-line" specimen with dispersion at t_μ = 100 s showed a significant increase in the Young's modulus from all of the other specimen types at all microwave exposure times (p<<0.001). The "single-line" specimen with dispersion at t_μ = 120 s was not significantly distinguishable from the "single-line" specimen with dispersion with t_μ = 80 s, but the two

were statistically different from the other groups (p<<0.001). At t_μ = 0 and 80 s, the "randomly oriented" specimen's Young's modulus was not discernable from the "measured polymer" specimens. However, the Young's modulus of all "randomly oriented" specimens were statistically different than the "processed polymer" specimens when compared at the same microwave exposure time. At t_μ = 0 s, the "single-line" specimens without dispersion's Young's modulus was also not statistically different from the "single-line" specimens with dispersion.

Figure 4.14 shows E normalized with E_{poly} as a function of t_μ for the "single-line" specimens (with and without dispersion) and the benchmark materials.

Figure 4.14 shows that, similar to the trend for σ_{UT}, exposure to microwave radiation produced a marked increase in E for the "single-line" specimens, both with and without dispersion, and that again the "single-line" specimens without dispersion (diamond marker) gave the highest result with E increasing by 600% relative to the "processed polymer". For the "randomly oriented" specimens (square marker), E was relatively unchanged with exposure to microwave radiation, with a maximum increase of 16.3%. This was unexpected, given that the microwave exposure increased the stiffness of the "processed polymer" (triangle marker) by 87-110%, and could indicate that the microwaves are selectively absorbed by the MWCNT [137] thus reducing the stiffening effect of the microwaves on the polymer matrix.

Figure 4.15 shows the modulus of toughness for the specimen types at microwave exposure times from 0 – 120s.

The "single-line" specimen with dispersion and t_μ = 120 s, had the most variability and showed no statistical significant difference in the modulus of toughness from all of the

other “single-line” specimen types that had exposure to microwave. The “single-line” specimen without dispersion at t_μ = 100 s had a modulus of toughness that was not significantly distinguishable from the “single-line” specimen with dispersion with t_μ = 100 s. However, all “single-line” specimens both with and without dispersion that had some microwave exposure were found to have modulus of toughness that was significantly different than all of the “randomly oriented”, “processed polymer”, and “measured polymer” specimens ($p<<0.001$).

Figure 4.14 shows U_T normalized with $U_{T,poly}$ as a function of t_μ for the “single-line” specimens (with and without dispersion) and the benchmark materials.

Figure 4.16 shows that for the “processed polymer” specimen (triangle marker) microwave radiation exposure had a small effect on modulus of toughness with an approximate 20% decrease at t_μ = 80 s, a 25% increase at t_μ = 100 s, and no statistically significant change at t_μ = 120 s. It is observed that for the “single-line” specimens, the maximum value of U_T occurred at t_μ = 100 s, with U_T increasing relative to the “processed polymer” by 235% and 265% for the specimens with dispersion (circle marker) and without dispersion (diamond marker), respectively. Relative to their respective values at t_μ = 0 s, this corresponds to an increase of 143.8% and 73.9% with exposure to microwave radiation. In light of the more significant increases in σ_{UT} and E, this suggests that exposure to microwave radiation was allowing strain softening to occur prior to failure.

Figure 4.17 shows the modulus of resilience for the specimen types at microwave exposure times from 0 – 120s.

The “single-line” specimen with dispersion t_μ = 100 s showed no statistically significant difference in the modulus of resilience from the “single-line” specimen without dispersion

at t_μ = 100 s. However, all "single-line" specimens both with and without dispersion that had some microwave exposure were found to have modulus of toughness that was significantly different than all of the "randomly oriented", "processed polymer", and "measured polymer" specimens.

Figure 4.18 shows U_R normalized with $U_{R,poly}$ as a function of t_μ for the "single-line" specimens (with and without dispersion) and the benchmark materials.

From Figure 4.18, it is observed that overall, the specimens had an increase in the modulus of resilience with microwave exposure with the exception of the "randomly oriented" specimen (square marker) at t_μ = 80 s which had a modulus of resilience similar to that with no microwave exposure. It is observed that the trends are similar to those observed for the Young's modulus, with a maximum increase of approximately 600% relative to the value of the "processed polymer", suggesting that the increase in U_R was primarily due to an increase in the initial elastic stiffness, rather than a delay in plastic deformation.

Figure 4.19 shows the stress-strain diagram for a microwaved exposed "single-line" specimen, a "single-line" specimen without exposure to microwave radiation, and a "processed polymer" specimen.

It is clear from Figure 4.19 that exposure to microwave radiation increased the stiffness, ductility, and ultimate tensile strength of the material, resulting in an increase in the moduli of toughness and resilience. The 310% σ_{UT} increase and 610% E increase achieved for "single-line" specimens with microwave radiation exposure are the highest increases achieved in this work and are the largest increases reported in the literature for polymer nanocomposite materials with aligned MWCNTs using bulk alignment methods.

4.4 Discussion of limitations

While this work represents a significant advancement in the state of the art for aligned CNT-reinforced polymer composite materials, the demonstration of mechanical property enhancement with the method was limited by certain aspects of the manufacturing process and analysis methods.

The development of the CNT-alignment method was guided by theoretical models and previous work, but the development process was largely empirical, because the models that describe ultrasound alignment of particles cannot adequately describe the complexities in this system, such as particle shape, CNT entanglement, changing temperature and viscosity, finite precision in the manufacture of the dogbone reservoir, and positioning of the parallel PZT plates. Improved theoretical models of the alignment process would enable more efficient optimization of the process parameters.

The scope of the work was limited to a single material set (polymer matrix/surfactant/MWCNT type), which restricted the options for improving dispersion and alignment. The operating frequency was limited to a range near the center frequency of the available PZT plates and the need to obtain a standing wave in the fixture, so it was not possible to investigate the effect of significantly varying the frequency on alignment efficiency, MWCNT concentration, or polymer degradation.

The wave propagation velocity and viscosity of the urethane resin both change during hardening, and both likely depend on temperature, as does the rate of hardening. The hardening reaction is exothermic, and heat is added to the system from operation of the PZT transducers, but the heat loss is dependent on the geometry of the reservoir and the temperature of the surroundings. The fixture geometry (and thus the temperature profile during curing) differed between the single-line and multi-line fixtures, and the PZT plates

were operated at different frequencies for the two fixtures, but it is unknown how the difference in temperature and operating frequency affected the performance of the materials. Extending the work to include a study of "processed polymer" and "randomly oriented" materials fabricated in both of the fixture types would provide data to assess these effects.

The results showed that dispersion of MWCNT was a critical factor in determining mechanical performance, but the preliminary work to optimize the surfactant-to-MWCNT ratio was conducted for parts with a MWCNT weight fraction in the range of 0.1 to 0.3 wt. %. While an optimal ratio was clearly observed for the parts in this range, the effect of surfactant-to-MWCNT ratio was not tested at the higher weight fractions obtained in the "single-line" specimens. Further optimization of this ratio through the full range of weight fractions (0.1 to 10 wt. %) could potentially improve performance of the high weight fraction specimens.

The results showed that the mechanical properties of the MWCNT-reinforced specimens with alignment were limited do to the polymer degradation that occurred during processing, as evidenced by the difference between the "processed polymer" and "measured polymer". The effect of ultrasound energy on polymer solutions and the resulting degradation of elastic properties has been studied by Price and Smith [138] and Kost *et al.* [139], who observed similar degradation due to shear gradients formed around cavitation bubbles in the solution.

Figure 4.20 shows an x-ray CT image of a "randomly oriented" specimen and a "single-line" specimen. It is not possible to distinguish the MWCNT from the polymer matrix material in these images; however, air pockets and particles of NaDDBs are clearly seen.

These air pockets could be caused by the ultrasound transducers, the tip sonication, or casting/mixing. This “randomly oriented” specimen showed more of the air pocket defects than the “single-line” specimen. It is possible that the slightly higher-energy ultrasound transducer operating frequency of the “randomly oriented” part produced more air pockets, or that the air pockets in the “single-line” specimen are displaced as the MWCNTs move toward the alignment node, or the difference could simply be part-to-part variation. An imaging study of a statistically significant number of specimens would be needed to make this determination.

In estimating the mass fraction of MWCNT in the “single-line” specimens (Section 3.3.5), the effect of air pockets on the bulk density is neglected. While this assumption is consistent with the observation of few air pockets for the “single-line” specimens, it is a potential source for error in the analysis.

Air bubbles could also have affected the mechanical properties of the specimens. A detailed fracture analysis was not completed on the test specimens, because imaging the interface between the MWCNT and matrix requires challenging sample preparation (*e.g.*, for TEM) that may cause additional mechanical degradation. In a few cases, it was observed that failure initiated at a visible defect such as an air pocket or undispersed aggregate bundle of MWCNT. From the stress-strain diagram, it is shown that the specimens that were reinforced with MWCNTs were more brittle than the unreinforced polymer specimens, so the presence of these defects may have been significant. In future work, the fracture surface of the specimens could be examined to help determine the exact mode of failure, which could guide optimization of the process.

The study spanned a wide parameter space, varying from specimen type, weight

fraction, dispersion amount, etc., so with the resources available to the project, it was only possible to fabricate seven to fourteen of each specimen type. Sections 4.1 through 4.3 reported the variability in the measured results, but the sample size may be insufficient to fully characterize the variability resulting from the manufacturing method.

Mold evacuation, material removal in preparation of the "single-line" specimens, and isolation of the concentrated alignment region for gravimetric analysis were all manual procedures and thus introduced the potential for part-to-part variation and nonuniformity. The trimming and sanding of the excess polymer may have affected the mechanical properties of the final part because of surface defects that were introduced. Additionally, the largest width and thickness in the gage section of the dogbone specimen was used to compute the cross sectional area prior to tensile testing. As a result, the analysis could have underestimated the mechanical properties of the material, particularly if a specimen broke at a smaller portion of the gage section.

In spite of these limitations, it was clear from the obtained results that the alignment/concentration method for producing high weight percent MWCNT-reinforced polymer composite materials has the potential for application in enhancing and customizing the mechanical properties of these composite materials in a way not possible with other bulk alignment methods. Addressing these limitations is expected to further enhance this capability, and is therefore a promising directions for future research.

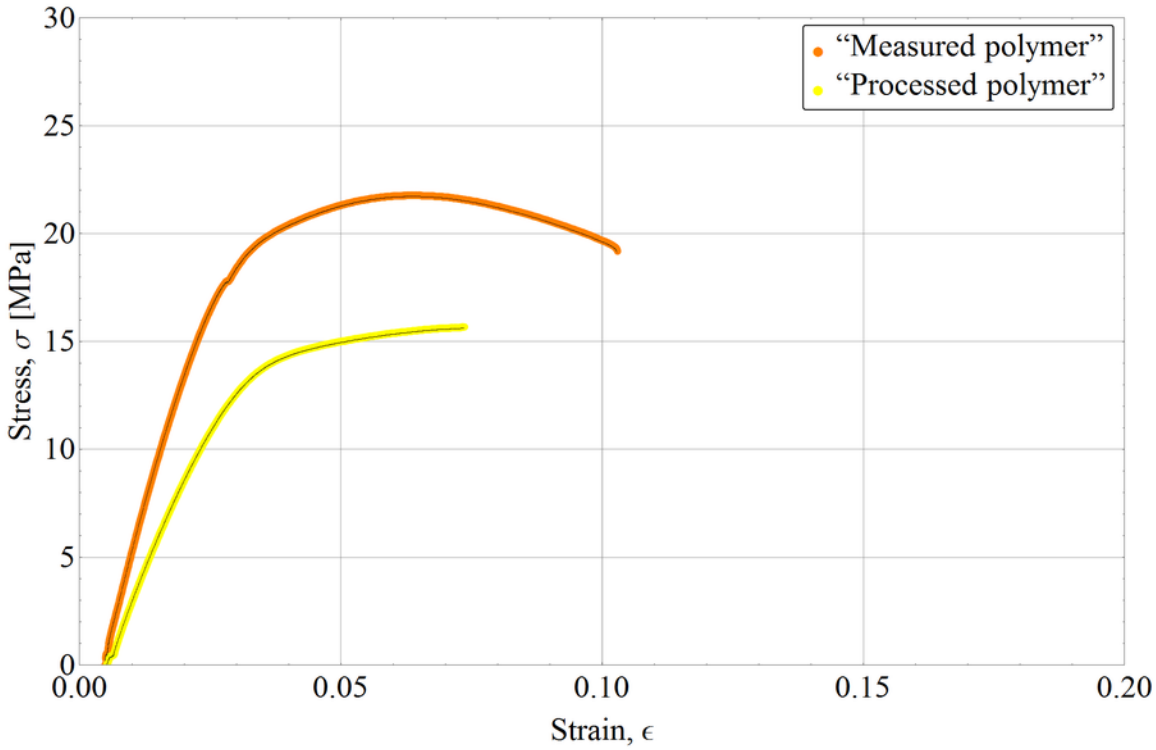

Figure 4.1 Stress-strain diagram for the "measured polymer" and "processed polymer".

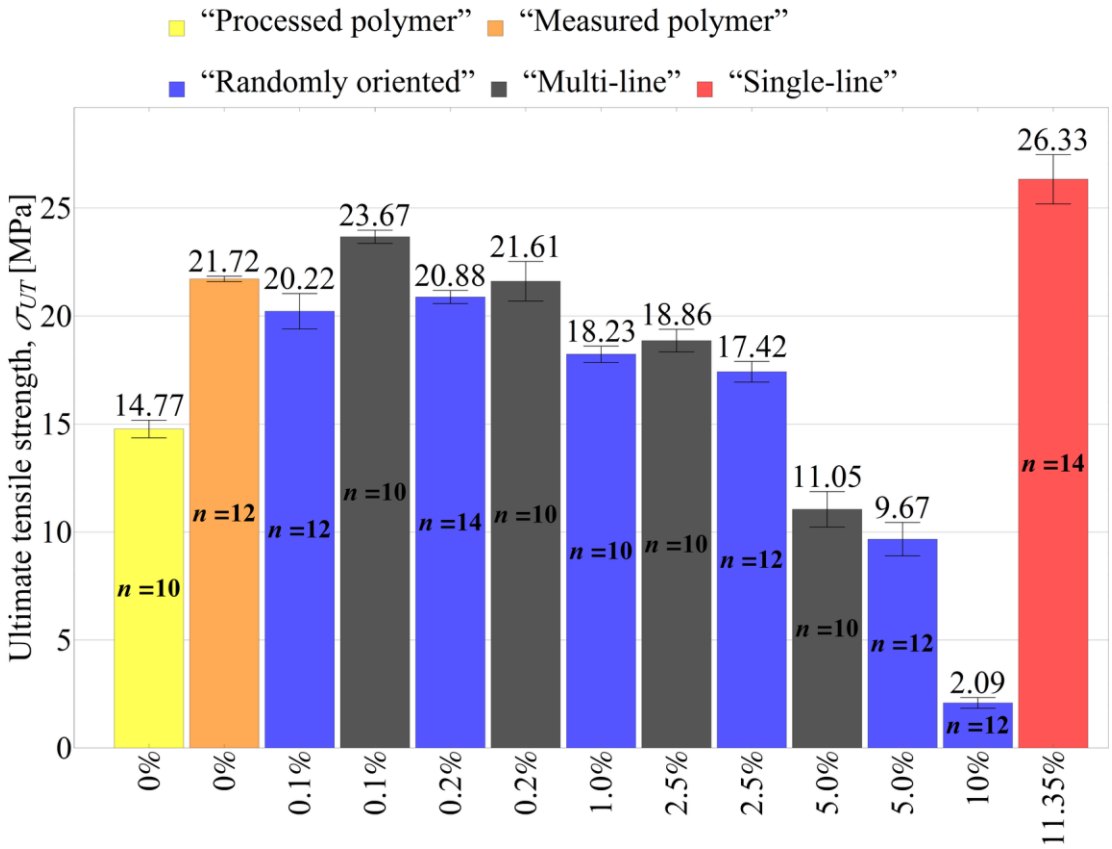

Figure 4.2 Ultimate tensile strength versus weight fraction for various specimen types.

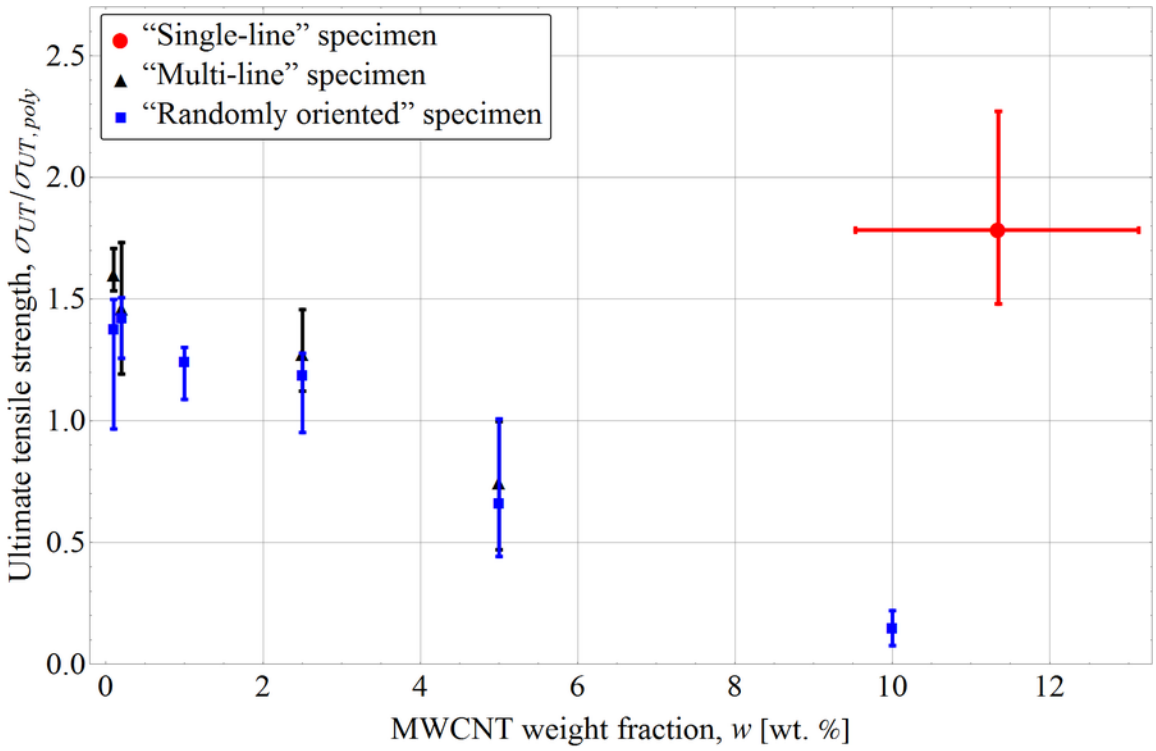

Figure 4.3 Ultimate tensile strength normalized by the ultimate tensile strength of the "processed polymer" versus MWCNT weight fraction.

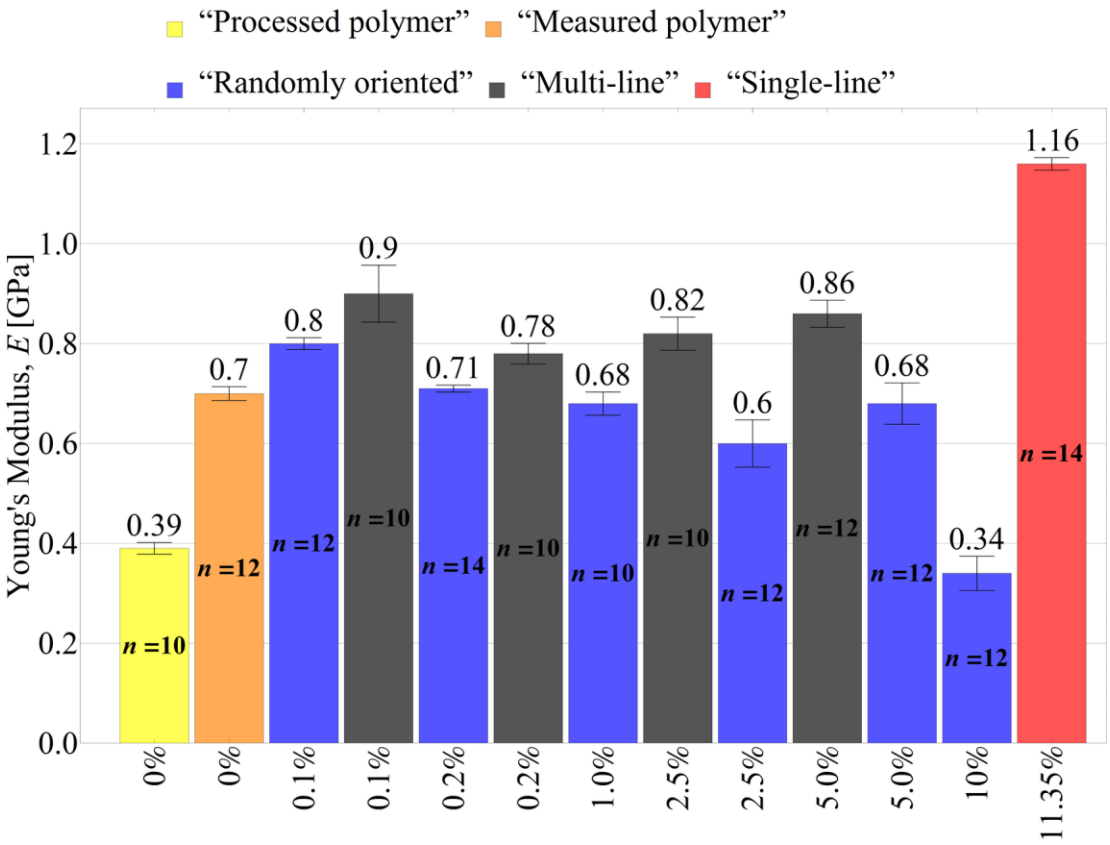

Figure 4.4 Young's modulus versus weight fraction for various specimen types.

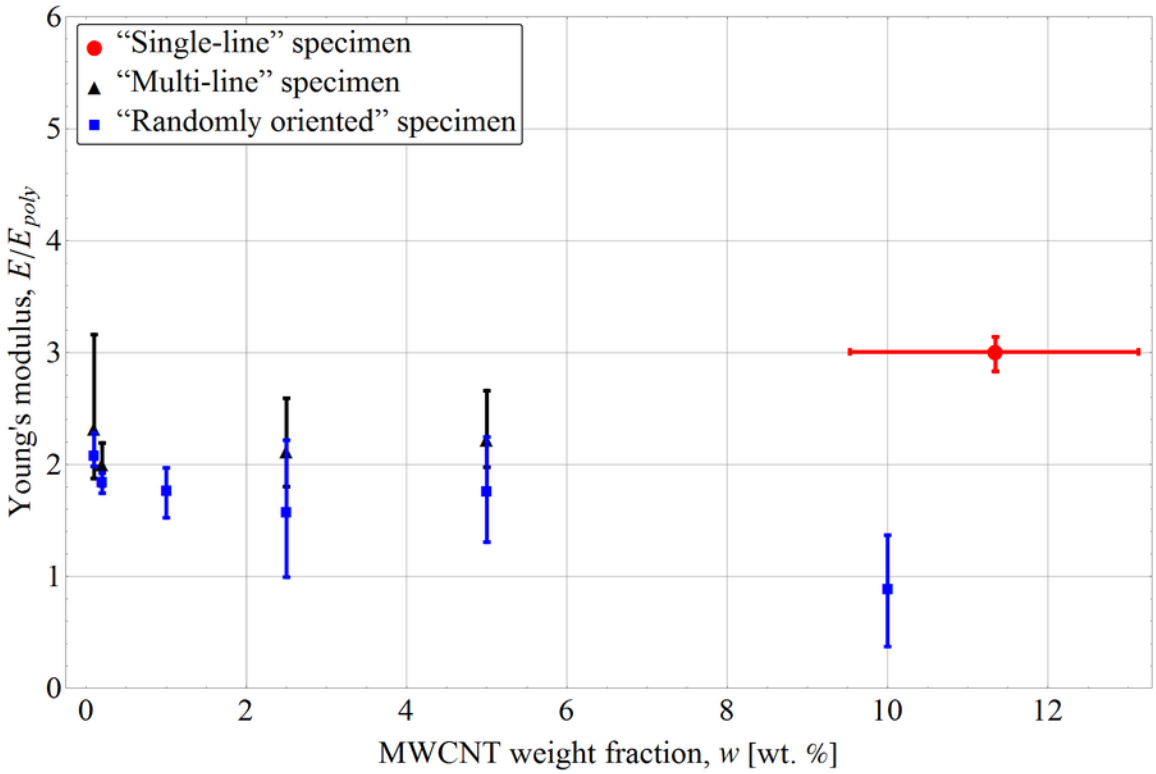

Figure 4.5 Young's modulus normalized by Young's modulus of the "processed polymer" versus MWCNT weight fraction.

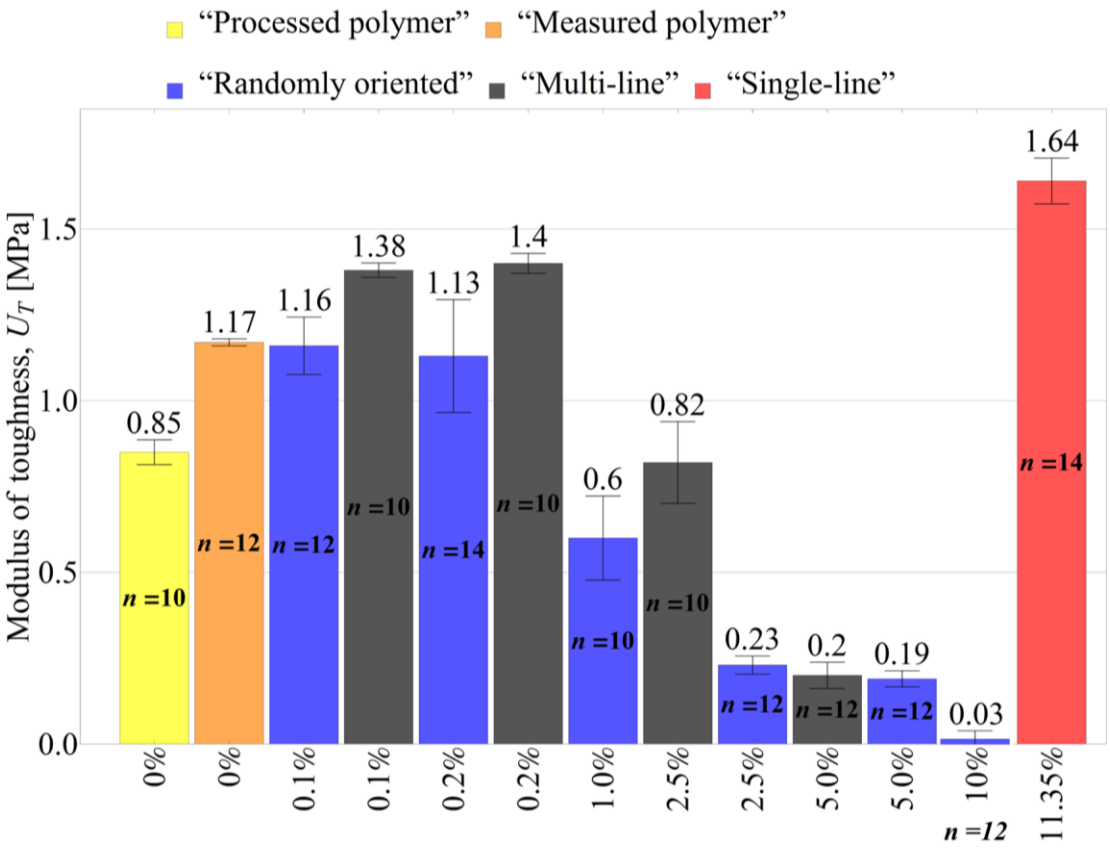

Figure 4.6 Modulus of toughness versus weight fraction for various specimen types.

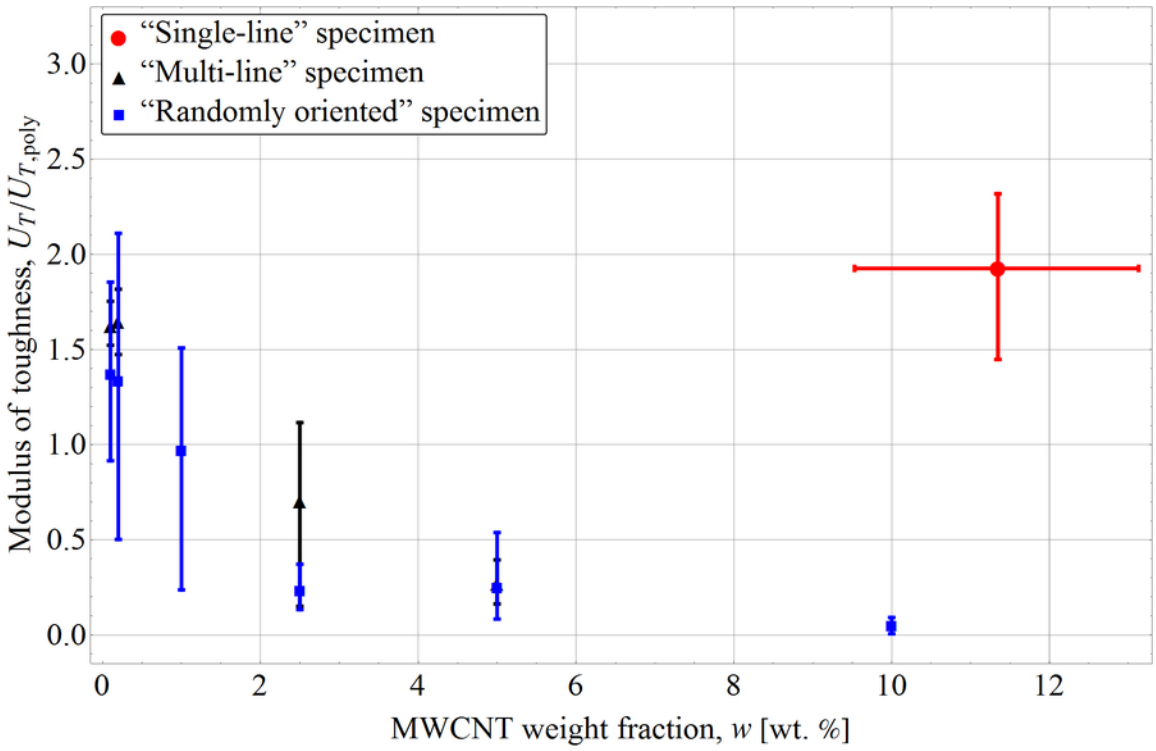

Figure 4.7 Modulus of toughness normalized by modulus of toughness of the "processed polymer" versus MWCNT weight fraction.

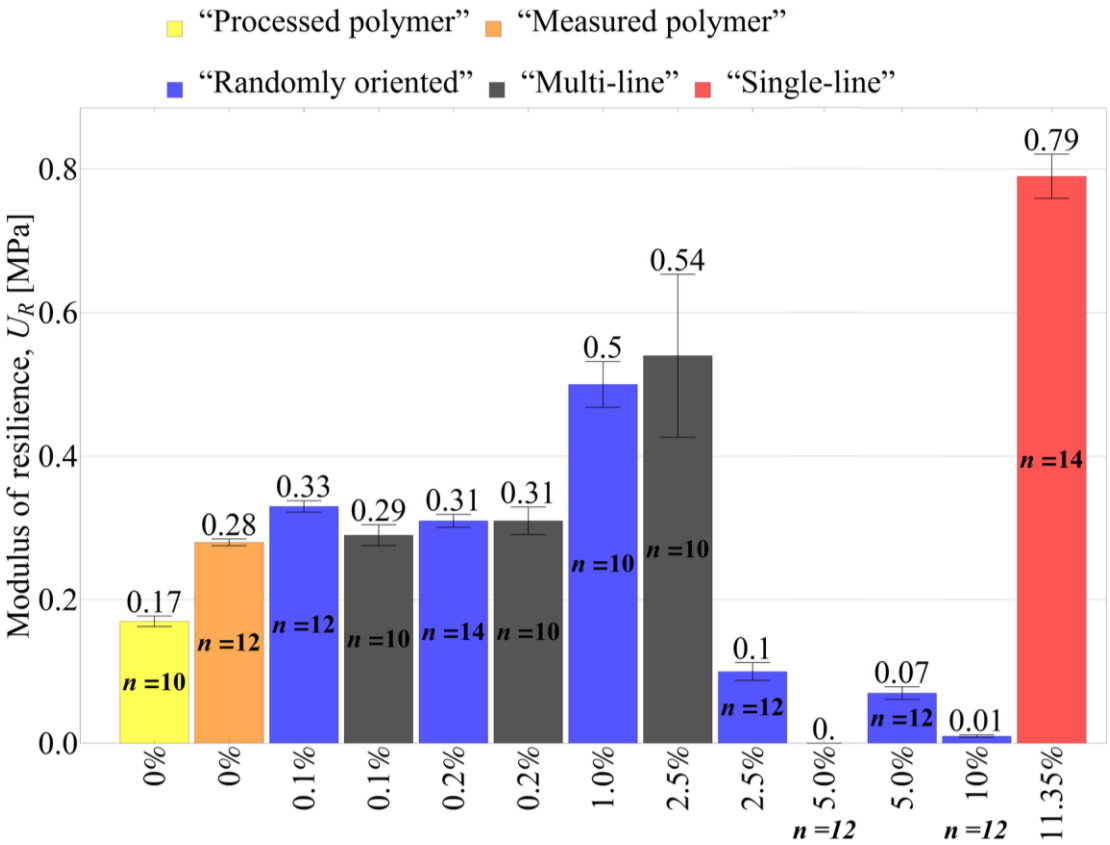

Figure 4.8 Modulus of resilience versus weight fraction for various specimen types.

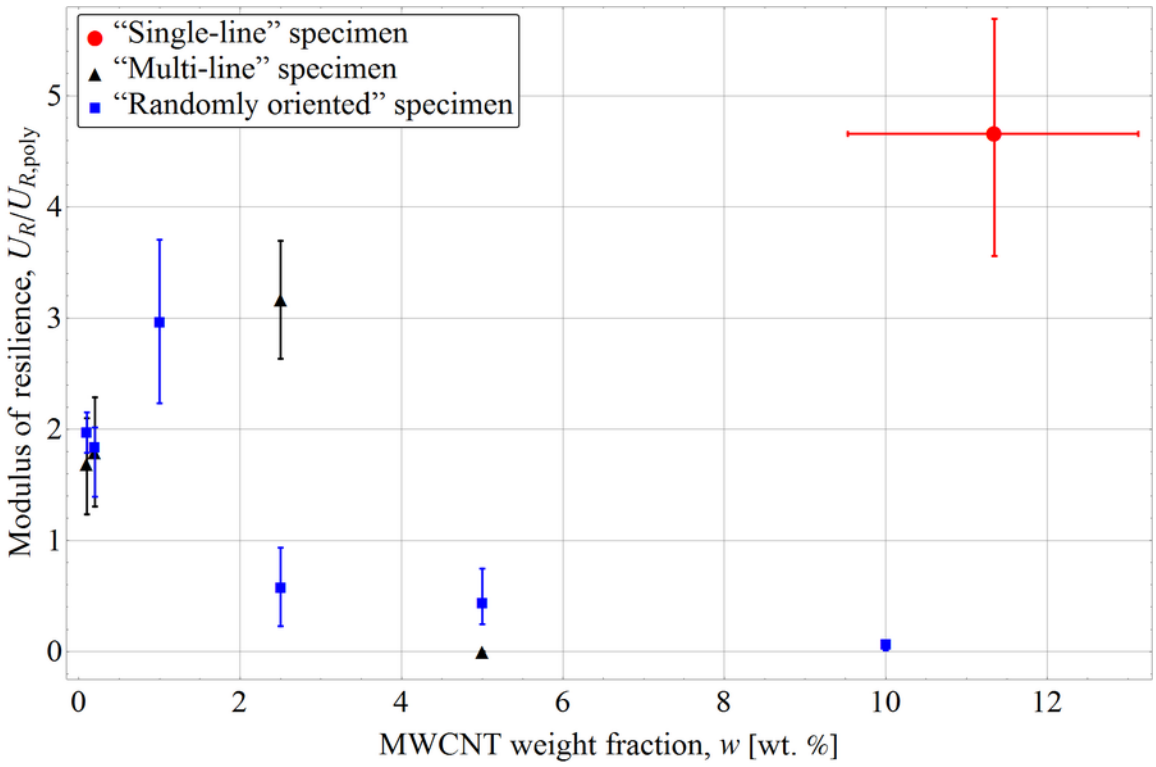

Figure 4.9 Modulus of resilience normalized by modulus of resilience of the "processed polymer" versus MWCNT weight fraction.

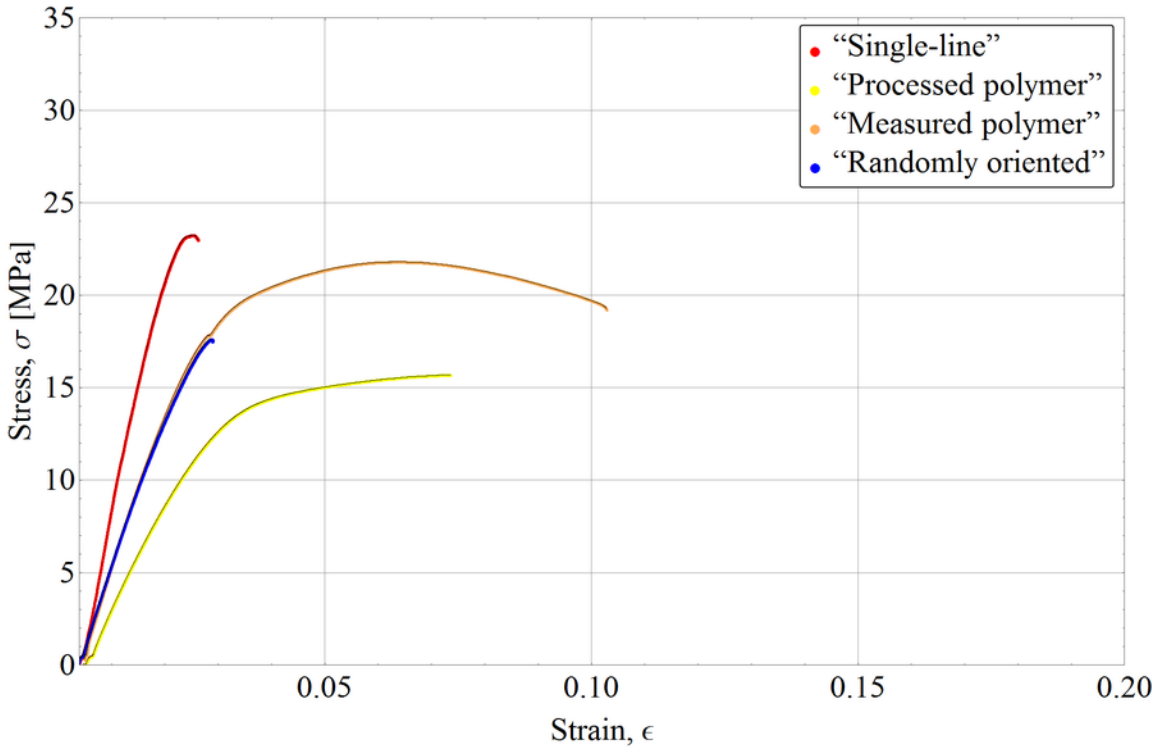

Figure 4.10 Stress-strain diagram for the "single-line", "randomly oriented", "measured polymer", and "processed polymer" specimens.

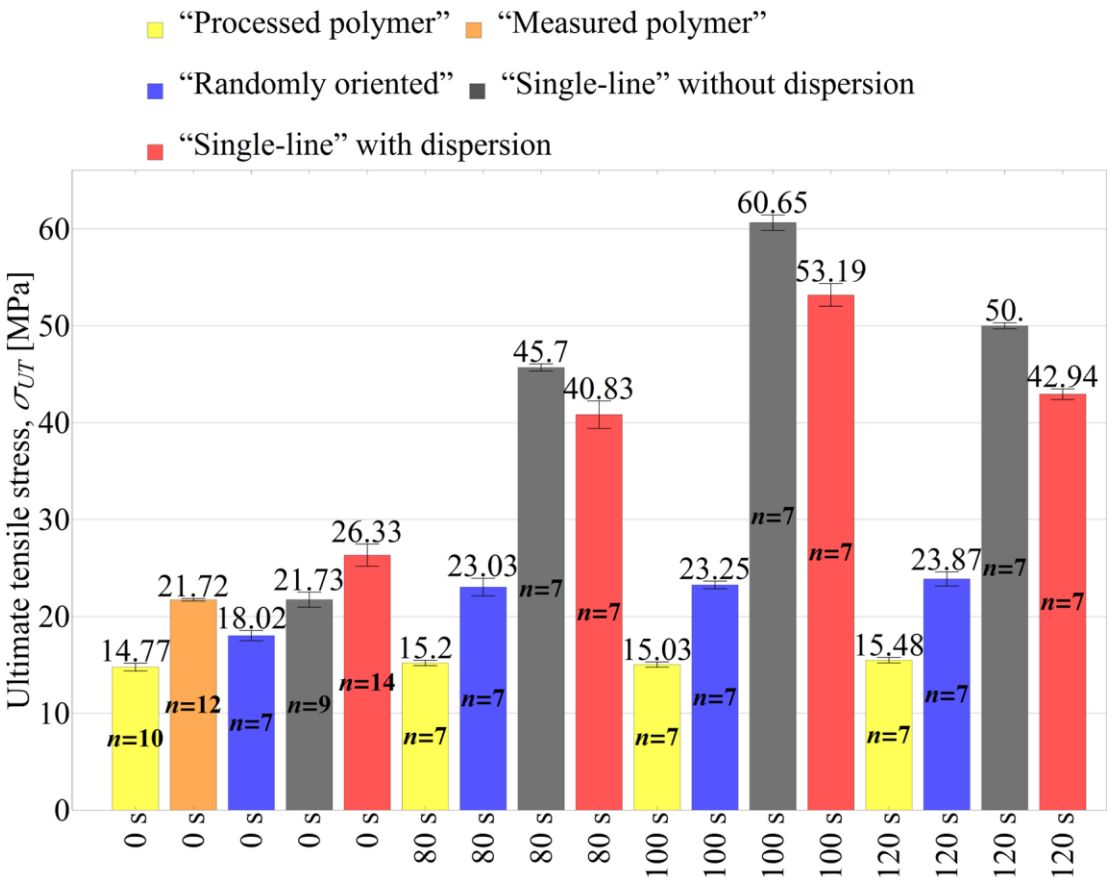

Figure 4.11 Ultimate tensile strength versus microwave exposure time for various specimen types.

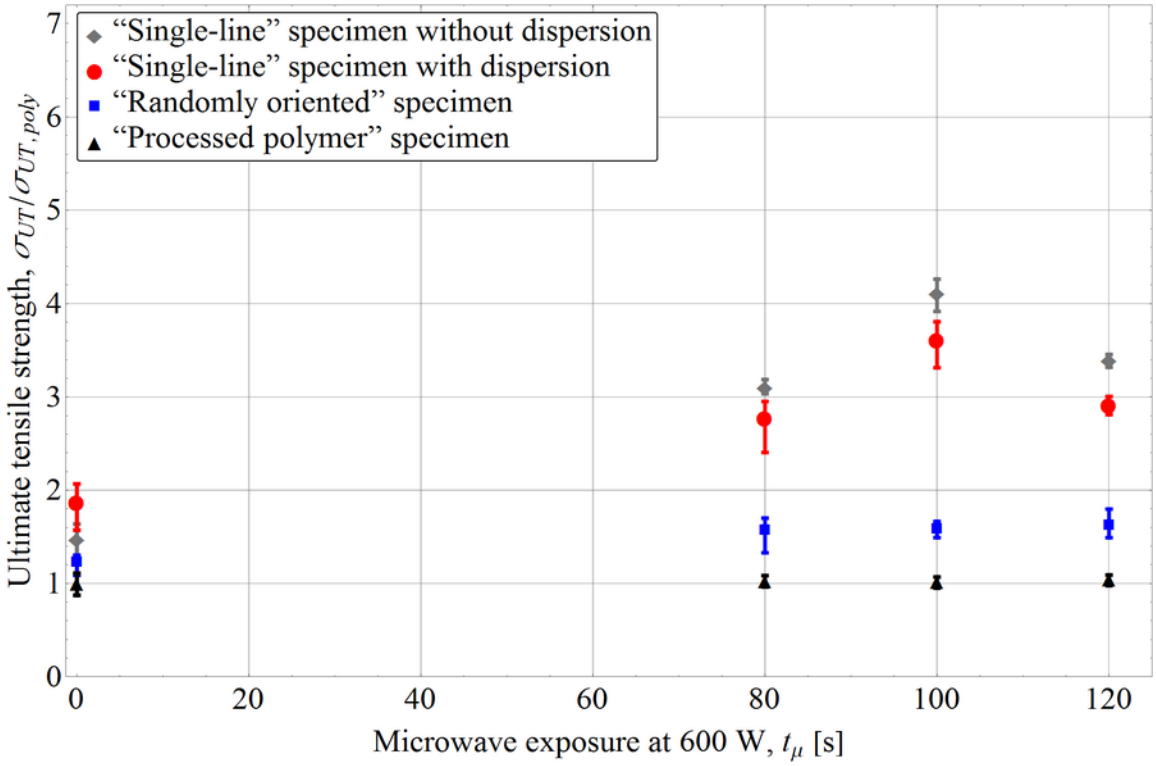

Figure 4.12 Ultimate tensile strength normalized by ultimate tensile strength of the "processed polymer" versus microwave radiation exposure time for "single-line" specimen with and without dispersion and for benchmark materials.

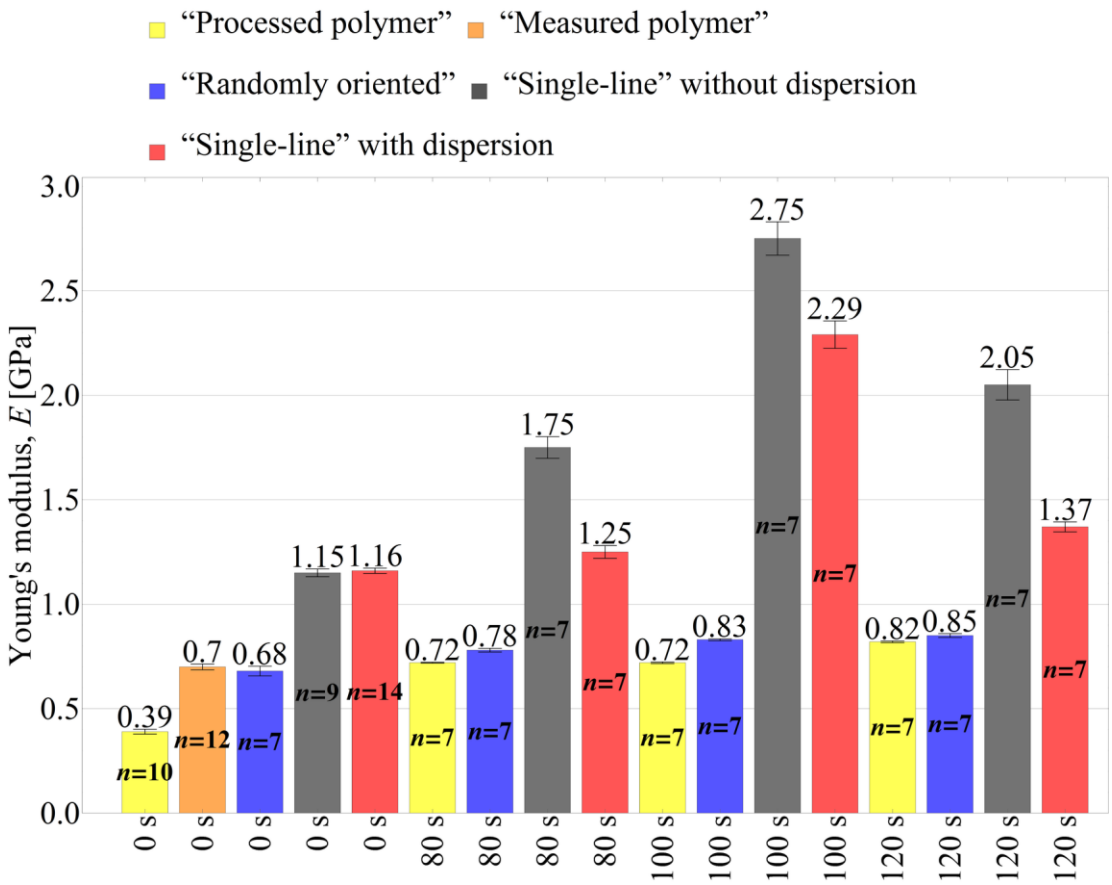

Figure 4.13 Young's modulus versus microwave exposure time for various specimen types.

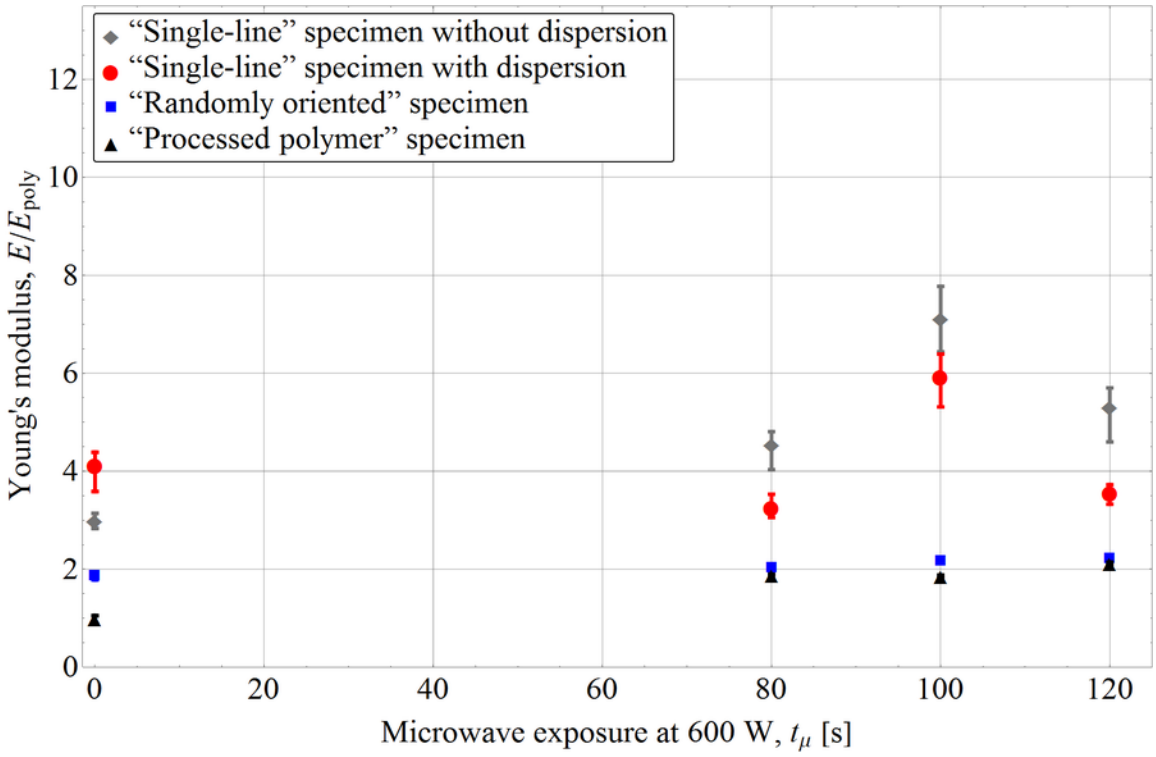

Figure 4.14 Young's modulus normalized by Young's modulus of the "processed polymer" versus microwave radiation exposure time for "single-line" specimens with and without dispersion and for benchmark materials.

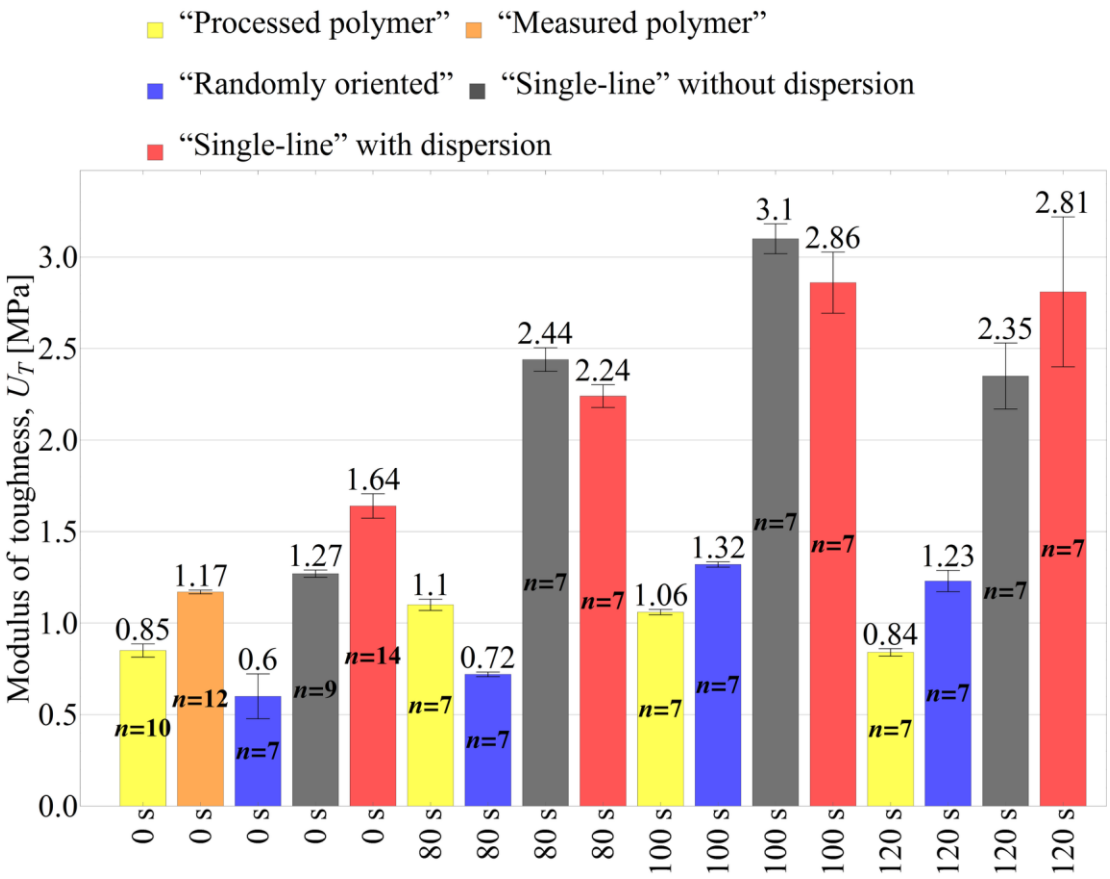

Figure 4.15 Modulus of toughness versus microwave exposure time for various specimen types.

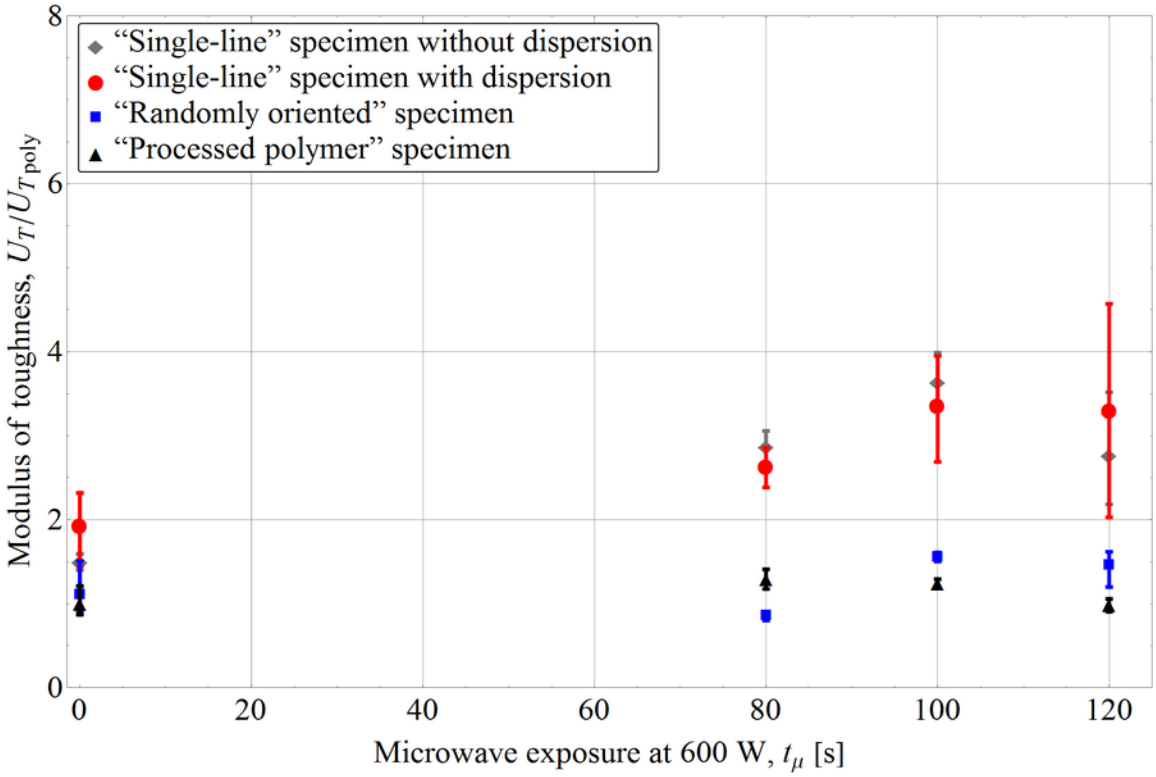

Figure 4.16 Modulus of toughness normalized by modulus of toughness of the "processed polymer" versus microwave radiation exposure time for "single-line" specimens with and without dispersion and for benchmark materials.

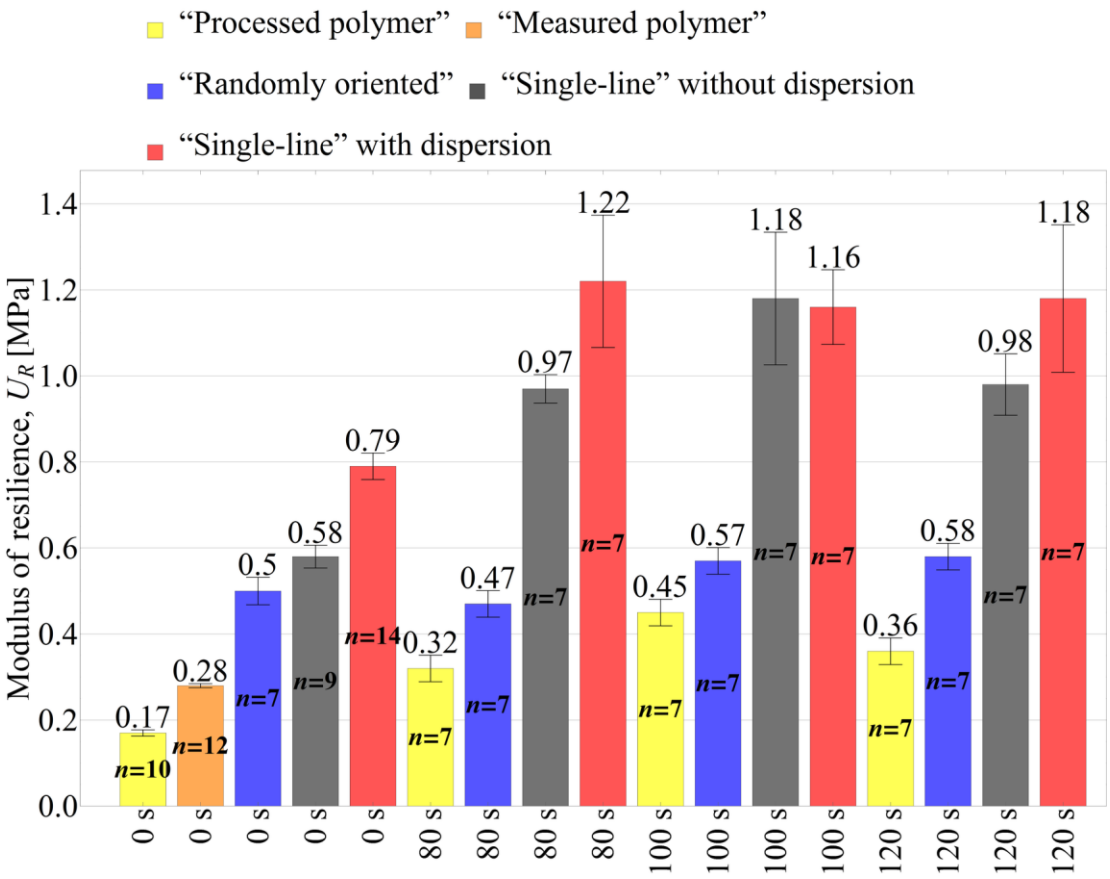

Figure 4.17 Modulus of resilience versus microwave exposure time for various specimen types.

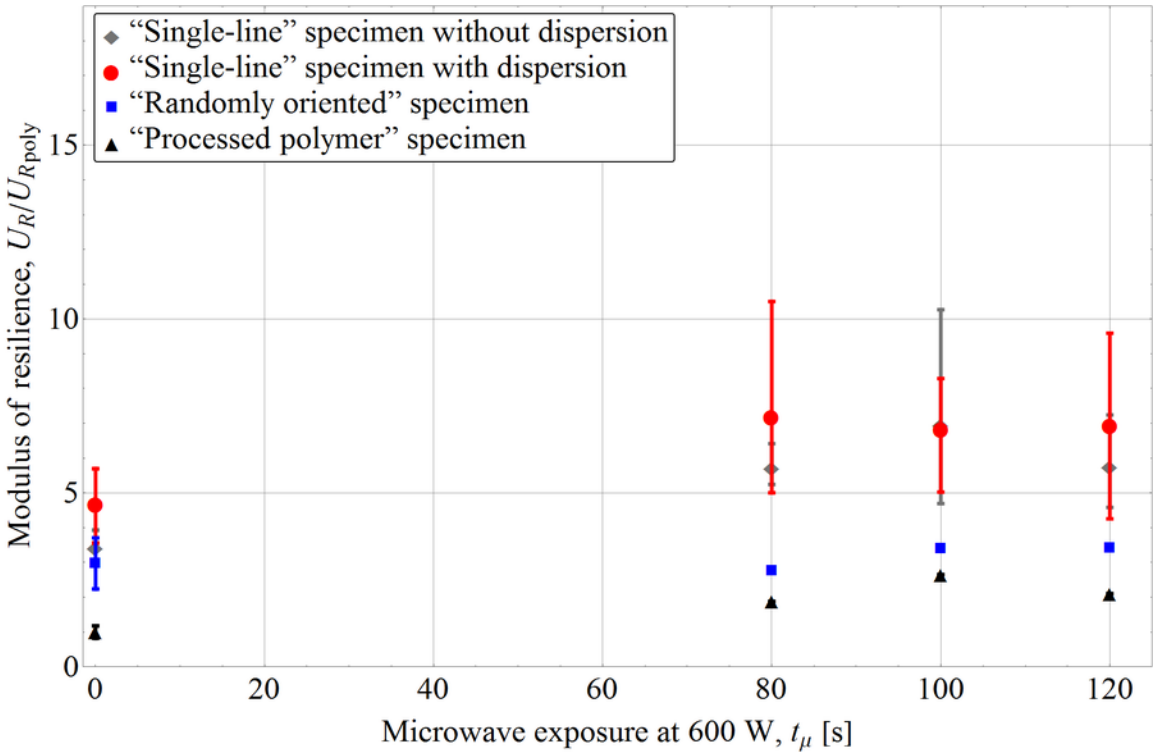

Figure 4.18 Modulus of resilience normalized by modulus of resilience of the "processed polymer" versus microwave radiation exposure time for "single-line" specimens with and without dispersion and for benchmark materials.

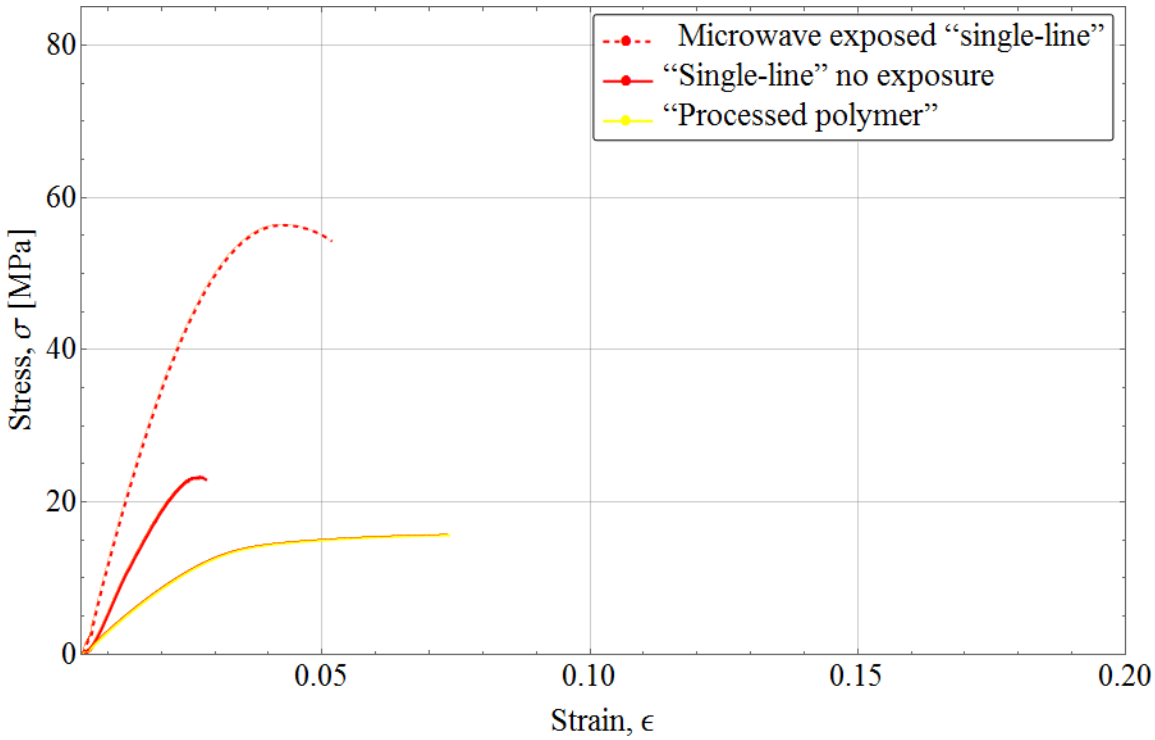

Figure 4.19 Stress-strain diagram for the "single-line" specimens with and without microwave exposure and the "processed polymer" specimens.

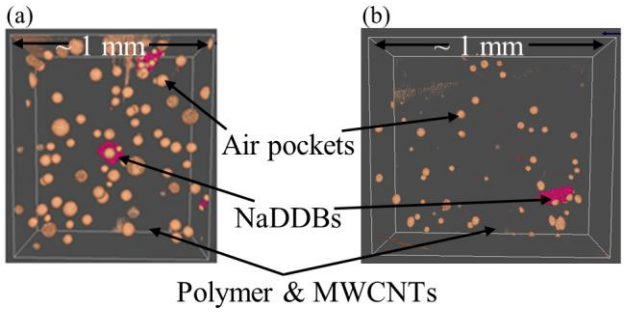

Figure 4.20 X-ray computed tomography (CT) reconstruction of a nanocomposite material highlighting the bubble defects within a (a) "randomly oriented" specimen and (b) "single-line" specimen. The pink material is the NaDDBs, the orange-yellow are air pockets.

Table 4.1 Mechanical properties of the cured urethane resin at different stages of the fabrication process.

Specimen type	Average Young's modulus, E [GPa]	Average ultimate tensile strength, σ_{UT} [MPa]
Cured urethane resin (manufacturer specification)	0.961	21.
"Measured polymer" specimen: cured urethane resin	0.704 ± 0.048	21.7 ± 0.4
Cured urethane resin with surfactant	0.771 ± 0.061	23.2 ± 2.4
"Processed polymer" specimen: cured urethane resin with surfactant, tip sonication, and ultrasound exposure	0.369 ± 0.037	14.8 ± 1.3

CHAPTER 5

CONCLUSIONS

This thesis presented a method to concentrate and align MWCNTs within polymer nanocomposite material using standing ultrasound waves, and characterize the mechanical properties of these materials.

5.1 Novel contributions to the current state of knowledge

This research led to important contributions to the state-of-the-art in fabricating CNT polymer composite materials.

- The concentrate/align/excise methodology was developed to achieve weight fraction of aligned MWCNTs of ~11.35±3.5 wt. %; previous acoustic alignment methods got just 0.15 wt. %.
- This methodology was demonstrated to increase strength (185%) and stiffness (200%) of the MWCNT nanocomposite material relative to the processed polymer benchmark; previous work showed strength increases of just 6 %.
- The research demonstrated that density measurements and a rule of mixtures was sufficient to characterize the weight fraction of MWCNT in randomly oriented specimens when the fiber density was equal to the bulk density of the MWCNT; this revealed that the best available dispersion methods were still leaving a

significant quantity of undispersed MWCNT.

- Density measurements of excised portions of the specimens were used to obtain the first estimates of the local weight fraction of MWCNT in the concentrated region at the nodes of the standing wave –a previously unknown value.
- The research demonstrated a 310% increase in ultimate tensile strength and a 610% increase in Young's modulus relative to the "processed polymer" from microwave exposure to MWCNT polymer nanocomposite materials, including coupled effects with dispersion that hint at underlying mechanisms. While the precise mechanism governing the observed enhancement to mechanical properties is not known, these results clearly show the potential for the combination of microwave processing with ultrasound-aligned MWCNTs in polymer nanocomposite materials.

In support of this experimental effort the research, several key advances were made that may aid future development of this technology.

- The work quantified the effect of surfactant-to-MWCNT ratio on the mechanical performance of "randomly oriented" MWCNT polymer nanocomposite material specimens, and showed that a ratio of 0.6 was optimal for this system over a range of MWCNT weight fractions.
- An alternative configuration of the ultrasound transducer alignment apparatus was used to directly measure the acoustic wave propagation velocity in the curing urethane resin, an important parameter in designing the alignment fixture and operating conditions.
- It was demonstrated that while the addition of surfactant had a negligible effect on the ultimate tensile strength of the urethane resin, the strength of the polymer was

degraded by exposure to either tip sonication or to standing ultrasound waves.

These observations and methods may guide future development of MWCNT urethane resin composite materials.

5.2 Future work

These results suggested that this methodology could be a promising new avenue to achieve synthesis and processing of polymer nanocomposite materials with ultra-high weight fraction of MWCNTs (> 10 wt. %). Based on this research, several areas were identified for future work to build upon this effort.

- The results showed a critical need to better understand the degradation caused by ultrasound energy on polymer materials, so that steps can be taken to mitigate this degradation. Studying the effect on polymer mechanical properties and defect formation (as determined from density measurements or x-ray CT imaging) of varying concentrations of surfactant and the power and duration of the ultrasound exposure could guide the process optimization.
- For both aligned and randomly oriented specimens, it was shown that the current performance was limited by incomplete dispersion of the MWCNT, even when concentrated from an initially low wt. %. Development of better dispersion methods will certainly enable advances in performance for these polymer nanocomposite materials.
- The results obtained for microwave-exposed polymer nanocomposite materials with aligned MWCNT are encouraging, and exploring this approach with other systems should be an active area of research.
- The alignment method could be applied to a variety of geometries, including

continuous processing with in-situ alignment of filament or UV-cured bath-based additive manufacture; in particular, extending this work with multiple sets of ultrasound transducers to achieve uniaxial alignment (rather than in-plane alignment) should result in an immediate increase in mechanical properties.

With continued development, the processes that this research developed and demonstrated in this work will lead to next-generation polymer nanocomposite materials with aligned MWCNTs with desirable mechanical traits exceeding those available with existing technology.

REFERENCES

[1] S. Iijima, “Helical microtubules of graphitic carbon,” *Nature*, vol. 354, no. 6348, pp. 56–58, 1991.

[2] A. Desai and M. Haque, “Mechanics of the interface for carbon nanotube-polymer composites,” *Thin Wall. Struct.*, vol. 43, no. 11, pp. 1787–1803, 2005.

[3] X. Xie *et al.*, “Dispersion and alignment of carbon nanotubes in polymer matrix: A review,” *Mater. Sci. Eng.: R: Rep.*, vol. 49, no. 4, pp. 89–112, 2005.

[4] J. Coleman *et al.*, “Small but strong: A review of the mechanical properties of carbon nanotube-polymer composites,” *Carbon*, vol. 44, no. 9, pp. 1624–1652, 2006.

[5] H. Cebeci *et al.*, “Multifunctional properties of high volume fraction aligned carbon nanotube polymer composites with controlled morphology,” *Compos. Sci. Technol.*, vol. 69, no. 15–16, pp. 2649–2656, 2009.

[6] C. Sweeney *et al.*, “Microwave induced welding of carbon nanotube-thermoplastic interfaces for enhanced mechanical strength of 3D printed parts,” in *Meeting Amer. Phys. Soc.*, 2016.

[7] D. Adams, "Engineering composite materials," *Composites*, vol. 18, no. 3, pp. 261, 1987.

[8] M. Groover, *Fundamentals of Modern Manufacturing: Materials Processes, and Systems*, 3rd Edition. John Wiley & Sons, 2007.

[9] N. Chand and M. Fahim, *An Introduction to Tribology of FRP Materials*. Allied Publishers, 2000.

[10] M. Tamin, *Damage and Fracture of Composite Materials and Structures*. Springer, 2012.

[11] H. Binici *et al.*, “Thermal isolation and mechanical properties of fibre reinforced mud bricks as wall materials,” *Constr. Build. Mater.*, vol. 21, no. 4, pp. 901–906, 2007.

[12] Y. Yuming *et al.*, “Bamboo diversity and traditional uses in Yunnan, China,” *Mt. Res. Dev.*, vol. 24, no. 2, pp. 157–165, 2004.

[13] J. Karni and E. Karni, “Gypsum in construction: origin and properties,” *Mater. Struct.*, vol. 28, no. 2, pp. 92–100, 1995.

[14] Berkeley National Lab, "Roman seawater concrete holds the secret to cutting carbon emissions". 2013.

[15] B. Brown, “Aggregates for concrete,” *Concrete*, vol. 32, no. 5, pp. 12–14, 1998.

[16] S. Moskowitz, *The Advanced Materials Revolution: Technology and Economic Growth in the Age of Globalization*. John Wiley & Sons, 2014.

[17] B. Mitchell, *An Introduction to Materials Engineering and Science for Chemical and Materials Engineers*. John Wiley & Sons, 2004.

[18] D. Askeland and W. Wright, *Essentials of Materials Science & Engineering*. Cengage Learning, 2013.

[19] G. Akovali, *Handbook of Composite Fabrication*. iSmithers Rapra Publishing, 2001.

[20] Z. Gürdal *et al.*, *Design and Optimization of Laminated Composite Materials*. John Wiley & Sons, 1999.

[21] A. Bunsell and J. Renard, *Fundamentals of Fibre Reinforced Composite Materials*. CRC Press, 2005.

[22] J. Reddy and A. Miravete, *Practical Analysis of Composite Laminates*, vol. 1. CRC Press, 1995.

[23] N. Cheremisinoff, *Handbook of Ceramics and Composites*. M. Dekker, 1990.

[24] U. Vaidya, *Composites for Automotive, Truck and Mass Transit, Materials, Design, Manufacturing*. 2011.

[25] R. Vajtai, *Handbook of Nano-materials*. Springer Science & Business Media, 2013.

[26] R. Gibson, *Principles of Composite Material Mechanics*, 3rd Edition. CRC Press, 2012.

[27] W. Rankin, *Minerals, Metals and Sustainability: Meeting Future Material Needs*. CSIRO Publishing, 2009.

[28] S. Lee, *Handbook of Composite Reinforcements*. Wiley-VHC, 1992.

[29] P. Mallick, *Fiber-reinforced Composites: Materials, Manufacturing, and Design*. CRC press, 2007.

[30] S. Hoa, *Principles of the Manufacturing of Composite Materials*. DEStech Publications, Inc, 2009.

[31] E. Barbero, *Introduction to Composite Materials Design*. CRC press, 2010.

[32] A. Strong, *Fundamentals of Composites Manufacturing,* 2nd Edition. Society of Manufacturing Engineers, 2008.

[33] M. Yu, "Strength and breaking mechanism of multiwalled carbon nanotubes under tensile load," *Science*, vol. 287, no. 5453, pp. 637–640, 2000.

[34] G. Carter and D. Paul, *Materials Science and Engineering*. ASM International, 1991.

[35] S. Peters, *Handbook of Composites*. Springer Science & Business Media, 2013.

[36] G. Staab, *Laminar Composites*. Butterworth-Heinemann, 1999.

[37] A. Kelly, *Concise Encyclopedia of Composite Materials*. Elsevier, 2012.

[38] G. Carter and D. Paul, *Materials Science and Engineering*. ASM International, 1991.

[39] W. Callister, *Materials Science and Engineering,* 7th Edition. Wiley, 2011.

[40] K. Chawla, *Composite Materials: Science and Engineering*. Springer Science & Business Media, 2012.

[41] D. Chung, *Carbon Fiber Composites*. Butterworth-Heinemann, 1994.

[42] F. Campbell, *Structural Composite Materials*. ASM international, 2010.

[43] R. Budynas and K. Nisbett, *Shigley's Mechanical Engineering Design,* SI Version. McGraw-Hill Education, 2009.

[44] M. Ashby *et al.*, "The mechanical properties of natural materials. I. Material property charts," in *Proc. R. Soc. A*, 1995, vol. 450, pp. 123–140, 1995.

[45] "Cambridge engineering selector." [Online]. Available: http://www.grantadesign.com/images/ces/Youngs-Density-2012-large.jpg. [Accessed: 01-Jan-2015].

[46] P. Morgan, *Carbon Fibers and Their Composites*. CRC Press, 2005.

[47] C. Journet *et al.*, "Large-scale production of single-walled carbon nanotubes by the electric-arc technique," *Nature*, vol. 388, no. 6644, pp. 756–758, 1997.

[48] C. Baddour and C. Briens, "Carbon nanotube synthesis: A review," *Int. J. Chem. React. Eng.*, vol. 3, no. 1, 2005.

[49] V. Popov, "Carbon nanotubes: properties and application," *Mater. Sci. and Eng.: A*, vol. 2003, no. 3, pp. 61–102, 2004.

[50] P. Avouris *et al.*, "Carbon nanotubes: synthesis, structure, properties, and

applications," *J. Phys. Chem. Lett.*, pp. 6–53, 2000.

[51] D. Venegoni *et al.*, "Parametric study for the growth of carbon nanotubes by catalytic chemical vapor deposition in a fluidized bed reactor," *Carbon*, vol. 40, no. 10, pp. 1799–1807, 2002.

[52] S. Fu *et al.*, "Effects of particle size, particle/matrix interface adhesion and particle loading on mechanical properties of particulate-polymer composites," *Composites, Part B*, vol. 39, no. 6, pp. 933–961, 2008.

[53] O. Breuer and U. Sundararaj, "Big returns from small fibers: A review of polymer/carbon nanotube composites," *Polym. Compos.*, vol. 25, pp. 630–645, 2004.

[54] G. Milton, *The Theory of Composites*. Cambridge University Press, 2002.

[55] C. Ru, "Effect of van der Waals forces on axial buckling of a double-walled carbon nanotube.," *J. Appl. Phys.*, vol. 87, no. 10, pp. 7227–7231, 2000.

[56] P. Ma *et al.*, "Dispersion and functionalization of carbon nanotubes for polymer-based nanocomposites: A review," *Compos. Part A: Appl. Sci.*, vol. 41, no. 10, pp. 1345–1367, 2010.

[57] V. Choudhary *et al., Carbon Nanotubes and Their Composites*. InTech, 2013.

[58] X. Gong *et al.*, "Surfactant-assisted processing of carbon nanotube/polymer composites," *Chem. Mater.* vol. 12, no. 4, pp. 1049–1052, 2000.

[59] L. Vaisman *et al.*, "The role of surfactants in dispersion of carbon nanotubes," *Adv. Colloid Interfac.*, vol. 128–130, pp. 37–46, 2006.

[60] E. Thostenson *et al.*, "Advances in the science and technology of carbon nanotubes and their composites: A review," *Compos. Sci. Technol.*, vol. 61, no. 13, pp. 1899–1912, 2001.

[61] J. Zhu *et al.*, "Fiber-reinforced polymer composites containing functionalized carbon nanotubes". United States Patent and Trademark Office US20100143701, June 10, 2010.

[62] G. Caneba *et al.*, "Novel ultrasonic dispersion of carbon nanotubes," *J. Miner. Mater. Charact. Eng.*, vol. 9, no. 3, pp. 165–181, 2010.

[63] V. Choudhary and A. Gupta, "Polymer/carbon nanotube nanocomposites," *Carbon Nanotubes: Polym. Nanocompos.*, pp. 65–90, 2011.

[64] O. Matarredona *et al.*, "Dispersion of single-walled carbon nanotubes in aqueous solutions of the anionic surfactant NaDDBS," *J. Phys. Chem. C*, vol. 107, no. 48, pp. 13357–13367, 2003.

[65] Y. Li *et al.*, “Direct spinning of carbon nanotube fibers from chemical vapor deposition synthesis,” *Science*, vol. 304, no. 5668, pp. 276–278, 2004.

[66] A. Kenneth *et al.*, "Fiber-reinforced polymer composites containing cross-functionalized carbon nanotubes". United States Patent and Trademark Office US20128187703, May 29, 2012.

[67] M. Islam *et al.*, “High weight fraction surfactant solubilization of single-wall carbon nanotubes in water,” *Nano Lett.*, vol. 3, no. 2, pp. 269–273, 2003.

[68] M. Byrne and Y. Gun’ko, “Recent advances in research on carbon nanotube-polymer composites,” *Adv. Mater.*, vol. 22, no. 15, pp. 1672–1688, 2010.

[69] M. Haslam and B. Raeymaekers, “A composite index to quantify dispersion of carbon nanotubes in polymer-based composite materials,” *Composites, Part B*, vol. 55, no. 1, pp. 16–21, 2013.

[70] M. Shokrieh and R. Rafiee, “Investigation of nanotube length effect on the reinforcement efficiency in carbon nanotube based composites,” *Compos. Struct.*, vol. 92, no. 10, pp. 2415–2420, 2010.

[71] H. Wagner and R. Vaia, “Nanocomposites: Issues at the interface,” *Mater. Today*, vol. 7, no. 11, pp. 38–42, 2004.

[72] Y. Li *et al.*, “Pull-out simulations on interfacial properties of carbon nanotube-reinforced polymer nanocomposites,” *Comput. Mater. Sci.*, vol. 50, no. 6, pp. 1854–1860, 2011.

[73] E. Wong, “Nanobeam mechanics elasticity strength and toughness of nanorods and nanotubes,” *Science*, vol. 277, no. 5334, pp. 1971–1975, 1997.

[74] E. Thostenson *et al.*, “Advances in the science and technology of carbon nanotubes and their composites: A review,” *Compos. Sci. Technol.*, vol. 61, no. 13, pp. 1899–1912, 2001.

[75] R. Haggenmueller *et al.*, “Aligned singlewall carbon nanotubes in composites by melt processing methods,” *Chem. Phys. Lett.*, vol. 330, no. 3, pp. 219–225, 2000.

[76] P. Pötschke *et al.*, “Orientation of multiwalled carbon nanotubes in composites with polycarbonate by melt spinning,” *Polymer*, vol. 46, no. 23, pp. 10355–10363, 2005.

[77] J. Gao *et al.*, “Continuous spinning of a single-walled carbon nanotube-nylon composite fiber,” *J. Am. Chem. Soc.*, vol. 127, no. 11, pp. 3847–3854, 2005.

[78] W. Salalha *et al.*, “Single-walled carbon nanotubes embedded in oriented polymeric nanofibers by electrospinning,” *Langmuir*, vol. 20, no. 22, pp. 9852–9855, 2004.

[79] F. Ko *et al.*, “Electrospinning of continuous carbon nanotube-filled nanofiber

yarns," *Adv. Mater.*, vol. 15, no. 14, pp. 1161–1165, 2003.

[80] R. Andrews *et al.*, "Nanotube composite carbon fibers," *Appl. Phys. Lett.*, vol. 75, no. 9, pp. 1329–1331, 1999.

[81] A. Dalton *et al.*, "Super-tough carbon-nanotube fibres," *Nature*, vol. 423, no. 6941, p. 703, 2003.

[82] B. Vigolo *et al.*, "Improved structure and properties of single-wall carbon nanotube spun fibers," *Appl. Phys. Lett.*, vol. 81, no. 7, pp. 1210–1212, 2002.

[83] L. Dai and A. Mau, "Controlled synthesis and modification of carbon nanotubes and C60: carbon nanostructures for advanced polymeric composite materials," *Adv. Mater.*, vol. 13, no. 12–13, pp. 899–913, 2001.

[84] P. Bradford *et al.*, "A novel approach to fabricate high volume fraction nanocomposites with long aligned carbon nanotubes," *Compos. Sci. Technol.*, vol. 70, no. 13, pp. 1980–1985, 2010.

[85] R. Cervini *et al.*, "Aligned silane-treated MWCNT/liquid crystal polymer films," *Nanotechnology*, vol. 19, no. 17, p. 175602, 2008.

[86] B. Hinds *et al.*, "Aligned multiwalled carbon nanotube membranes," *Science*, vol. 303, no. 5654, pp. 62–65, 2004.

[87] L. Pei *et al.*, "Processing of thin carbon nanotube-polyimide composite membranes," *Nanosci. Nanotechnol. Lett.*, vol. 3, no. 4, pp. 451–457, 2011.

[88] Y. Jung *et al.*, "Aligned carbon nanotube-polymer hybrid architectures for diverse flexible electronic applications," *Nano Lett.*, vol. 6, no. 3, pp. 413–418, 2006.

[89] W. Lim *et al.*, "Alignment of carbon nanotubes by acoustic manipulation in a fluidic medium," *J. Phys. Chem. C*, vol. 111, no. 45, pp. 16802–16807, 2007.

[90] T. Kimura *et al.*, "Polymer composites of carbon nanotubes aligned by a magnetic field," *Adv. Mater.*, vol. 14, no. 19, pp. 1380–1383, 2002.

[91] P. Gonnet *et al.*, "Thermal conductivity of magnetically aligned carbon nanotube buckypapers and nanocomposites," *Curr. Appl. Phys.*, vol. 6, no. 1, pp. 119–122, 2006.

[92] E. Choi *et al.*, "Enhancement of thermal and electrical properties of carbon nanotube polymer composites by magnetic field processing," *J. Appl. Phys.*, vol. 94, no. 9, pp. 6034–6039, 2003.

[93] H. Lu *et al.*, "Magnetically aligned carbon nanotube in nanopaper enabled shape-memory nanocomposite for high speed electrical actuation," *Appl. Phys. Lett.*, vol. 98, no. 17, p. 174105, 2011.

[94] J. Hone *et al.*, "Electrical and thermal transport properties of magnetically aligned single wall carbon nanotube films," *Appl. Phys. Lett.*, vol. 77, no. 5, pp. 666–668, 2000.

[95] B. Smith *et al.*, "Structural anisotropy of magnetically aligned single wall carbon nanotube films," *Appl. Phys. Lett.*, vol. 77, pp. 663–665, 2000.

[96] J. Lagerwall *et al.*, "Nanotube alignment using lyotropic liquid crystals," *Adv. Mater.*, vol. 19, no. 3, pp. 359–364, 2007.

[97] M. Haslam and B. Raeymaekers, "Aligning carbon nanotubes using bulk acoustic waves to reinforce polymer composites," *Composites, Part B*, vol. 60, pp. 91–97, 2014.

[98] P. Ajayan *et al.*, "Aligned carbon nanotube arrays formed by cutting a polymer resin-nanotube composite," *Science*, vol. 265, no. 5176, pp. 1212–1214, 1994.

[99] J. Wood *et al.*, "Orientation of carbon nanotubes in polymers and its detection by Raman spectroscopy," *Composites, Part A*, vol. 32, no. 3–4, pp. 391–399, 2001.

[100] C. Wang *et al.*, "Strong carbon-nanotube-polymer bonding by microwave irradiation," *Adv. Funct. Mater.*, vol. 17, no. 12, pp. 1979–1983, 2007.

[101] M. Rosato and D. Rosato, *Reinforced Plastics Handbook*. Elsevier, 2004.

[102] M. Yu, "Strength and breaking mechanism of multiwalled carbon nanotubes under tensile load," *Science*, vol. 287, no. 5453, pp. 637–640, 2000.

[103] R. Baughman *et al.*, "Carbon nanotubes-the route toward applications," *Science*, vol. 297, no. 5582, pp. 787–792, 2002.

[104] H. Li *et al.*, "Carbon nanodots: synthesis, properties and applications," *J. Mater. Chem.*, vol. 44, no. 46, pp. 24230–24253, 2012.

[105] "Stainless steel mechanical properties," 2012. [Online]. Available: http://www.ezlok.com/TechnicalInfo/MPStainlessSteel.html. [Accessed: 21-Apr-2015].

[106] ASTM Standard D638, ASTM: D638, Standard test method for tensile properties of plastics. 2013.

[107] "Smooth-Cast 300 series bright white liquid plastic." [Online]. Available: http://www.smooth-on.com/Urethane-Plastic-a/c5_1120_1209/index.html. [Accessed: 01-Jan-2015].

[108] "Cheaptubes.com is the source for multi walled carbon nanotubes - MWNTs." [Online]. Available: http://cheaptubes.com/MWNTs.htm. [Accessed: 27-Sep-2013].

[109] M. Islam *et al.*, "High weight fraction surfactant solubilization of single-wall carbon nanotubes in water," *Nano Lett.*, vol. 3, no. 2, pp. 269–273, 2003.

[110] X. Xin *et al.*, "Dispersion and property manipulation of carbon nanotubes by self-assemibles of amphiphilic molecules," *Phys. Chem. Prop. Carbon Nanotubes*, S. Suzuki, Ed. InTech, 2013.

[111] M. Clark *et al.*, "Understanding surfactant aided aqueous dispersion of multi-walled carbon nanotubes," *J. Colloid Interface Sci.*, vol. 354, no. 1, pp. 144–151, 2011.

[112] B. Mensah *et al.*, "Carbon nanotube-reinforced elastomeric nanocomposites: A review," *Int. J. Smart Nano Mater.*, vol. 6, no. 4, pp. 211–238, 2016.

[113] J. Greenhall *et al.*, "Continuous and unconstrained manipulation of micro-particles using phase-control of bulk acoustic waves," *Appl. Phys. Lett.*, vol. 103, no. 7, p. 74, 2013.

[114] J. Greenhall *et al.*, "Ultrasound directed self-assembly of user-specified patterns of nanoparticles dispersed in a fluid medium," *Appl. Phys. Lett.*, vol. 108, no. 10, p. 103, 2016.

[115] B. Raeymaekers *et al.*, "Manipulation of diamond nanoparticles using bulk acoustic waves," *J. Appl. Phys.*, vol. 109, no. 1, p. 2338, 2011.

[116] L. V. King, "On the acoustic radiation pressure on spheres," in *Proc. R. Soc. London, Ser. A*, 1934, vol. 147, pp. 212–240, 1934.

[117] L. P. Gor'kov, "On the forces acting on a small particle in an acoustical field in an ideal fluid," *Dokl. Phys.*, vol. 6, p. 773, 1962.

[118] K. Yosioka and Y. Kawasima, "Acoustic radiation pressure on a compressible sphere," *Acoustica*, vol. 5, no. 3, pp. 167–173, 1955.

[119] A. T. Fenley *et al.*, "Calculation and visualization of atomistic mechanical stresses in biomolecules," *Biophys. J.*, vol. 106, no. 2, p. 461a, 2014.

[120] J. Hone *et al.*, "Thermal conductivity of single-walled carbon nanotubes," *Phys. Rev. B*, vol. 59, no. 4, pp. R2514–R2516, 1999.

[121] J. R. Lukes and H. Zhong, "Thermal conductivity of individual single-wall carbon nanotubes," *J. Heat Transfer*, vol. 129, no. 6, pp. 705–716, 2007.

[122] F. G. Mitri, "Radiation force acting on an absorbing cylinder placed in an incident plane progressive acoustic field," *J. Sound Vib.*, vol. 284, no. 1, pp. 494–502, 2005.

[123] N. Pßrez *et al.*, "Experimental determination of the dynamics of an acoustically levitated sphere," *J. Appl. Phys.*, vol. 116, no. 18, pp. 184903–1, 2014.

[124] A. A. Doinikov, “Acoustic radiation pressure on a rigid sphere in a viscous fluid,” *J. Fluid Mech.*, vol. 267, pp. 1–21, 1994.

[125] A. A. Doinikov, “Acoustic radiation force on a spherical particle in a viscous heat-conducting fluid. II. Force on a rigid sphere,” *J. Acoust. Soc. Am.*, vol. 101, no. 2, pp. 722–730, 1997.

[126] M. Kireš, “Archimedes’ principle in action,” *Phys. Edu.*, vol. 42, no. 5, pp. 484–487, 2007.

[127] B. Shaffer and A. H. Windle, “Fabrication and characterization of carbon nanotube/poly (vinyl alcohol) composites,” *Adv. Mater.*, vol. 11, no. 11, pp. 937–941, 1999.

[128] “ANOVA—Wolfram language documentation.” [Online]. Available: https://reference.wolfram.com/language/ANOVA/ref/ANOVA.html. [Accessed: 26-Mar-2017].

[129] Y. Huang and E. Terentjev, "Dispersion of carbon nanotubes: mixing, sonication, stabilization, and composite properties", *Polymer*, vol. 4. pp. 275-295, 2012.

[130] P. Greil, "Perspectives of nano-carbon based engineering materials", *Adv. Eng. Mater.*, vol. 17, no. 2, pp. 124–137, 2015.

[131] P. Pötschke *et al.*, “Rheological behavior of multiwalled carbon nanotube/polycarbonate composites,” *Polymer*, vol. 43, no. 11, pp. 3247–3255, 2002.

[132] J. H. Du *et al.*, "The present status and key problems of carbon nanotube based polymer composites," *Express Polym. Lett.*, vol. 1, no. 5, pp. 253–273, 2007.

[133] W. a. de Heer, “Nanotubes and the pursuit of applications,” *MRS Bull.*, vol. 29, no. 4, pp. 281–285, 2004.

[134] D. Qian *et al.*, “Load transfer and deformation mechanisms in carbon nanotube-polystyrene composites,” *Appl. Phys. Lett.*, vol. 2868, pp. 4–7, 2000.

[135] E. Thostenson and T. Chou, “Microwave processing: fundamentals and applications,” *Composites, Part A*, vol. 30, no. 9, pp. 1055–1071, 1999.

[136] V. K. Rangari *et al.*, “Microwave processing and characterization of EPON 862/CNT nanocomposites,” *Mater. Sci. Eng., B*, vol. 168, no. 1, pp. 117–121, 2010.

[137] X. Sun *et al.*, “Microwave absorption characteristics of carbon nanotubes,” *Carbon Nanotubes*, S. Suzuki, Ed. InTech, 2011.

[138] G. J. Price and P. F. Smith, “Ultrasonic degradation of polymer solutions: 2. The effect of temperature, ultrasound intensity and dissolved gases on polystyrene in

toluene," *Polymer*, vol. 34, no. 19, pp. 4111–4117, 1993.

[139] J. Kost *et al.*, "Ultrasound-enhanced polymer degradation and release of incorporated substances," in *Proc. Natl. Acad. Sci.*, vol. 86, no. 20, pp. 7663–7666, 1989.